

CRANFIELD UNIVERSITY

CHEN WANG

Transient Performance Simulation of Gas Turbine Engine Integrated
with Fuel and Control Systems

School of Aerospace, Transport, and Manufacturing
Aerospace Propulsion

Ph.D.
Academic Years: 2012 - 2015

Supervisor: Yiguang Li
Jan 2016

CRANFIELD UNIVERSITY

School of Aerospace, Transport, and Manufacturing
Aerospace Propulsion

Ph.D.

Academic Years 2012 - 2015

CHEN WANG

Transient Performance Simulation of Gas Turbine Engine Integrated
with Fuel and Control Systems

Supervisor: Yiguang Li
Jan 2016

© Cranfield University 2016. All rights reserved. No part of this
publication may be reproduced without the written permission of the
copyright owner.

ABSTRACT

Two new methods for the simulation of gas turbine fuel systems, one based on an inter-component volume (*ICV*) method, and the other based on the iterative Newton Raphson (*NR*) method, have been developed in this study. They are able to simulate the performance behaviour of each of the hydraulic components such as pumps, valves, metering unit of a fuel system, using physics-based models, which potentially offer more accurate results compared with those using transfer functions. A transient performance simulation system has been set up for gas turbine engines based on an inter-component volume (*ICV*). A proportional-integral (*PI*) control strategy is used for the simulation of engine control systems. An integrated engine and its control and hydraulic fuel systems has been set up to investigate their coupling effect during engine transient processes. The developed simulation methods and the systems have been applied to a model turbojet and a model turboshaft gas turbine engine to demonstrate the effectiveness of both two methods. The comparison between the results of engines with and without the *ICV* method simulated fuel system models shows that the delay of the engine transient response due to the inclusion of the fuel system components and introduced inter-component volumes is noticeable, although relatively small. The comparison of two developed methods applied to engine fuel system simulation demonstrate that both methods introduce delay effect to the engine transient response but the *NR* method is ahead than the *ICV* method due to the omission of inter-component volumes on engine fuel system simulation. The developed simulation methods are generic and can be applied to the performance simulation of any other gas turbines and their control and fuel systems.

A sensitivity analysis of fuel system key parameters that may affect the engine transient behaviours has also been achieved and represented in this thesis. Three sets of fuel system key parameters have been introduced to investigate their sensitivities, which are, the volumes introduced for *ICV* method applied to fuel system simulation; the time constants introduced into those first order lags to

simulate the valve movements delay and fuel spray delay effect; and the fuel system key performance and structural parameters.

Keywords:

Transient Performance, Inter Component Volume Method, Newton Raphson Method, Gas Turbine Simulation, Fuel System Simulation

ACKNOWLEDGEMENTS

I would like to express my sincere gratitude to my supervisor, Dr. Yiguang Li for providing valuable support and guidance throughout my research.

I truly appreciate Mr. Baoying Yang and Dr. Zhitao Wang, visiting researchers of Dr. Li, who provided me with a lot of knowledge and experience on my research project.

I would also like to thank my parents who supported me through my UK study and helped me whenever I needed them.

I also would like to thank my dear wife Yan Shi. Her great belief in me is the world's largest force encouraging me to implement my study!

Finally, I would like to thank my colleagues, room-mates, and friends in Cranfield who provided me a lot of advice and support through three years' study.

TABLE OF CONTENTS

ABSTRACT	i
ACKNOWLEDGEMENTS.....	iii
LIST OF FIGURES.....	vii
LIST OF TABLES	x
LIST OF EQUATIONS.....	xi
LIST OF ABBREVIATIONS.....	xvi
1 Introduction.....	1
2 Literature Review	3
2.1 Engine Performance Analysis Technology Development	3
2.1.1 Engine Steady State Prediction.....	3
2.1.2 Engine Transient Performance Prediction.....	6
2.2 Gas Turbine Engine Fuel and Control System Development.....	11
2.2.1 Control System Development from Hydro-mechanical System to FADEC System	11
2.2.2 Simulation Methods for Engine Control and Fuel System	16
2.2.3 Engine Control Laws	23
2.2.4 Accessory Components of FMU.....	29
3 Transient Performance Simulation Methodology of Engine and its Fuel and Control System.....	32
3.1 Engine Performance Simulation	32
3.1.1 Engine Design Point Simulation	32
3.1.2 Engine Transient Performance Simulation Inter-Component Volume (<i>ICV</i>) Method.....	37
3.1.3 Engine Components Calculation	40
3.2 Engine Control System Simulation.....	57
3.3 Engine Fuel System Simulation	61
3.3.1 Engine Fuel System Description	61
3.3.2 Engine Fuel System Performance Simulation Inter-Component Volume (<i>ICV</i>) Method.....	62
3.3.3 Engine Fuel System Performance Simulation Newton Raphson (<i>NR</i>) Method.....	65
3.3.4 Engine Fuel System Components Calculation	72
3.4 Integrated Engine, Control and Fuel System	84
4 Application, Results, and Analysis.....	86
4.1 Application of Engine and its Control and Fuel Systems.....	86
4.1.1 Model Engine System	86
4.1.2 Model Fuel System.....	88
4.1.3 Model Control System	93
4.2 Engine Model Validation	95
4.2.1 Off-Design Steady State Validation	95

4.2.2 Transient Validation.....	99
4.3 Engine Transient Performance Simulation Co-operating with its Control and Fuel System.....	100
4.3.1 Turbojet Engine with Fuel System Developed Using ICV Method..	100
4.3.2 Turbojet Engine with Fuel System Developed Using NR Method ..	103
4.3.3 Turbojet Engine with and without Fuel System Transient Simulation Results Comparison.....	106
4.3.4 Turbojet Engine with Fuel System Transient Simulation Results Comparison between the Developed ICV and NR Method Applied for Fuel System Simulation	111
4.3.5 Turboshaft Engine with Fuel System Developed Using ICV Method	115
4.3.6 Turboshaft Engine with Fuel System Developed Using NR Method	117
4.4 Sensitivity Analysis of Key Fuel System Parameters on Engine Transient Behaviour.....	119
4.4.1 The Sensitivity of Selected Volume of Fuel System Volume Chambers.....	120
The reason producing such phenomena is that the first and second volumes, HPP and CPDV form a closed fuel delivery loop to return the excess fuel from HPP outlet to its inlet. This fuel stream is not involved in the system fuel metering task but only used to maintain the system operation safety. Therefore, the amounts of the first and second volumes have less effect on the metered fuel injected into the engine combustor. On the contrary, the MU metered fuel has to flow through the third volume and the injector before it entering into the engine system. The variation of the volume amount of the third volume chamber largely affects the engine actual fuel trajectory.....	121
4.4.2 The Sensitivity of Fuel System Components' Delay Time Constant	121
4.4.3 The Sensitivity of Fuel System Components' Performance and Structural Key Parameters	123
5 Conclusion.....	125
6 Future Work.....	128
6.1 Model Accuracy Verification.....	128
6.2 Engine Transient Model Improvement	128
6.3 Fuel Control Algorithms	129
6.4 Engine Limit Protection Control Logic.....	129
6.5 Dynamic Flight Parameters Introduced into Engine Transient Performance Simulation.....	129
REFERENCES.....	130
APPENDICES	140

A.1 Engine System Simulation Flow Chart Using Inter-Component Volume (ICV) Method.....	140
A.2 Flow Chart of Inter-Component Volume (ICV) Method on Fuel System Simulation.....	141
A.2 Flow Chart of Newton Raphson (NR) Method on Fuel System Simulation	142

LIST OF FIGURES

Figure 2.1 Schematics of traditional centralized architecture and distributed architecture of engine control system [68]	15
Figure 2.2 Block Diagrams of Open-loop and Closed-loop Control Systems [2]	16
Figure 2.3 Block Diagram of a PID Controller.....	19
Figure 2.4 Block Diagram of a FMU Model in AMESim [87].....	23
Figure 2.5 Fuel Control Schedule Fuel Flow Rate versus Engine Shaft Speed [20]	25
Figure 2.6 Limit Protection of Accel and Decel Schedules on N Controller [28]	26
Figure 3.1 Schematic of Single-Spool Turbojet Model Engine Configuration ...	32
Figure 3.2 Schematic of Two-Spool Turboshaft Model Engine Configuration ..	33
Figure 3.3 Compressor Characteristic Maps [15]	34
Figure 3.4 Turbine Efficiency and Mass Flow Rate Characteristic Maps [92]...	35
Figure 3.5 Fuel Schedule of Model Engine	57
Figure 3.6 Diagram of Coupled Engine Controller and Fuel Selection Logic....	59
Figure 3.7 Diagram of Coupled Engine Controller and Fuel Selection Logic....	60
Figure 3.8 Schematic of Engine Fuel System.....	61
Figure 3.9 Schematic of Inter-Component Volume.....	62
Figure 3.10 Newton Raphson Method on Finding X_n from Initial Value X_0	66
Figure 3.11 Schematic of Centrifugal Pump.....	73
Figure 3.12 Schematic of Gear Pump	73
Figure 3.13 Typical Centrifugal Pump Characteristic Map	74
Figure 3.14 Typical Gear Pump Characteristic Map	74
Figure 3.15 Schematic of Constant Pressure Differential Valve	77
Figure 3.16 Schematic of Metering Unit Valve	80
Figure 3.17 Schematic of Metering Unit Valve [104]	82
Figure 3.18 Schematic of Integrated Engine, Control and Fuel System	84
Figure 4.1 Low Pressure Pump Volumetric Flow Rate Map	90
Figure 4.2 High Pressure Pump Volumetric Flow Rate Map	90

Figure 4.3 Low Pressure Pump Efficiency Map.....	91
Figure 4.4 High Pressure Pump Efficiency Map	91
Figure 4.5 Turbojet Engine Fuel Schedule and Steady State Fuel Lines	94
Figure 4.6 Turboshaft Engine Fuel Schedule and Steady State Fuel Lines	94
Figure 4.7 Off-Design Steady State Results Comparison at Sea Level, ISA Condition between TurboMatch and Newly Simulated Engine Models.....	97
Figure 4.8 Off-Design Steady State Results Comparison at Sea Level, ISA Condition between GasTurb and Newly Simulated Engine Models.....	97
Figure 4.9 Transient Trajectories Comparison at Sea Level, ISA Condition between GasTurb and Newly Simulated Engine Models	100
Figure 4.10 Model Turbojet Engine PCN vs. Time at Sea Level, ISA Condition	102
Figure 4.11 Model Turbojet Engine Wff vs. Time at Sea Level, ISA Condition	102
Figure 4.12 Model Turbojet Engine Wff vs. PCN at Sea Level, ISA Condition	103
Figure 4.13 Model Turbojet Engine PCN vs. Time at Sea Level, ISA Condition	104
Figure 4.14 Model Turbojet Engine Wff vs. Time at Sea Level, ISA Condition	105
Figure 4.15 Model Turbojet Engine Wff vs. PCN at Sea Level, ISA Condition	106
Figure 4.16 Model Turbojet Engine Wff vs. Time Comparison at Sea Level, ISA Condition between Engine with and without Fuel System Transient Simulation.....	107
Figure 4.17 Model Turbojet Engine Wff vs. PCN Comparison at Sea Level, ISA Condition between Engine with and without Fuel System Transient Simulation.....	109
Figure 4.18 Model Turbojet Engine PCN vs. Time Comparison at Sea Level, ISA Condition between Engine with and without Fuel System Transient Simulation.....	109
Figure 4.19 Model Turbojet Engine TET vs. Time Comparison at Sea Level, ISA Condition between Engine with and without Fuel System Transient Simulation.....	110
Figure 4.20 Model Turbojet Engine P_3 vs. Time Comparison at Sea Level, ISA Condition between Engine with and without Fuel System Transient Simulation.....	110
Figure 4.21 Model Turbojet Engine Wff vs. Time Comparison at Sea Level, ISA Condition between the Developed ICV and NR Methods Applied on the Fuel System Transient Simulation	111

Figure 4.22 Model Turbojet Engine Wff vs. PCN Comparison at Sea Level, ISA Condition between the Developed ICV and NR Methods Applied on the Fuel System Transient Simulation	112
Figure 4.23 Model Turbojet Engine PCN vs. Time Comparison at Sea Level, ISA Condition between the Developed ICV and NR Methods Applied on the Fuel System Transient Simulation	113
Figure 4.24 Model Turbojet Engine TET vs. Time Comparison at Sea Level, ISA Condition between the Developed ICV and NR Methods Applied on the Fuel System Transient Simulation	114
Figure 4.25 Model Turbojet Engine P_3 vs. Time Comparison at Sea Level, ISA Condition between the Developed ICV and NR Methods Applied on the Fuel System Transient Simulation	114
Figure 4.26 Model Turboshaft Engine PCN vs. Time at Sea Level, ISA Condition	115
Figure 4.27 Model Turboshaft Engine Wff vs. Time at Sea Level, ISA Condition	116
Figure 4.28 Model Turboshaft Engine Wff vs. PCN at Sea Level, ISA Condition	117
Figure 4.29 Model Turboshaft Engine PCN vs. Time at Sea Level, ISA Condition	117
Figure 4.30 Model Turboshaft Engine Wff vs. Time at Sea Level, ISA Condition	118
Figure 4.31 Model Turboshaft Engine Wff vs. PCN at Sea Level, ISA Condition	119
Figure 4.32 Engine Actual Fuel Trajectories Comparison for Fuel System Volume Sensitivity Analysis	120
Figure 4.33 Engine Actual Fuel Trajectories Comparison for Fuel System Components' Delay Time Constant Sensitivity Analysis.....	122
Figure 4.34 Engine Actual Fuel Trajectories Comparison for Fuel System Components' Performance and Structural Key Parameters' Sensitivity Analysis	124

LIST OF TABLES

Table 2-1 Sensors and Actuators of Multivariable Engine Controller [88]	28
Table 4-1 Turbojet Model Engine Performance Specification at Design Point and Key Parameters	86
Table 4-2 Turboshaft Model Engine Performance Specification at Design Point and Key Parameters	87
Table 4-3 Fuel System Parameters at Design Point for Turbojet Model	88
Table 4-4 Fuel System Parameters at Design Point for Turboshaft Model	89
Table 4-5 PI Controller Gains for Turbojet Engine Model	93
Table 4-6 PI Controller Gains for Turboshaft Engine Model	93
Table 4-7 Off-Design Key Performance Parameters Comparison between Newly Simulated Engine Model and TurboMatch Simulated Engine Model (%) ..	98
Table 4-8 Key Performance Parameters Comparison between Newly Simulated Engine Model and GasTurb Simulated Engine Model (%)	99

LIST OF EQUATIONS

(2-1).....	20
(3-1).....	36
(3-2).....	36
(3-3).....	36
(3-4).....	36
(3-5).....	36
(3-6).....	36
(3-7).....	37
(3-8).....	37
(3-9).....	37
(3-10).....	39
(3-11).....	40
(3-12).....	41
(3-13).....	41
(3-14).....	41
(3-15).....	41
(3-16).....	41
(3-17).....	41
(3-18).....	41
(3-19).....	41
(3-20).....	42
(3-21).....	42
(3-22).....	42
(3-23).....	42
(3-24).....	42
(3-25).....	42
(3-26).....	42
(3-27).....	43

(3-28).....	44
(3-29).....	44
(3-30).....	44
(3-31).....	44
(3-32).....	44
(3-33).....	44
(3-34).....	45
(3-35).....	45
(3-36).....	45
(3-37).....	45
(3-38).....	45
(3-39).....	46
(3-40).....	46
(3-41).....	46
(3-42).....	46
(3-43).....	47
(3-44).....	47
(3-45).....	47
(3-46).....	48
(3-47).....	48
(3-48).....	48
(3-49).....	48
(3-50).....	48
(3-51).....	49
(3-52).....	49
(3-53).....	49
(3-54).....	51
(3-55).....	51
(3-56).....	51

(3-57).....	51
(3-58).....	52
(3-59).....	52
(3-60).....	52
(3-61).....	52
(3-62).....	52
(3-63).....	52
(3-64).....	52
(3-65).....	54
(3-66).....	54
(3-67).....	54
(3-68).....	54
(3-69).....	54
(3-70).....	54
(3-71).....	55
(3-72).....	55
(3-73).....	55
(3-74).....	55
(3-75).....	55
(3-76).....	55
(3-77).....	56
(3-78).....	56
(3-79).....	56
(3-80).....	56
(3-81).....	60
(3-82).....	61
(3-83).....	63
(3-84).....	63
(3-85).....	63

(3-86).....	63
(3-87).....	63
(3-88).....	64
(3-89).....	64
(3-90).....	64
(3-91).....	65
(3-92).....	65
(3-93).....	65
(3-94).....	65
(3-95).....	66
(3-96).....	66
(3-97).....	66
(3-98).....	67
(3-99).....	67
(3-100).....	68
(3-101).....	68
(3-102).....	68
(3-103).....	68
(3-104).....	68
(3-105).....	69
(3-106).....	69
(3-107).....	69
(3-108).....	69
(3-109).....	70
(3-110).....	70
(3-111).....	70
(3-112).....	70
(3-113).....	71
(3-114).....	71

(3-115).....	71
(3-116).....	71
(3-117).....	72
(3-118).....	75
(3-119).....	76
(3-120).....	76
(3-121).....	76
(3-122).....	76
(3-123).....	76
(3-124).....	76
(3-125).....	78
(3-126).....	78
(3-127).....	78
(3-128).....	79
(3-129).....	79
(3-130).....	79
(3-131).....	79
(3-132).....	79
(3-133).....	79
(3-134).....	81
(3-135).....	81
(3-136).....	81
(3-137).....	81
(3-138).....	82
(3-139).....	83
(3-140).....	83
(4-1).....	87

LIST OF ABBREVIATIONS

A	Area (m ²)
AW	Auxiliary Work (W)
B	Bulk Modulus (Pa)
BE	Base Error
Cd	Orifice Discharge Flow Coefficient
CN	Shaft Corrected Rotational Speed
CNC	Compressor Corrected Rotational Speed Relative to Design Point Value
CNT	Turbine Corrected Rotational Speed Relative to Design Point Value
Cp	Specific Heat at Constant Pressure (J/kg·K)
CPDV	Constant Pressure Differential Valve
CW	Compressor Work (W)
D	Derivative
DH	Enthalpy Drop Ratio
dm	Volume Stored Air Mass Variation (kg)
dP	Derivative of Pressure (kPa)
dT	Derivative of Temperature (K)
dV	Derivative of Volume (m ³)
E	Energy (kJ)
e(t)	Controller Input Error
EL	External Load (W)
FAR	Fuel Air Ratio
HPP	High Pressure Pump
I	Shaft Inertia (kg·m ²)
ICV	Inter Component Volume
K	Spring Stiffness (kN/m)
k	Valve Opening Area Coefficient (m ²)
K _i	Integral Gain
K _p	Proportional Gain
LHV	Low Heating Value (J/kg)
LPP	Low Pressure Pump

m	Mass (kg)
Ma	Mach Number
MFC	Mass Flow Continuity
MU	Metering Unit
NT	Net Thrust
P	Total Pressure (kPa)
PCN	Shaft Relative Rotational Speed
PI	Proportional and Integral
PR	Pressure Ratio
PSP	Pump Shaft Power (kw)
Q	Fuel Volumetric Flow Rate (m ³ /s)
R	Gas Constant (J/kg·K)
RES	Residual Equation Set
SFC	Specific Fuel Consumption (g/kN·s)
SP	Engine Shaft Surplus Power (W)
T	Total Temperature (K)
TET	Turbine Entry Temperature (K)
T _f	Time Constant of Injector Fuel Spray Delay (s)
T _i	Time Constant of Integral Action (s)
T _m	Time Constant of Mechanical Movement Delay (s)
T _s	Time Constant of Sensor Delay (s)
TW	Turbine Work (W)
u(t)	Controller Output Signal
V	Volume Chamber Volume (m ³)
Vs	Speed (m/s)
W	Mass Flow Rate (kg/s)
Xd	Valve Opening Distance (m)
Δt	Calculation Step (s)

Greek Letters:

∂	Partial Differential
α	Thermal Expansion Coefficient (K ⁻¹)
Δ	Difference
ε	Intake Pressure Recovery Coefficient

η	Efficiency
κ	Heat Producing Coefficient of Valve (K)
κ_T	Isothermal Compressibility (Pa ⁻¹)
ξ	Prescribed Convergence Value of NR Iterations (kg/per calculation step)
ρ	Density (kg/m ³)
τ	CPDV Spring Pre-pressurized Distance (m)
ϕ	Thermal Energy (J)

Subscripts:

A	Component Inlet
AMB	Ambient
B	Component Outlet
ff	Fuel Flow
i	Previous Time Step
I	Integral
$i+1$	Current Time Step
in	Inlet
j	Sampling J Point
out	Outlet
P	Proportional
P	Constant Pressure
T	Constant Temperature

1 Introduction

Performance simulations have been widely used in modern gas turbine engine designs in order to shorten design cycles and reduce development costs. Such simulations can be classified into design point, off-design steady state, and transient performance simulations depending on how the engines are operated. Engine transient performance simulation is very useful in the initial stage of engine development. For example, it will be able to assess the safety of transient operations of new engines including acceleration and deceleration, and to provide a numerical test-bed for the development of control systems including the investigation of the control system dynamic behaviour and the coupling between the engines and their control systems.

In recent years, the developed engine models based on system performance simulations has drawn the interest of researchers or engineers to not only use them on new system development, but also on the real engine operations in recent years. Numerical engine models are capable of predicting some important indirectly measured control variables which are required through engine operations such as compressor stall margin (*SM*), turbine entry temperature (*TET*), and engine net thrust. With the huge progress of modern Full Authority Digital Electronic Control (*FADEC*) systems, researchers tried to integrate the developed engine performance models into the Electronic Engine Controller inside the *FADEC* to build a new generation of engine systems which were named "Intelligent Engines". This concept was first investigated in American Versatile Affordable Advanced Turbine Engines (*VAATE*) program. [1]

An engine system, a controller, sensors, and a hydraulic fuel system are four basic elements of a gas turbine propulsion system. Most currently developed engine models only focus on the simulation of engine systems and their controllers but ignore the sensors and actuators or treat them as first order lags.[2] Such simplification ignores the non-linear effect of these physical components and their impact on the whole systems and may cause noticeable prediction errors. In the operation of gas turbine systems, the flow rate of fuel injected into an engine combustion chamber is not only decided by the controller,

but also affected by the execution of fuel control actuators including pumps, valves, and metering units. [3] Therefore, fuel output delay and fluctuation due to fuel system response will directly affect engine combustion and engine performance during transient processes.

To investigate the fuel system effect on engine transient performance simulation, fuel system transient performance model are required to be established and integrated into the engine system simulation. However, it is found in relevant literature that no available method has been analysed. Thus, it is worthwhile to develop a new method for the fuel system transient performance prediction to investigate the fuel system effect on engine system transient simulation.

An inter-component volume (*ICV*) method has already been analysed and widely applied to the transient performance prediction of a series of engine systems. To an engine fuel system with highly incompressible working fluid fuel, this method can be extended to establish the new method for the fuel system transient performance prediction. The simulation results of an integrated model engine coupled with its fuel and control systems will be compared with the model engine only with its controller to estimate the effect of fuel system introduced into the engine transient performance simulation.

In addition, as the *ICV* method has to introduce compressibility into a system where the working fluid fuel oil is always considered incompressible, a Newton Raphson method that ignores the fluid compression behaviour is also developed as an alternative simulation method to compare with the *ICV* method simulation results. In this thesis, both of these methods are introduced to establish the engine with its fuel and control system models and the difference is estimated by comparing the simulation results between these two models.

2 Literature Review

2.1 Engine Performance Analysis Technology Development

2.1.1 Engine Steady State Prediction

Engine performance calculations play an important role in the engine concept stage and development program since they can shorten the design cycle and reduce the development cost, and are even required throughout the system operation. Before the 1960s, most of these calculations were implemented by hand, although some computer programs had been developed for particular engines calculations. The performances of individual components were first predicted especially for the axial flow compressors such as Howell summarizes in Refs. 4, 5.

After components' performance prediction work had been completed, the engine system steady state performance prediction was needed by the researchers and engineers to determine the required component characteristics and understand the components' operation and interaction. Mallinson et al [6] and Goldstein et al [7] presented good examples on how to implement such work manually, without adequate computing facilities, in the early stage of engine performance calculations. Component performances were represented through charts with all the necessary parameters. Those charts are still indispensable tools of modern engine system performance simulations.

In the late 1960s, digital computers became more and more popular to establish computer engine models for the engine steady state performance calculation. The advantages of using those computer models were speed, economy, flexibility, reliability and extreme accuracy. [8] In the early stages, a computation program was only written to a particular researched engine case. However, to free the researchers and engineers so that they did not need to spend so much time on writing similar programs when they would start new case studies, flexibility became an important issue in designing the calculation programs. Typical examples of the developed simulation programs applied to different engine type simulations at that time were represented by Chappell and Cockshutt

et al [9-10], Palmer and Annand [11-12], McKinney [13-14], and Koenig and Fishbach [15-16], Macmillan [17], etc.

References 9-12 introduced two design point (*DP*) programs including the NRC programs and 'TURBOCODE' program. Engine DP is a particular operating steady state point where the engineers decide the engine configuration and the required components' performance. This point calculation is undoubtedly the starting point of each engine performance prediction study. Details of each program have been sufficiently introduced in these references. The progress of these programs were the introduction of a three-level building block approach into the program development to improve the flexibility of these programs. The three levels include the top level master control program, and two lower levels called engine component subroutines and thermodynamic data generators. Through the engine simulation, the master segment handles the calculation sequence and calls the required subroutines from the bottom two levels.

In the NRC programs, as the computation sequences had been pre-described in the system, each developed program could not be altered for other types of engine simulation. This arrangement restricted the flexibility of programs and soon was changed by the TURBOCODE program. In TURBOCODE program, the three-level structure was inherited, but users were permitted to arrange calculation sequences between the top level and the bottom two levels. This design approach largely increased the flexibility of the program and such an arrangement was still taken on some simulation programs in service. Another feature of the TURBOCODE program is its "loop" ability on incrementing some engine or component parameters each time. This can reduce re-input times when the users want to study the important parameters' effects with different values.

The DP program was only used for one specific point calculation. However, the capability of simulating one point is not enough for those programs when researchers need to perform off-design calculations. Engine off-design steady state simulation aims to establish a "balanced" engine at each operating condition. The calculation has to solve a series of non-linear aerodynamic and thermodynamic equations using some iteration. Some constraints, like air flow

continuity, power balances, and some conservation laws, etc. have to be satisfied and details of these constraints are illustrated in Ref. 17. As engine operation is the co-operation of those constituent components such as compressors, combustors, and turbines, these non-linear equations are expressed by the component characteristics form instead of a linear algebraic form. The non-linear nature of these characteristics requires a trial and error approach to obtain a final solution of the performance simulation. Macmillan has illustrated the development of this trial and error approach from a basic iteration technique to the most widely applied Newton-Raphson method taken in SMOTE, GENENG, TURBOCODE, etc. Detail descriptions of engine steady state calculation procedure are exhibited by Walsh et al [18] and Pachidis [19] for different selected engine configurations.

A great advantage of SMOTE, summarized by McKinney, was the component map scaling method which had been widely adopted in most modern performance programs. To a theoretical or hypothetical engine in the concept design stage, those component maps used for engine simulation cannot be taken from actual existing ones. This method provides the possibility to scale new maps from old ones for the purpose of simulation. However, the SMOTE program was only developed for turbofan engines and the illustrations were quite simple. Macmillan inherited McKinney's method and provided a more detailed and generalized illustration of scaling method on each required component of engine simulation. To improve the flexibility of a developed program, Palmer proposed a modular design concept which tried to build a set of subroutines called "Bricks" under the program master segment. These bricks can either be the engine components or the connecting interface between those components. Users who simulated their engines only needed to organize these bricks and the calculation sequence of the program was decided by these arrangements. This largely increased the flexibility of the program, so that users could analyse many configurations of fixed and variable engines, as did Macmillan, and this idea was referenced by many followers in developing their programs.

2.1.2 Engine Transient Performance Prediction

Engine transient performance simulation is used to estimate the engine dynamic behaviour from one steady state condition to another, such as that during acceleration or deceleration processes. Although the continuation of energy, mass, and momentum is still satisfied, equilibrium of work, mass flow, and heat transfer within an engine system will be broken during a transient process. It was first carried out to fulfil the engine control requirement in the early 1950s. For this purpose, engine behaviour was described as a first-order lag system with a time constant. The real non-linear operation procedure such as acceleration was simplified as a linear differential equation which is the function of engine fuel flow and shaft speed near a steady state operating point. [20] Otto et al [21] first fulfilled this research on both acceleration and deceleration analysis of a typical single-spool turbojet engine with a centrifugal compressor. The simulation was carried out on a set of inlet conditions but altitude was kept constant. The results showed that such a linear approximation only provided good transient characteristics near the steady state operating regions. Within a large transient procedure, the author pointed out that there was only a fair agreement with experimental results on acceleration but a poor level of agreement on deceleration process. The reasons which produced such differences were the linear model assumption and the constant burning efficiency assumed in the simulation.

Similar research on the same engine type was taken by Heidmann [22] to analyse engine time constant and turbine entry temperature (*TET*) overshoot due to the effect of the variation of some independent variables such as compressor tip Mach number, ram pressure ratio and component efficiency. Engine time constant is a characteristic that measures the time of engine speed response to the fuel flow change and *TET* overshoot is the result produced by the step change of fuel flow. In this research, a corrected time constant was used by considering the effects of engine size and operation altitude.

A series of transient behaviour researches based on the linear engine model were carried out for different engine configuration applications like a turboprop engine,

an engine with afterburner and two shafts turbojet engine. Moreover, fuel control systems were designed by using the developed linear engine models. It should be noted that in Novik [23], a second order lag linear system instead of a first order linear system was introduced to specify different spool speed responses of multi-spool engines. More research work during this period by using linear engine system simulation were described by Palidis [24].

Linear system models described by simple time constants and partial derivatives are proved to be accurate only at small perturbations from steady state operating points. To better represent the non-linear engine operation on a transient phase, a non-linear system simulation method is required. Two main developed methods have been fully researched and calculation processes are well established including the “Mass Flow Continuity (*MFC*)” method and “Inter Component Volume (*ICV*)” method. The first *MFC* method on transient research was carried out with the analogue computer by Larowe et al [25]. The researchers made use of a number of special electro-mechanical “map-readers” and utilized dc analogue voltages to represent practical variables of engine systems. By connecting different analogue engine “components” to form the simulation model, mass flow continuity was satisfied automatically.

Before the late 1960s, most engine performance predictions were investigated based on an analogue simulation where the *MFC* method had been used. That research exhibited that analogue simulation proved more powerful in exploratory studies. However, due to the advantages of digital simulation, more emphases were placed on digital simulation, by engineers such as Dennison [26], Mueller [27], Durand [28], Bates [29], Bauerfeind [30], etc. Dennison and Mueller established their models for control purposes but paid less attention to representing the thermodynamic behaviour of engine systems. Durand’s simulation of a one-spool turbojet engine exhibited a good match between the simulation results and experimental tests. Bates and Bauerfeind both carried out their research on two-spool turbofan engines. In Bates’ work, engine simulation was fulfilled on two numerical platforms based on FORTRAN and MIMIC. The comparison showed that the FORTRAN program was running much faster than

the MIMIC program. In Bauerfeind's research, the heat soakage effect on an engine system was introduced throughout the simulation.

In the early 1970s, Fawke and Saravanamuttoo [31-32] compared the relative advantages of engine simulation on both analogue and digital computers. At the same time, Fawke and Saravanamuttoo [33] first introduced the ICV method and summarized both the two aforementioned simulation methods: i.e. the iterative method (or *MFC* method) and the ICV method, on digital computer simulations. The iterative method assumes the working fluid air/gas continuity through the whole system and the entire operating time. This requires some parameters which values are guessed such as compressor pressure ratio and non-dimensional turbine flow, plus a series of iteration cycles to force the engine to directly jump from one operating point to another. [34] In the ICV method, assumed volumes are added between adjacent components to store or release extra air produced by the imbalance of mass flow rates between two components appertaining to the volume. A transient engine model developed by using this method can estimate the system's dynamic behaviour during each required individual short period throughout the entire transient process.

To a specific engine study, computing time by using either of these two methods is almost the same except for the large inertia of a high bypass turbofan's low pressure shaft which largely increases the calculation time of the ICV method.[35] Unlike the *MFC* method, which only simulates engine dynamic behaviour due to shaft rotational speed changes affected by the variation of the injected fuel flow rate, the ICV method provides a more accurate description of transient processes by considering the air/gas compression phenomenon between the connecting components inside the system. However, both methods are proved to be accurate in some applications. Li et al pointed out some suitable cases for each method. [36]

Generally, the use of the ICV method was only adding assumed volumes between connecting components like compressor, combustor, turbine and nozzle. However, Seldner et al [37] not only used this method to simulate the whole engine dynamic behaviour but also introduced it into the conjunction

volume calculation between each of the two neighbouring stages of both compressor and turbine to consider the inter-stage gas dynamics. Generally, these inter-stage gas dynamics were ignored by using the traditional component characteristic map simulation method.

With more research being carried out to predict engine dynamic modes, the mismatching between simulation and experimental results invoked the realization of additional issues affecting on engine transient operation. These issues can be summarised as heat storage effect, mass storage effect, combustion inefficiencies effect and heat transfer. Research development about these affecting issues on engine transient behaviour was introduced in Prof. Palidis [24] Doctoral Thesis. In his research, various such issues were analysed, including:

- a) component inefficiencies;
- b) clearance movements including blade tip clearances and seal clearances;
- c) heat transfer effects produced by the component heat capacities and compressor characteristic variations;
- d) engine reheat operation;
- e) degree of mixing in a mixed nozzle configuration;
- f) the pressure effect due to the value of air specific heat value; and
- g) the selection of engine fuel schedule types, etc.

Particular research was focused on the tip clearance variation caused by the heat transfer effect, however, the author also mentioned another issue which was that the axial movements between the rotary and stationary components should be specified in the future work. This research was implemented on the thermal and mechanical model of one simplified stage. Similar research on more specified whole engine model was carried out by Nylor [38].

Researches described above were mostly off-line simulations to investigate engine transient behaviours. However, with the development of digital engine controls, integrated flight-propulsion controls, and engine diagnostic systems, Daniele [39] concluded that real-time engine simulations should be taken to facilitate more advanced control technology development.

Simulations were first carried out successfully on hybrid computers such as Szuch et al [40-41], for two low-bypass, twin spool, augmented turbofan engines TF30-P-3 and F100-PW-100. Both results had proved that the requirements of simulations had been satisfied and that the accuracies were maintained. However, Richard et al [42] pointed out that the difficulty of programming, lack of portability, and high costs were great considerations in restricting the development of this kind of simulation. Another available method is to use simplified process models (or called “piecewise linear models”) by linearizing the non-linear models at some selected operating points. However, as linear models are not accurate enough to describe the non-linear system operation, this type of simulation is not an appropriate method for further application. Richard and Daniele reported an acceptable simulation method at NASA Lewis Centre by using high speed microprocessors and a parallel processing simulation technique. DIGTEM, a digital real time simulation computer program for two spool turbofan engines had been developed based on this method. [43]

Owing to the large enhancement of digital computer capability and maturity of transient performance calculation methods, a variety of digital computer simulation platforms have been developed and reported in the 21st century. Typical examples are NPSS [44-46], C-MAPSS [47-48], GasTurb [49-50], GSP [51], TERTS [52], etc. Users with these platforms can implement both engine steady state and transient simulations and even engine control researches on different engine applications. An object-oriented graphical user interface (*GUI*) of each system is provided to ensure a quick understanding and easy operation of the simulation environment.

Performance evaluation, controls design, engine test direction and analysis, and engine health monitoring are the most important applications of engine mathematical models development. [53] The conventional engine models for performance evaluation can be referred to as Component Level Models (*CLMs*). Most engine models in previous introductions belong to this type. The *CLMs* consist of a number of individual components (like intake, compressor, combustor, turbine and nozzle) and these components are arranged following the

real installation of engine systems. Each component model is represented by a series of aerodynamic and thermodynamic equations, maps, or tables, etc. By giving the values of a number of input parameters, one component will generate one or more output variables to the following components' calculation. With the calculation of engine components one by one and by use of the introduced steady state or transient simulation method, the engine performance will be analysed. In addition to the CLMs, Sun [54] has also summarized other developed engine model types like state variable models, adaptive models, and intelligent models for more advanced engine control and health monitoring technology development.

2.2 Gas Turbine Engine Fuel and Control System Development

2.2.1 Control System Development from Hydro-mechanical System to FADEC System

To ensure the optimum running of a gas turbine engine in given conditions, a control system is required to control a series of actuators installed in the engine system. The increased complexity of engine systems over the past several decades leads to the development of control systems from original hydro-mechanical fuel control systems to modern full authority digital electronic control (FADEC) systems. The usage of fuel flow for engine shaft speed control, developed in the first generation control system, is still the main control strategy in most modern aircraft propulsion systems. [55]

Control systems can be manually or automatically operated to regulate engine behaviour. The first to be developed was a throttle lever, to allow pilots to manually control fuel flow into combustors of Whittle engines in the early 1940s.[56] In 1950s, the effects of flight altitude and speed change, and the variations of air speed, temperature, and density, on engine systems, had been recognized. These inputs had to be adjusted by the pilot manually at first. [57-58] However, manual operations were soon found to be difficult and dangerous and could cause a series of problems like compressor stalling, combustor lean die-out or rich blow-out, turbine over-temperature. [59] In the early stages, control

systems were simple mechanisms consisting of a number of cams and levers and they were developed for specific applications.

In the 1960s, analogue computers were introduced into the hydro-mechanical control systems of Rolls-Royce Conway, Spey, and RB211 engines with five limited trimming control functions including the fuel flow of combustor and augmentor, position of inlet guide vane (*IGV*) and variable stator vane (*VSV*), bleed/cooling valve settings, exhaust nozzle position, and rotor speed feedback. [60] The mechanical part was developed to be a combination of a number of valves, springs, levers, cams, shafts, and seals like the Hamilton Standard JFC-60 till 1970s. [61]

The fuel flow was regulated by a fuel metering unit (*FMU*) and a speed governor which were the main parts of a hydro-mechanical control system. The pressure difference between both ends of the *FMU* was always maintained at an even value and, in that case, the metered fuel flow rate was only proportional to the adjusted opening orifice area inside the *FMU*. This kind of fuel metering method has been inherited by modern applications. The speed governor was initially applied on a steam turbine engine control and employed in jet engines by changing its material composition and miniaturizing the sizes. The centrifugal force of rotating two bob weights which are the main parts of the speed governor controls the cam displacement through a combination of springs and levers to detect the engine shaft speed and adjust the pressure difference of the *FMU*. According to the detected rotational speed, the required engine fuel flow rate can be automatically measured and injected into combustion chamber.

Notwithstanding that the hydro-mechanical control systems had reached a high level of sophistication and reliability by the 1970s, the higher requirements for engine system development like high thrust engines, high bypass-ratio engines, or over-boost and over-temperature avoidance made the engineers realize the shortcomings of hydro-mechanical control systems. In addition, the high weight, large volumes, difficult operation, and high cost of maintenance were also compelling reasons to force engineers to find a better solution for the coming

problems. Digital electronic devices such as microprocessors, therefore, were utilised to design the new generation of engine control systems. [62]

In the early 1970s, high level regulatory functions were introduced into the American engines owing to the newly-designed digital electronic control units (*ECUs*) such as the Digital Electronic Engine Control (*DEEC*) unit for P&W F100 engine. The purpose of its regulatory function is to calculate speed or temperature set-points and provide sole control responsibilities for some non-critical controlled variables.[20] In the early 1980s, a first flight investigation of DEEC system on an F100 engine in a F15 military aircraft was carried out by NASA cooperating with U.S. Air Force and Pratt & Whitney. [63] The success of system tests resulted in the full production of F100 DEEC units before the end of the program.[64] The application of DEEC unit on jet engine control was a milestone, representing the transition of engine control systems from traditional hydro-mechanical types to digital control. However, because of the high reliability of hydro-mechanical control system, this type of control system has not been discarded but installed on the propulsion system with a smaller size to be a “backup” safe guarantee.

Full authority digital electronic control (*FADEC*) system is a further improvement of digital electronic control units. “Full Authority” which in an ECU is considered to be its ability to control an entire engine operation from start-up to shutdown according to the pilot’s throttle command. [20] It was first applied as a single channel FADEC system but then changed to its modern appearance as a dual channel FADEC system to improve the system redundancy and reliability. Joby [65] mentioned that the first civil twin-channel FADEC system flight test was carried out on Rolls-Royce Olympus engine in 1976. In Link et al [20] report, the first dual-channel FADEC flight test on a military engine deployed F100 DEEC system.

In the 1990s, Pratt & Whitney developed a FADEC system which eliminated the back-up hydro-mechanical control system, since it was proved to provide enough redundancy and reliability. [60] The FADEC system has been chosen to be the only control system for air propulsion engines since that phase. Except for the control functions on regulating engine operation at maximum efficiency for which

control systems had been designed, more test functions were attempted to be integrated into FADEC systems such as: a) the embedded mathematical engine models to improve engine performance and diagnostic ability; b) the usage and life tracking algorithms, and c) the improvement of microprocessor speeds and memory technologies. Accessory actuation systems governed by the FADEC displayed a great improvement by accepting more electro-mechanical components. New sensors were developed and applied especially for engine health management. [20]

In the last ten years, advanced electrical technology and new mathematical control algorithms have been developed and are being used to achieve better hardware and software for FADEC systems. Typical examples are multi-variable control systems, intelligent control systems, and distributed engine control systems. Control system for only one parameter control like speed control is named as “single input single output” (S/SO) system. However, the requirements of more control signals and higher performance and functionality for more complex engines promotes the development of “multi-input multi-output” (MIMO) control systems for multi-variables control tasks. FADEC system provides the availability for multivariable control of engine systems. Successful applications of MIMO system developed by the industry were F414-GE-400 and F135 engines’ FADEC systems.[66]

Intelligent engine control (*IEC*) systems and distributed engine control (*DEC*) systems are still in research, performing through lab tests but not in practice. The concept of aircraft intelligent engine control was taken from aerospace reusable propulsion engines to increase their reliability, durability, and maintainability. Those in designed rocket control systems integrated a variety of control and diagnostic functions including: life extending control; adaptive control; real-time engine diagnostics and prognostics; component condition monitoring; real-time identification, and sensors/actuators fault tolerances. [67] Owing to the development of aero-propulsion FADEC systems, the benefits brought to rocket engines were recognized and absorbed by the researchers and engineers to further improve the capability of FADEC systems.

The main feature of IEC systems is the integration of mathematical engine models into the digital computers inside FADEC to represent the real engine behaviour. With the feature, to describe engine operation mathematically, the control and diagnostic functions mentioned on rocket IEC systems can be all achieved to improve engine performance such as reducing the maintained safety margins on traditional sensor-based control system and providing some indirect measured variable control methods such as thrust or surge margin control.

The DEC system is also a research hotspot of the aircraft propulsion industry currently. The traditional used control system is always centralized architecture (Fig. 2.1(a)) which means that there exists only one FADEC system as a brain to control other parts of the propulsion system like FMU, VSV, VBV, etc. However, just as the name says, the centralized architecture has been attempted to be changed as a distributed architecture described in Fig. 2.1(b). The integrated FADEC system has been replaced by a number of “smart nodes” receiving digital data from the controller through a robust data bus and controlling each specific actuator by themselves. Great benefits are brought by using these DEC systems described in Ref. 68 including increased engine performance, mission success improvement and life cycle cost reduction.

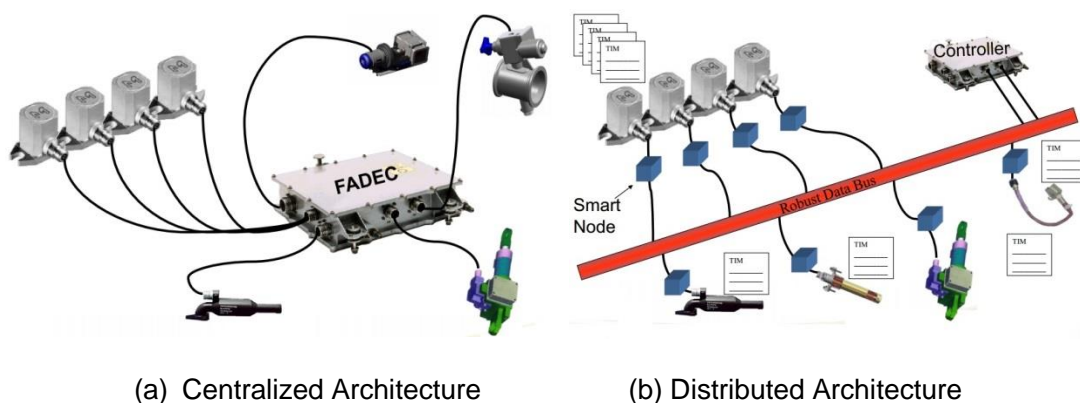


Figure 2.1 Schematics of traditional centralized architecture and distributed architecture of engine control system [68]

2.2.2 Simulation Methods for Engine Control and Fuel System

2.2.2.1 Engine Control and Fuel System Description

Control systems can be mainly divided into two categories including open-loop (or feed-forward) and closed-loop (or feedback) systems, represented in Fig. 2.2.[2] Generally, open-loop control is faster than closed-loop control, however, this type of control has to follow a prescribed schedule and control accuracy cannot be guaranteed. In contrast, as closed-loop control is based on the modification of error between desired output response from the command and measured actual output value from the engine system, this control type is more accurate and widely accepted to control gas turbine engines.

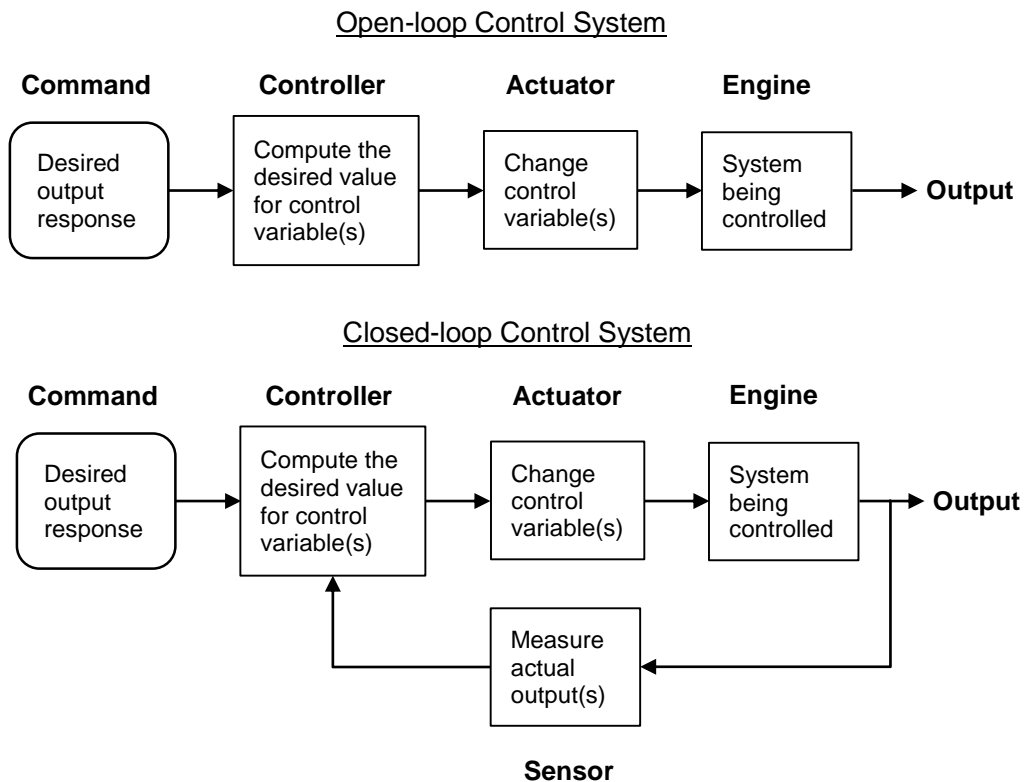


Figure 2.2 Block Diagrams of Open-loop and Closed-loop Control Systems [2]

An Engine, a controller, actuators, and sensors are four basic elements needed to construct a gas turbine engine control system. An engine controller for the gas

turbine system can be compared to the brain in human beings. It receives command orders to recognize operators' requirements; processes sensors' monitored data to observe the current situation of the engine system; determines the proper control orders from the embedded control algorithms and control laws; and governs actuators with these orders to regulate engine's next step operation. In advanced control applications, engine embedded numerical models and measured health data for diagnostics and prognostics are all stored in the controllers.

Actuators are devices which execute orders from the controller to control engine system operations. According to the roles which actuators play on engine system control, they can be mainly divided into three categories: fuel control actuators (e.g. fuel metering valves); position control actuators (e.g. VSVs, VGVs, and thrust vectoring of military engines); and air/gas flow actuators (e.g. air bleed valves). In addition, actuators can also be distinguished within their working mediums including hydraulic actuators such as load-bearing actuators (or a piston-rod-cylinder) and servo valve actuators, pneumatic actuators such as bellows valves, and electric actuators such as torque motors and stepper motors.

Sensors are used to measure specific properties of engine systems. The measured data values can be taken as the feedback for the control system or used to estimate the health of engine systems. According to their functions, the applied sensors can be divided into five categories including gas path sensors, vibration sensors, oil and debris sensors, actuator feedback sensors, and damage sensors. [2]

An engine fuel system meters the required fuel flow rates for engine combustors and afterburners. It is a combination of a FMU and a number of accessory fuel flow delivery components such as pumps, valves and filters. A typical FMU consists of a fuel metering valve and a control mechanism combination to adjust the metering valve opening position. This control mechanism can be designed to be of different types according to the selection of the fuel metering valve. A rack and pinion mechanism driven by a stepper motor is designed to adjust the position of a needle valve for fuel metering. A linear variable differential

transformer (*LVDT*) combined with an electrohydraulic servo valve will alternatively be applied to control the movement of a load-bearing type actuator to meter fuel flow rate. [69]

The two mentioned types of FMUs are designed based on the principle that the fuel flow rate is the function of both the valve opening area and the pressure difference between the inlet and outlet ports of the valve. If the pressure difference is kept constant, the metered fuel flow rate is proportional to the orifice opening area. In addition to this basic fuel metering principle, Rowen [70] has illustrated another type of FMU by adjusting the excess fuel given by the fuel pump to achieve the fuel metering task. In this FMU, a bypass valve driven by two LVDTs and a servo valve is allocated to recirculate the excess fuel back to the inlet of the pump.

2.2.2.2 Simulation Methods of Control System

Simulation of control and fuel systems can be classified as digital simulation, semi-physical simulation, or physical simulation. Due to the expense, difficulty of modification, and long-term testing, semi-physical and physical simulations are mostly used by the industry to test their products' stability and reliability because they use real components and can fully represent system behaviour in the experiments. On the contrary, simulations based on digital computer can be much cheaper and more easily modified. The mathematical representations of system models and operating states provide researchers with a direct and easier understanding. In this section, only the developed digital method for control and fuel system simulation will be introduced.

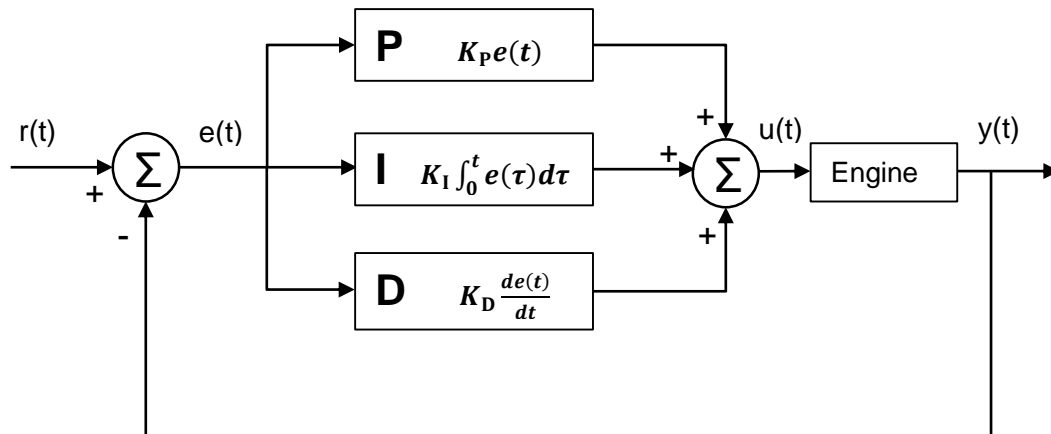


Figure 2.3 Block Diagram of a PID Controller

Proportional-Integral-Derivative (*PID*) control is by far the only accepted control algorithm applied to control real engine operation and the most commonly used method on controller simulation. A developed controller based on this method is called a PID controller (see Fig. 2.3). It aims to minimize the error $e(t)$ between setpoint $r(t)$ and engine output $y(t)$ through three prescribed actions: proportional (*P*), integral (*I*), and derivative (*D*) actions to be the input for engine adjustment.

According to the mathematical expression shown in Fig. 2.3, output of proportional (*P*) action is simply proportional to the control error. This action can quickly eliminate the error but will produce a system residual error between the system output and control set-point. The function of integral (*I*) action is to accumulate the instantaneous error and offset the oscillations or the system residual error. The derivative control action aims to speed up the system response and improves the system stability by predicting the error change rate. However, this action cannot eliminate the system residual error. This action is mainly used in the systems which have an obvious time lag to the disturbance of control variables. For most industry applications which have no obvious time lag effect to the control variables, only PI instead of PID has been applied. A mathematical version of PID controller is described in Eq. 2-1. [71]

$$u(t) = K_c \left[e(t) + \frac{1}{T_i} \int_0^t e(\tau) d\tau + T_d \frac{de(t)}{dt} \right] \quad (2-1)$$

As shown in Eq. 2-1, controller gain K_c , integral time T_i , and derivative time T_d are three corresponding adjustable parameters to a PID controller. [72] Tuning of these parameters to find their optimum values for the desired control response is very difficult. Several methods like Ziegler and Nichols' tuning method [73] or IMC tuning method [74] have been developed and applied on control parameters' tuning. Manual tuning is the simplest of these methods. A great advantage of this method is that it does not need any mathematical correlation of these three parameters' relationships on different controlled system applications but only settles the value of each parameter and observe the system behaviour. However, better tuning with this method requires vast experience and costs a lot of time.

With the development of modern control theory, more advanced control methods have been applied to achieve better performance and add more functions to the engine control systems. Linear quadratic regulator (*LQR*) is a time-domain method which has been applied on aero-engine multivariable control (*MVC*) method development to account for multi-loop interactions and to optimize engine performance since the 1970s. [75] *LQR* is taken to derive the optimal control law of a linear dynamic system at minimum cost described by a quadratic function. The solution process of this method on a general time-varying linear system is described in Ref. 76. In the F100 Multivariable Control Synthesis program developed by Air Force Aero-Propulsion Laboratory (*AFAPL*) and NASA Lewis Centre, *LQR* was applied to design and test a practical multivariable control of an F100 engine based on a hybrid simulation. [77]

The Inverse Nyquist Array (*INA*) method is a frequency-domain method also used for *MVC* of aero-engines. Frequency domain methods are very popular in the control design because they are not sensitive to the model order and modelling error. However, as computers always process calculations in the time-domain, these frequency methods are not widely applied until some professional programs such as MATLAB based programs have been developed for the simulation. Traditionally used frequency domain methods such as root locus and

Bode plot are not appropriate in the MVC design because MVC requires transfer functions to synthesize the controller. INA was first developed by Rosenbrock [78] for the multivariable control systems design application using inverse transfer function matrix. It aims to achieve an approximate decoupled dynamic system by using matrix transformation to allow those classical control methods applied on each of the engine transfer functions. [2] McMarron [79] used this method on a new low-order multivariable controller development of a 4th-order linearized aero-engine model.

H_∞ control is also a frequency domain method in the optimization theory to mitigate the effect of parameter uncertainty and stabilize the control system.[80] It seeks to maintain the influence of exogenous inputs on a designer-defined performance output below a prescribed value. [81] The strength of the input influence is measured by infinity-norm. In the CMAPSS-40k program, Richter [81] illustrated the H_∞ synthesis method used to obtain the control gains of a two-spool turbofan engine to control the fan speed. Similarly, based on a CMAPSS-40k two-spool turbofan engine model, Kolmanovsky et al [82] established an H_∞ controller to track three set-point commands including engine pressure ratio (*EPR*), *VSV*, *VBV* with three control inputs: the fuel flow rate, commanded *VSV* and *VBV* positions.

A suitable controller designed to control a system requires an accurate model established to represent the system behaviour. However, in some complex systems such as aero-engines, mathematical descriptions of system models cannot accurately be easily achieved. Fuzzy set theory proposed by Zadeh [83,84] found that using linguistic variables and fuzzy algorithms could provide an effective and more accurate description of such complex systems. By using this theory, a fuzzy logic controller is designed and has been used on a variety of applications such as a steam-engine boiler combination, a communication satellite, a servomotor and an aircraft flight control. [85] Balakrishnan et al [85] have reported a fuzzy computing algorithm developed to control a single spool turbojet fuel flow rate based on the prescribed TET data logic. To further improve the fuzzy control strategy, Balakrishnan et al [86] reported a rule-based fuzzy

logic controller designed to control a two-spool turbofan engine under development.

2.2.2.3 Simulation Methods of Fuel System

Previous simulations of engine fuel system mostly focused on the delay effect of fuel metering actions on engine dynamic behaviour. In this case, typically, a used fuel metering valve (actuator) was treated as a first order lag but other accessory components were omitted. [2] Owing to the development of professional digital simulation environments, fuel systems' traditional physical simulations based on real components are allowed to be replaced by numerical simulations with mathematical component models. A typical example of such a simulation environment is AMESim.

AMESim is a one-dimensional lumped time domain platform developed for engineering systems simulation. It is made up of many sets of standard pictorial symbols integrated into different libraries including mechanical, control, hydraulic, pneumatic and thermal libraries. Simulation of researched systems first builds the sketch of system models by adding those selected icons to a drawing area. The icons are integrated with the mathematical descriptions of system components. Components' designed features and parameters can be set by clicking the icons. After the system model has been established and parameters are set, a simulation running is initiated. To test the accuracy of model establishment and operational behaviour of simulated models, graphs are plotted to interpret the results. Wang et al [87] has used this simulation platform to establish a servo valve-controlled FMU model (Fig. 2.4) to investigate the temperature fluctuation effect on FMU operation. The simulation results are compared with testing experiments and a good level of correlation between numerical simulation and experiment results has been presented.

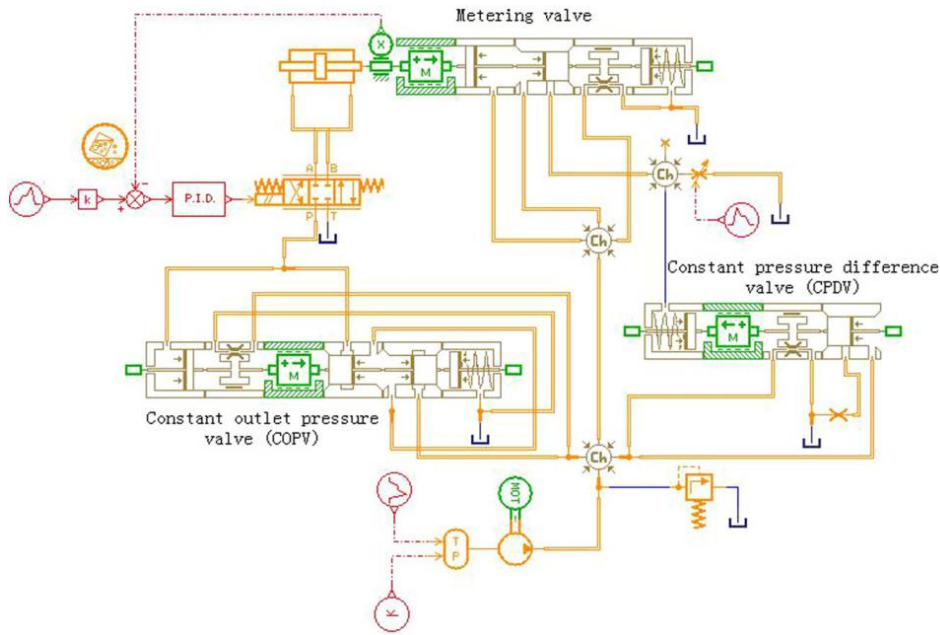


Figure 2.4 Block Diagram of a FMU Model in AMESim [87]

As shown in Fig. 2.4, component models of a FMU such as metering valve, constant pressure difference valve (*CPDV*) and constant outlet pressure valve (*COPV*) are built with a set of mechanical sub-components to represent detailed structures of each component. A PID controller receives commands to regulate the metering valve orifice opening through an electrohydraulic servo valve. Steady state and dynamic behaviours of FMU are simulated based on the numerical calculation of each subcomponent.

2.2.3 Engine Control Laws

Previous sections have illustrated a variety of methods developed to build numerical models of engines and their control and fuel systems. In addition to the establishment of each individual system, a control strategy is required to be a connecting bridge to ensure the cooperation of all three systems. Engine control law is such a strategy which is the relationship between the control variable such as fuel flow rate and measured engine parameters. In the controller, the sensor measured current state engine parameter (e.g. engine pressure ratio, or shaft speed) value is compared with the transferred parameter required value from the

cockpit power level angle (*PLA*) command. The difference between the command and engine current status is used to decide the required fuel flow rate ordered into the engine combustor from those prescribed control laws. The controller then transfers this fuel flow rate order into the opening movement order of the metering valve of FMU. The operation of FMU components will meter the proper fuel flow rate and inject it into the engine system. By using the new incoming fuel flow rate, engine system will be adjusted, thus reaching another new state.

According to the engine operation conditions, control laws can be mainly divided into two categories including set-point and transient control law. The set point control (or steady state control) is to regulate the engine performance close to a desired operating condition through the control of engine speed or pressure ratio. Although most of engine manoeuvres are in a steady state operation, the control law design for this phase only accounts for one quarter of total engine control law design tasks.

Different from engine steady state control, which keeps maintaining a fixed power or thrust production, engine transient control is always aiming to vary the engine operation covering the speed range of different steady state points but not exceeding its physical limitations. Therefore, most control law design and development effort is required on the transient control. Some typical engine limits include: maximum shaft speed, maximum TET, maximum burner pressure, compressor and fan stall (or surge). The transient control law design is mainly to establish a series of control strategies between the control variable fuel flow rate and the measured command variables in order to fulfil the required manoeuvre.

A commonly used control strategy is to plot the fuel flow (or fuel ratio unit) versus engine shaft speed, as shown in Fig. 2.5 below. A large transient operation from the engine idle power to the maximum power is shown in the envelope. It should be noted that if the large transient operation can be fulfilled safely by the control system, a small transient operation within the safe operating region can be achieved without worrying about the excess of engine limits.

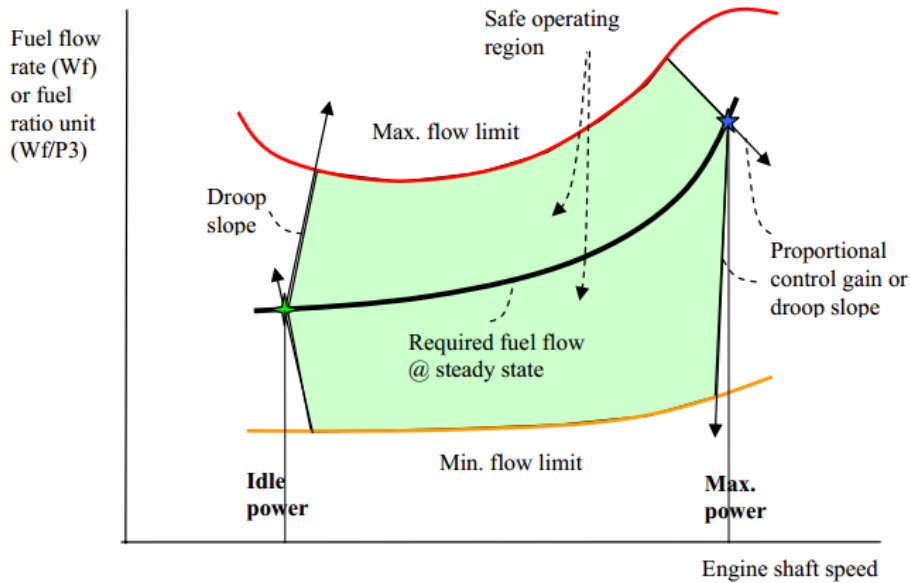


Figure 2.5 Fuel Control Schedule Fuel Flow Rate versus Engine Shaft Speed [20]

Two different control variables, i.e. the fuel flow rate or fuel ratio unit can be used in this control law establishment. Fuel ratio unit ($RU \equiv W_{ff}/P_3$) is widely used especially in traditional hydro-mechanical control units. Jaw et al [2] listed the benefits of the utilization of fuel ratio unit instead of fuel flow rate. If the inlet air conditions are maintained during the transient, the fuel-air-ratio can be directly obtained as it is proportional to the fuel ratio unit. Thus, the turbine entry temperature can be directly obtained from the fuel ratio unit. As P_3 is the compressor exit pressure, when the compressor suffers surge, it provides a self-recovery feature. In addition, the control law is also simplified due to the reduction of control gain constants. In the modern electronic controller, this control method is taken as a back-up of the N-dot type control.

N-dot control strategies are widely applied in the turbofan and turbojet engine control. This control method uses the rotor acceleration rate (\dot{N}) as the feedback command variable. As no two existing manufactured engines are identical, due to their manufactured variations, ages, and deteriorations, an optimal control law fitted to one engine cannot provide the same operational behaviour in another engine. However, by using this method, consistent transient performance can be obtained for a given operating condition without worrying about the engine

differences since the acceleration rates of different shafts can be kept the same. This is favourable particularly to the control of twin-engine aircraft. Because the rotor acceleration is directly measured, the transient response of the controller is much faster than other command variable based controllers. In addition, by using the N_{dot} control, higher-gain control laws are allowed due to the high stability of the control loop. [2]

Although the N-dot control has many advantages and been widely applied in the modern engine controller establishment, some limitations of this control schedule should be noticed. The tendency to catastrophic engine situations like stall, surge, or flame out is the most serious limitation of N-dot control. Therefore, limit acceleration and deceleration protection schedules are also introduced if choosing this control strategy. Fig. 2.6 shows the diagram of the limit protection concept of a N_{dot} controller.

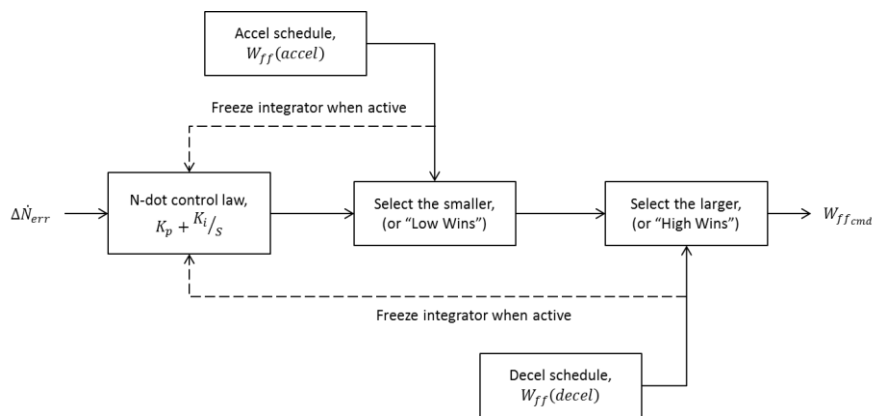


Figure 2.6 Limit Protection of Accel and Decel Schedules on \dot{N} Controller [28]

As shown in Fig. 2.6 above, two limit protection bricks (“Low-Wins” and “High-Wins”) are allocated to regulate the required fuel supply. “Low-Wins” (select the smaller control variable value) works for the engine acceleration and “High-Wins” (select the larger control variable value) works for the engine deceleration. The “Accel schedule” and “Decel schedule” are the prescribed optimal fuel schedules. \dot{N}_{err} (Speed Error) given to the “N-dot control law” brick is used to decide how much fuel should be supplied by the fuel system. However, due to the engine

restriction, the calculated fuel flow from \dot{N}_{err} has to be compared with the optimal fuel supply from the prescribed schedules. For example, in the engine acceleration, if the required engine fuel supply calculated from the N_{dot} error is larger than the prescribed maximum fuel flow rate, the actual fuel quantity will be decided by the “Accel Schedules” which is the smaller of the two compared values.

Thrust management is another type of engine control mode. As the thrust produced by the aero-propulsion system is the function of the shaft speed and the engine pressure ratio, this kind of fuel schedule measures these two parameters to control the engine thrust. Taking a two shaft turbofan engine as an example, fan speed and the overall pressure ratio which is the ratio between compression process inlet and the outlet are handled. As the thrust is proportional to the air flow through the engine, these two parameters can directly measure the engine thrust since they both affect the quantity of air flow.

The idea of thrust control is to establish the linear relationship between the throttle position and thrust. Thus, if this relationship can be implemented by the controller, the pilot can alter the throttle position to find the required thrust settings within the flight envelope. Spang et al [88] has listed the typical required thrust settings including take-off thrust, maximum continuous thrust, maximum climb rating, flight idle, and ground idle.

A new method called Model-based control mentioned in section 2.2.1 is another way to control the engine thrust. From the thrust control point of view, unlike the previously mentioned thrust control method to establish a check-up table containing all the throttle position versus demanded shaft speed or engine overall pressure ratio, the new system is designed to be more intelligent as the controller can offer the required thrust at any point within the flight envelope. In the new controller, a real time, numerical, simulated, on-board engine model is running to represent the physical engine operation behaviour. As this model is running in the computer, all the required parameters like thrust and compressor surge margins can be directly calculated and predicted. With these calculated control variables, the engine operation can be easily regulated.

The three, previously indicated engine control types are mainly fulfilled by a single closed fuel control loop. These SISO control loops are adequate to meet the control requirements of most commercial aircraft engines. However, traditional SISO approach is not suitable to the control of military engines when the after-burner is working. As a result of the after-burner working to add more thrust through engine take-off, climb or acceleration from subsonic to supersonic, both the combustion at main combustor and after-burner will affect the thermal variation at each engine state position. The interaction between these simultaneously occurring combustions leads to the ambiguity of fuel injection at each injector. Therefore, a multivariable approach (also called MIMO multi-input/multi-output approach) is introduced to allow two control loops established with approximately the same response time. Another application using MIMO control is the variable cycle engine (VCE) which has a variable area bypass injector (VABI) to vary the engine behaviour between turbojet and turbofan type.

Multivariable control (MVC) is based on an optimization approach which achieves a closed-loop control design that maximizes (or minimizes) an objective function of key performance indices of the engine. [2] The research of this approach application is based on the linear engine models valid for small signal analysis and avoid the limit protection problem. For most engine operating regimes, a 3×3 controller shown in table 2-1 is taken and a 2×2 controller is used for low power settings when the IGVs are fully closed. Moreover, the controller may expand to a 4×4 controller during the transition and hover to regulate the ejector and ventral thrust using the ejector and ventral area actuators. [88]

Table 2-1 Sensors and Actuators of Multivariable Engine Controller [88]

Sensors	Actuators
Fan Speed or Engine Pressure Ratio	Fuel Flow
Compressor Speed	Inlet Guide Vanes
Bypass Duct Mach Number	A_8 Nozzle Areas

2.2.4 Accessory Components of FMU

2.2.4.1 Pumps

Pumps are playing an essential part in the gas turbine industry. Oil is provided through these components to operate landing gear, control surfaces, flaps, steering mechanisms, and wheel brakes in the aircraft system. From the engine perspective, the pumps are mainly used as fuel pumps, lubricant pumps, and hydraulic pumps.

The working fluid of a fuel pump is fuel oil. This type of pump is used to provide oil for combustion in the combustor and afterburner. The lubricant pump can provide lubricating oil to the engine's rotary component such as engine bearings to reduce the friction between contacting surfaces. A hydraulic pump is mainly used to power the actuator to control the engine nozzle or change the angle of variable stator vanes.

Pumps installed in the engine control system are mainly driven by the gas turbine engine. These power driven pumps can be distinguished according to their operating principle as positive displacement pumps and non-positive displacement pumps. Positive displacement pumps can be further classified as fixed displacement pumps or variable displacement pumps. Due to the difference of the pump action, positive displacement pumps can be specified as a gear type pump, a vane type pump or a piston type pump. Non-positive displacement pumps can also be specified such as centrifugal pumps, vapour core pumps, and axial flow pumps. [89]

Generally, non-positive displacement pumps are defined as the devices producing successive flow. The rotary component of the pump forces the fluid from the inlet port to the outlet and transfers the mechanical energy of the component to the kinetic and pressure energy of the fluid. On the contrary, if the discharging period is discontinuous, this kind of pump is referred to as a positive displacement pump. From the amount of output fluid perspective, the fixed displacement pump discharges the same fluid quantity on each cycle, however, in the variable displacement pump, the displacement for each cycle can be varied.

The pressure of the flow out of the pump is produced by the restriction or obstruction at the outlet flow path of the pump. This restriction is normally the work accomplished by the system such as fuel spray at the combustor fuel nozzle or is provided by the lines, fittings, and valves installed in the system. If no restriction is provided, fluid pressure will not be produced.

Engine pump types are selected according to their applications. Piston and gear type pumps are generally applied to supply fuel oil to the combustor and low-thrust afterburner. For the afterburner producing large thrust, centrifugal or vapour core pumps are chosen to pump the required large quantity of fuel oil. Lubrication pumps are also gear type pumps but have lower pressure and quantity compared to the fuel gear pumps. In order to move engine actuators more efficiently, hydraulic pumps have to be piston pumps or gear pumps with low fuel flow but could produce high pressures of hydraulic oil. [89]

2.2.4.2 Valves

Valves are the devices to regulate the quantity, direction, or pressure of working fluid through the system. When a valve is open, the fluid is forced to flow from the high pressure side of the valve to the low pressure side. The flow quantity is decided by the opening area of the valve. When it is closed, the incoming fluid is blocked. The blocked fluid then has to flow another way or the fluid pressure is increased if no other access can be found. The feature of the valve makes it widely used in multi-domain fields to adjust the system fluid flow quantity or to alter the direction of flow. Unlike the pumps which are only used to pressurize the fuel oil, the installed valves have different purposes.

According to their applications, they can mainly be divided into pressure control valves, quantity control valves, and direction control valves. Typically used pressure control valves are overflow valves, safety valves, sequence valves, reducing valves and pressure regulators. The flow quantity control valves include throttle valves and speed control valves. Reversing valves, check valves, bypass valves, block valves, and pressure regulators, etc. can be used to control the direction of system fluid. In an engine fuel delivery system, the generally used

valves are constant pressure differential valves, constant outlet pressure valve and fuel metering valves. [87]

2.2.4.3 Stepper Motor

Unlike the generally used dc (digital current) or brushless dc motor, a stepper motor is an electromechanical device which converts electrical comment pulses into discrete mechanical movements. [90] The operation of the stepper motor is directly decided by the applied input pulses, for example, the motor shaft rotation direction is decided by the sequence of the pulses, rotation speed is controlled by the pulses' frequency, and rotation length is related to the number of applied pulses.

Ref. 90 has listed the advantages and disadvantages of this device. The feature of this component makes it quite a good choice when the system requires control of the rotation angle, speed, position, and synchronism. In the aircraft fuel metering unit devices, if the fuel supply quantity, which is directly affected by the open area of the orifice is controlled by a needle valve, the stepper motor is introduced to control the position of the needle valve from the pulse order given by the controller.

Stepper motors can be classified according to their motor construction, drive topology, and stepping pattern. [91] Distinguished by their construction, typical stepper motors are variable reluctance (*VR*) stepper motor, permanent magnet (*PM*) stepper motor, and hybrid stepper.

2.2.4.4 Fuel Filter

The oil flowing through the fuel system always contains some contaminations like dust, impurities, and metal particulates produced by the abrading caused by the hydraulic components operation. These impurities will lead to the blockage of the valves, ducts, or some small orifices. Some physical impurities like metal particles can also diminish the lubrication of the relative slip surfaces which reduces the service life of broken components. To ensure the proper function and increase the system components' service life, a fuel filter is necessarily introduced to clean the oil before it flows into the fuel system.

3 Transient Performance Simulation Methodology of Engine and its Fuel and Control System

3.1 Engine Performance Simulation

3.1.1 Engine Design Point Simulation

Engine “Design Point (DP)” is defined as a particular point in the operating range of a gas turbine to design engine components. At this point, the engine is running at a particular speed, pressure ratio and mass flow rate. Generally, this point is selected at sea level ISA condition where relative rotational speed is 1.0, altitude is 0, and Mach number is 0. At this condition, inlet air pressure is 101.325 kPa and temperature is 288.15 °C.

Figs. 3.1 and 3.2 show the diagrams of a typical single-spool turbojet model engine and a turboshaft model engine addressed in this study. The turbojet engine consists of an intake, a compressor, a splitter which extracts an air stream at the compressor outlet for turbine blade cooling, a combustor, a mixer to simulate the thermodynamic cooling effect, a turbine driving the compressor, and a nozzle. In the turboshaft engine, a free turbine driving a propeller is introduced after the gas generator turbine to produce the required power driving the propeller. In both types of engines, the working fluid is assumed to be air in cold sections and gas in hot sections of the model engines.

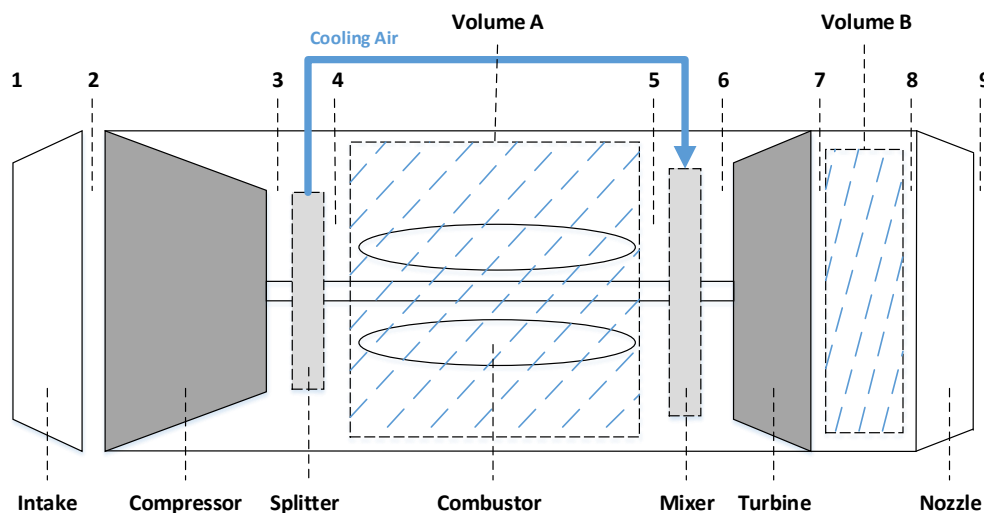


Figure 3.1 Schematic of Single-Spool Turbojet Model Engine Configuration

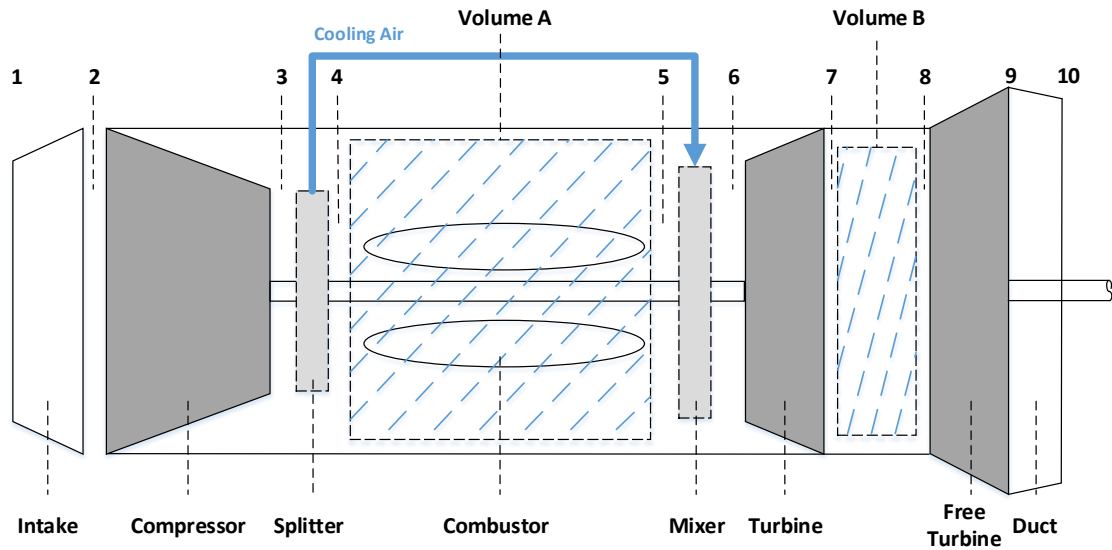
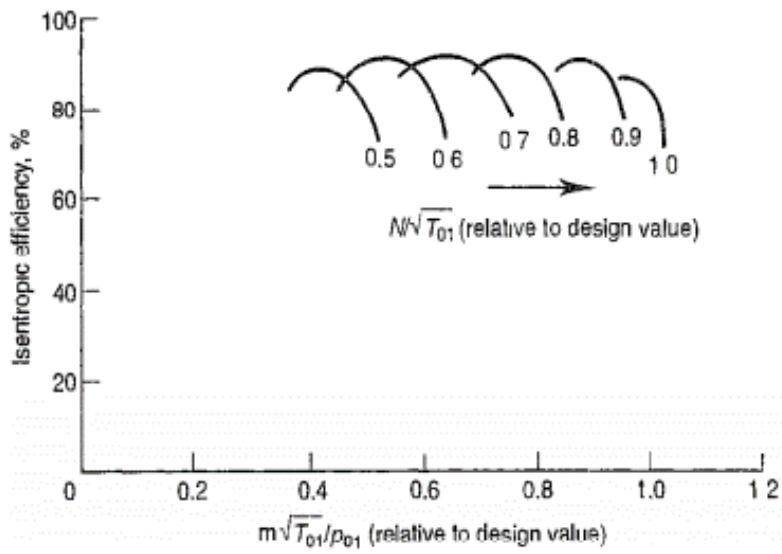


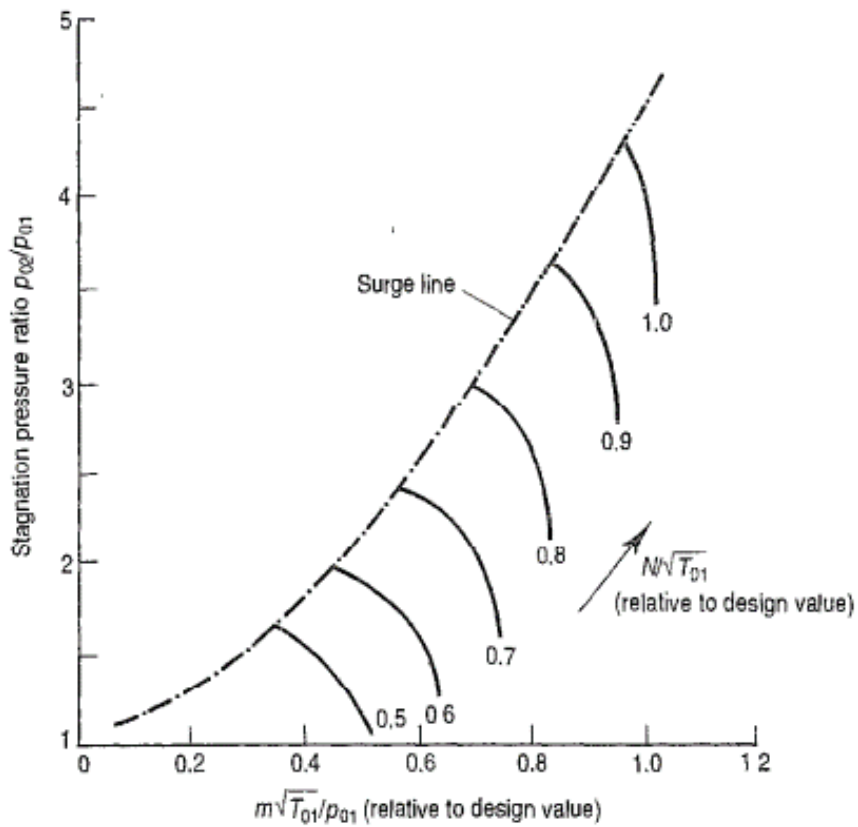
Figure 3.2 Schematic of Two-Spool Turboshaft Model Engine Configuration

DP simulation aims to specify some overall performance parameters' requirements such as thrust and specific heat consumption (*SFC*) on each of the constituent component performance requirements. Components' performances are represented by eight performance and structure parameters including fuel air ration (*FAR*), mass flow rate, static pressure, total pressure, static temperature, total temperature, area, and air speed on both inlet and outlet of the components. For some of the system components, only several parameters' values are required. To obtain these values for each component, inlet mass flow rate, compressor pressure ratio (*PR*), combustor exit temperature, and each component's efficiencies, etc. are required to be first specified.

Characteristic map scaling of turbomachinery (compressor and turbine) is the second task in the design point calculation for the following steady state and transient simulation. For a newly designed engine system under development or on the concept stage, no existing characteristic maps are available to be used. To solve this problem and to provide designers with cogent maps to implement the design, Koening et al introduced the map scaling method to obtain new required maps from existing ones. [15]



(a) Compressor Efficiency Characteristic Map



(b) Compressor Mass Flow Rate Characteristic Map

Figure 3.3 Compressor Characteristic Maps [15]

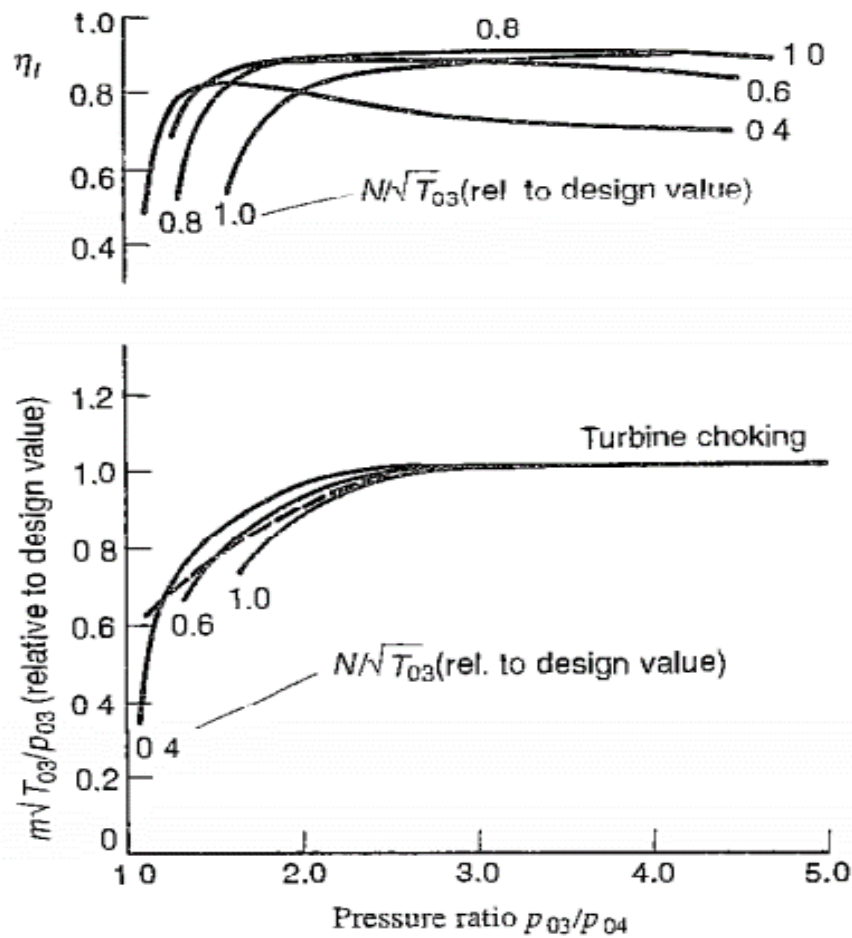


Figure 3.4 Turbine Efficiency and Mass Flow Rate Characteristic Maps [92]

Mass flow rate and efficiency maps are two characteristic maps used for both compressor and turbine simulation. Compressor maps plotted in Fig. 3.3 are represented by four parameters: PCN (shaft relative rotational speed), PR (pressure ratio), NDMF (non-dimensional mass flow), η (isentropic efficiency). Turbine maps in Fig. 3.4 are also represented by four parameters: CNT (corrected rotational speed relative to design point value), PR (pressure ratio) or DH (enthalpy drop ratio), NDMF (non-dimensional mass flow), η (isentropic efficiency).

To scale new characteristic maps, the same working condition should be selected for both the original and the new engine characteristic maps. As the working condition for a newly designed system is chosen at ISA SLS condition and PCN

is 1.0, the eight parameter values for the original maps should be provided based on the same condition. Scaling factors of each compressor and turbine parameters are calculated from Eqs. 3-1 to 3-9.

Compressor:

Pressure Ratio Scaling Factor (*PRSF*)

$$PRSF = \frac{PR_{DP} - 1}{PR_{DP,Map} - 1} \quad (3-1)$$

Non-Dimensional Mass Flow Scaling Factor (*NDMFCSF*)

$$NDMFCSF = \frac{NDMF_{DP}}{NDMF_{DP,Map}} \quad (3-2)$$

Isentropic Efficiency Scaling Factor (*ETACSF*)

$$ETACSF = \frac{\eta_{DP}}{\eta_{DP,Map}} \quad (3-3)$$

Turbine:

Work Function Scaling Factor (*DHSF*)

$$DHSF = \frac{DH_{DP}}{DH_{DP,Map}} \quad (3-4)$$

Non-Dimensional Mass Flow Scaling Factor (*NDMFTSF*)

$$NDMFTSF = \frac{NDMF_{DP}}{NDMF_{DP,Map}} \quad (3-5)$$

Isentropic Efficiency Scaling Factor (*ETATSF*)

$$ETATSF = \frac{\eta_{DP}}{\eta_{DP,Map}} \quad (3-6)$$

Compressor PCN (Eq. 3-7) is considered to be 1.0 at design point condition. Therefore, PCN scaling factor PCNSF is 1.0. Turbine rotational speed CNT (Eq. 3-8) is a corrected speed relative to the design value.

$$PCN = N/N_{DP} \quad (3-7)$$

$$CNT = \frac{N}{\sqrt{T_{in}}} \div \left(\frac{N}{\sqrt{T_{in}}} \right)_{DP} \quad (3-8)$$

To both compressor and turbine installed on the same shaft sharing the same rotational speed, compressor PCN has to be transformed to CNT used on turbine map interpolation. Scaling factor of turbine CNT is given by Eq. 3-9.

Non-dimensional Rotational Speed CNT Scaling Factor (*CNTSF*)

$$CNTSF = \frac{CNT_{DP,Map} \times \sqrt{T_{in,DP}}}{PCN_{DP,Map}} \quad (3-9)$$

3.1.2 Engine Transient Performance Simulation Inter-Component Volume (ICV) Method

Engine transient performance simulation is used to investigate the engine dynamic behaviour from one steady state condition to another, such as that during the acceleration or deceleration processes. The simulation of this process has to be divided into two steps: first is the starting steady state point calculation and second is to calculate those following transient points. Both these calculations use the same ICV method but follow different fuel schedules.

Steady state points (also including design point) are the points where not only the continuation of energy, mass and momentum is satisfied but also where equilibrium of work, mass flow, and heat transfer within an engine system is kept. Before the simulation environment recognises transient starting order, only the engine system has been “established” from design point but is not “running” at specified starting steady state point. Therefore, the engine model has first to reach its aimed starting steady state point before the transient simulation is processed.

After the simulation is starting, the current engine situation is determined by the design point and the system is in equilibrium. To break this balance for ICV method simulation, a fuel flow rate relating to the desired steady state point is

provided. This given fuel flow rate will result in a power imbalance between compressor and turbine power on the same shaft. As a result, shaft rotational speed will be altered. The fuel schedule through this process is to keep the given fuel flow rate constant. Over a period of calculation using transient ICV method (introduced below), the model engine will realign to its new balance situation and its performance parameters and rotational speed will remain at specific steady state values relating to the given fuel flow rate.

Transient simulation still retains the continuation of energy, mass and momentum but breaks the equilibriums of work, mass flow, and heat transfer within the engine system, which is different from that at the steady state engine operating conditions. Two different transient performance simulation methods are available, one is the Mass Flow Continuity (*MFC*) method [25] and the other is the Inter-Component Volume (*ICV*) method [33]. In this study, the ICV method is used to simulate the transient behaviour of gas turbine engines.

ICV method is introduced into engine transient simulation because of the existence of mass flow imbalance between connecting components. The assumed volumes added between adjacent components can absorb this flow mismatch by releasing or storing the extra air flow. As the working fluid keeps flowing through the engine system, it is assumed that the volumes are filled with air during the whole transient process. Therefore, the change of air mass inside the volume will generate a new volume pressure at each calculation time step. Since the work and mass flow equilibriums cannot be kept during transient simulation, the PCN is affected by work imbalance and the volume pressure affected by mass flow mismatch keeps changing until the system reaches a new steady state operating condition. After that, work and mass flow are restored to new equilibriums. The system's situation will not cause any changes of the rotational speed and volume pressure until another transient process is introduced.

Volume position selection is a very important issue when the ICV method is applied. Theoretically, it can be allocated between any two different components installed on the engine system. According to its principle, volume pressure

variation is produced by the mismatch between the mass flow rates entering and exiting the volume. Some of the engine components could calculate air or gas flow rate from these characteristics. To facilitate system simulation, those assumed volumes should be introduced between these components such as compressor, turbine, and nozzle. For example, in the turbojet engine shown in Fig. 3.1, one is between the compressor and the turbine (Volume A) and the other is between the turbine and the nozzle (Volume B).

After the volume positions have been selected, the following three important factors have to be considered in transient performance simulation processes using the ICV method.

The first is the imbalance of work between the components on the same shaft. For example, if the work produced by a turbine is more than the work consumed by a compressor, the engine will be driven into an acceleration process based on the rotordynamic equation represented by Eq. 3-10.

$$\frac{dN}{dt} = \frac{3600 SP}{4 \pi^2 I N} \quad (3-10)$$

where N is the shaft rotational speed, I the shaft inertia and SP the surplus power which is the difference between the generated and consumed power.

The second is the consideration of volume dynamics in a volume between adjacent components where the mass flow going into the volume may be different from that going out of the volume causing accumulation or dispersion of mass in the volume. As the temperature variation within a gas turbine engine is mainly caused by the compression, expansion or combustor in key gas path components, the minor temperature variation in inter-component volumes may be ignored. Therefore, by assuming a constant temperature in the inter-component volumes during a tiny calculation time step [33, 93], the volume dynamics may be represented by Eq. 3-11 where the change of volume pressure is mainly affected by the change of volume storage mass based on the perfect gas state equation. [33, 94]

$$dP = \frac{R T}{V} dm \quad (3-11)$$

where P is the volume pressure, T the volume temperature, V the volume, m the air mass and R the universal gas constant.

The third factor is the fuel schedule provided by fuel control and fuel delivery systems. This will be discussed in more details in section 3.2.

3.1.3 Engine Components Calculation

Intake:

The purpose of the engine intake is to transform the inlet freestream flow conditions into the required air conditions at the entrance to the engine fan or compressor. [95] In the gas turbine performance simulation, this component is assumed to be a duct which only considers the pressure recovery of the intake outlet pressure. Total temperature at the intake outlet is assumed to be equal to the inlet air temperature. The input and output parameters and main calculation equations for this component are listed below.

Input:

Ma	Flight Mach Number
p_A	Inlet Static Pressure
t_A	Inlet Static Temperature
W_B	Outlet Mass Flow Rate
ε	Intake Pressure Recovery Coefficient

Output:

P_A	Inlet Total Pressure
P_B	Outlet Total Pressure
T_A	Inlet Total Temperature

T_B	Outlet Total Temperature
V_{SA}	Flight Speed
W_A	Inlet Mass Flow Rate

Inlet air static pressure and temperature are equal to the ambient condition air pressure and temperature. At design point at ISA SLS condition, ambient pressure is 101.325 kPa and ambient temperature is 288.15 K. In the transient process, the new ambient condition corrected by the flight condition (like Altitude 1000 m, Mach 0.5) can be calculated from Eqs. 3-12 to 3-17.

Sea Level to 11000m: [18]

$$P_{amb} = 101.325 \times \left(\frac{288.15}{T_{amb}} \right)^{-5.2588} \quad (3-12)$$

$$T_{amb} = 288.15 - 0.0065 \times Alt \quad (3-13)$$

11000 m to 24994m:

$$P_{amb} = 22.63253 / e^{0.000157689 \times (Alt - 10998.1)} \quad (3-14)$$

$$T_{amb} = 216.65 \quad (3-15)$$

24994m to 30000m:

$$P_{amb} = 2.5237 * (216.65 / T_{amb})^{11.8} \quad (3-16)$$

$$T_{amb} = 216.65 + 0.0029892 * (Alt - 24994) \quad (3-17)$$

where Alt is aircraft flight altitude.

Inlet air total pressure and temperature are given from formulae 3-18 and 3-19 by knowing the static pressure $p_A (= P_{amb})$ and temperature $t_A (= T_{amb})$.

$$\frac{P_A}{p_A} = \left(1 + \frac{\gamma - 1}{2} \times Ma^2 \right)^{\frac{\gamma}{\gamma - 1}} \quad (3-18)$$

$$\frac{T_A}{t_A} = 1 + \frac{\gamma - 1}{2} \times Ma^2 \quad (3-19)$$

where γ is the ratio of specific heats.

The outlet pressure and temperature are obtained from formulae 3-20 and 3-21.

$$P_B = P_A \times \varepsilon \quad (3-20)$$

$$T_B = T_A \quad (3-21)$$

Here, the pressure recovery coefficient ε can be calculated by using the US military standard.[96]

$$\varepsilon = 1.0 \text{ if } M \leq 1 \quad (3-22)$$

$$\varepsilon = 1.0 - 0.075 \times [(M - 1)^{1.35}] \text{ if } M > 1 \quad (3-23)$$

Air mass flow rate at the intake inlet is equal to the outlet mass flow rate. At design point calculation, the inlet air flow rate is initially specified. In the transient phase, the mass flow rate through the intake is determined by the subsequent compressor flowing capacity. Thus, the inlet and outlet mass flow rate (W_A and W_B) are obtained from the compressor calculation.

The flight speed calculation should first establish the local sonic speed a (Eq. 3-24) and use the flight Mach number and local sonic speed to calculate the value (Eq. 3-26).

$$a = \sqrt{\gamma \times R \times t_A} \quad (3-24)$$

$$Ma = \frac{V_{S_A}}{a} \quad (3-25)$$

$$V_{S_A} = a \times Ma \quad (3-26)$$

Compressor:

The purpose of the compressor is to pressurize the air stream to the required total pressure of the gas turbine cycle. This action is implemented through a set of compressor stage rotations. Each individual stage shares the responsibility to partially increase the air pressure. If the pressure increase provided by the compressor stages on one shaft is not enough, more compressor stages can be

introduced on other shafts to further pressurize the air stream. In the performance simulation, compressor simulation introduces the characteristic map to represent this component operation. Therefore, the multi-compressor stages on the same shaft are integrated into one component. A total pressure ratio which is the product of all the compressor stages pressure ratios on one shaft is used to represent the rise in pressure of the air passing through this component.

Input:

P_A	Inlet Total Pressure
P_B	Outlet Total Pressure
PCN	Shaft Rotational Speed Relative to the Design Point Value
T_A	Inlet Total Temperature

Output:

CW	Compressor Work
T_B	Outlet Total Temperature
W_A	Inlet Mass Flow Rate
W_B	Outlet Mass Flow Rate

In the design point calculation, compressor pressure ratio (PR) is first given to design the system cycle and scale the characteristic maps. In the transient simulation, compressor outlet total pressure is calculated from its concomitant volume. Thus, the pressure ratio of this component is known from Eq. 3-27.

$$PR_{Comp} = P_B/P_A \quad (3-27)$$

For the transient process in the engine flight envelope, corrected values of pressure and temperature (δ & θ) from Eqs. 3-28 and 3-29 are introduced as follows to consider the air flow rate affected by the flight altitude and Mach number.[18]

$$\delta = P_{AMB}/101.325 \times \left(1 + \frac{\gamma - 1}{2} \times Ma^2\right)^{\frac{\gamma}{\gamma - 1}} \quad (3-28)$$

$$\theta = T_{AMB}/288.15 \times \left(1 + \frac{\gamma - 1}{2} \times Ma^2\right) \quad (3-29)$$

According to the definitions of δ and θ from Eqs. 3-28 and 3-29, both these two parameters have to consider the local Mach number effect. However, for the multi-compressors on multi-shaft engines, it is difficult to determine the local Mach number of each compressor. This is because the engine internal structure and local air static temperature are unknown. Therefore, Eqs. 3-30 and 3-31 can be used to redefine δ and θ by introducing the component inlet total pressure and temperature into the definition equations.[18]

$$\delta = P_A/101.325 \quad (3-30)$$

$$\theta = T_A/288.15 \quad (3-31)$$

To interpolate the compressor rotational speed in the compressor, the compressor's real shaft speed has to be corrected from Eq. 3-32 by eliminating the effect of altitude and flight Mach number.

$$CN = N/\sqrt{\theta} \quad (3-32)$$

where, CN is the corrected shaft rotational speed.

The corrected shaft rotational speed relative to design point rotational speed used on compressor map interpolation CNC is represented in Eq. 3-33.

$$CNC = PCN \times \sqrt{\frac{T_{A,DP}}{T_A}} \quad (3-33)$$

With the values of PR and CNC , the non-dimensional mass flow rate ($NDMF_{comp}$) and isentropic efficiency ($\eta_{is_{comp}}$) can be interpolated from the scaled compressor characteristic map shown in Fig. 3.3.

The compressor mass flow rate is then corrected from the interpolated $NDMF_{comp}$.

$$W_{Comp} = NDMF_{Comp} \times \frac{\delta}{\sqrt{\theta}} \quad (3-34)$$

Using PR_{Comp} and the interpolated $\eta_{is_{comp}}$, temperature ratio (TR) can be calculated from formulae 3-35 and 3-36. Compressor outlet total temperature T_B is obtained by knowing TR and T_A .

$$\eta_{is_{comp}} = \frac{h'_B - h_A}{h_B - h_A} = \frac{T'_B - T_A}{T_B - T_A} = \frac{(PR_{Comp})^{\frac{\gamma-1}{\gamma}} - 1}{TR_{Comp} - 1} \quad (3-35)$$

$$TR_{Comp} = 1 + \frac{(PR_{Comp})^{\frac{\gamma-1}{\gamma}} - 1}{\eta_{is_{comp}}} \quad (3-36)$$

$$T_B = T_A \times TR_{Comp} \quad (3-37)$$

Compressor work (CW) is calculated from the enthalpy increase between the inlet and outlet (Eq. 3-38). The value is used to compare with turbine generated work to vary engine rotational speed during transient process.

$$CW = W_{Comp} \times [h(T_B) - h(T_A)] \quad (3-38)$$

Splitter:

Splitter aims to divide the incoming air stream into two flow streams. In the gas turbine engine model, hot devices which are cooling (like combustor and turbine), compressor bleed, bypass duct, or jet pipe will all need to separate a stream of air flow from the main air flow. In the single spool turbojet and two-spool turboshaft engine model shown in Fig. 3.1 and 3.2, this component is taken to separate a stream of the compressed air flow from the compressor outlet for the turbine blade cooling.

Input:

P_A	Splitter Inlet Air Total Pressure
T_A	Splitter Inlet Air Total Temperature

W_A	Splitter Inlet Air Mass Flow Rate
ΔP	Pressure Loss after Separation
ΔW	Mass Flow Rate Loss after Separation
λ_P	Remained Main Air Flow Pressure Coefficient after the Separation
λ_W	Remained Main Air Flow Rate Coefficient after Separation

Output:

P_{B1}	Main Flow Total Pressure through the Core Generator
P_{B2}	Cooling Air Total Pressure
T_{B1}	Main Flow Total Temperature through the Core Generator
T_{B2}	Cooling Air Total Temperature
W_{B1}	Main Flow Air Mass Flow Rate through the Core Generator
W_{B2}	Cooling Air Mass Flow Rate

The coefficients of main air flow rate and pressure (λ_W & λ_P) are defined from formulae 3-39 and 3-40.

$$\lambda_W = \frac{W_{B1}}{W_A} \quad (3-39)$$

$$\lambda_P = \frac{P_{B1}}{P_A} \quad (3-40)$$

The outlet air mass flow rates (W_{B1} & W_{B2}) are then calculated from Eqs. 3-41 and 3-42.

$$W_{B1} = \lambda_W \times W_A - \Delta W \quad (3-41)$$

$$W_{B2} = W_A - W_{B1} \quad (3-42)$$

The same holds true with the main air flow rate calculation from Eq. 3-41, and so the main flow total pressure is given from Eq. 3-43. The split cooling air pressure is equal to this value. (Eq. 3-44)

$$P_{B1} = \lambda_p \times P_A - \Delta P \quad (3-43)$$

$$P_{B2} = P_{B1} \quad (3-44)$$

It is assumed that the flow separation in the splitter is an adiabatic process, thus, no temperature loss has been considered. Both the outlet temperatures (T_{B1} & T_{B2}) are equal to the inlet total temperature.

$$T_{B2} = T_{B1} = T_A \quad (3-45)$$

Combustor:

A combustor is the device which burns the injected fuel to provide enough energy for the exit gas expansion in the turbines. Through the combustion, the fuel oil chemical energy is transformed into component exit gas thermal energy. Fuel burning is assumed to be an isentropic process. Mass and energy conservation laws are adhered to in order to calculate the outlet gas mass flow rate and total temperature. The component outlet total pressure calculation has to consider an actual 5% pressure loss from the inlet air to the exit gas.

Input:

P_A	Inlet Total Pressure
T_A	Inlet Total Temperature
W_A	Inlet Mass Flow Rate
W_{ff}	Fuel Flow Rate
$\Delta \epsilon$	Pressure Loss Coefficient, = 5%
η_{Burn}	Combustion Efficiency

Output:

P_B	Outlet Total Pressure
T_B	Outlet Total Temperature

W_B Outlet Mass Flow Rate

Outlet gas mass flow rate and fuel air ratio (FAR) are calculated from Eqs. 3-46 and 3-47.

$$W_B = W_A + W_{ff} \quad (3-46)$$

$$FAR = \frac{W_{ff}}{W_A} \quad (3-47)$$

Outlet total temperature calculation using the energy conservation law shown in Eq. 3-48.

$$h(T_B) = \frac{h(T_A) + FAR \times (LHV \times \eta_{Burn} + h(T_{ff}))}{1 + FAR} \quad (3-48)$$

where LHV is the low heating value of jet fuel.

Outlet total temperature is:

$$T_B = \frac{h(T_B)}{C_p} \quad (3-49)$$

Outlet total pressure is:

$$P_B = P_A \times (1 - \Delta\varepsilon) \quad (3-50)$$

Mixer:

Mixer is an assumed component which aims to mix the separated cooling air from the compressor outlet with the combustor hot exit gas. On the contrary, with the flow separation process in the splitter, the mixer is combining the two flow streams to be a flow stream passing through the following components. This mixing process is assumed to be an adiabatic process and the mass and enthalpy conservation laws are followed.

Input:

P_{A1} Inlet Total Pressure from the Combustor Exit Gas

T_{A1} Inlet Total Temperature from the Combustor Exit Gas

T_{A2} Inlet Total Temperature of the Separated Cooling Air

W_{A1} Inlet Mass Flow Rate from the Combustor Exit Gas

W_{A2} Inlet Mass Flow Rate of the Separated Cooling Air

Output:

P_B Outlet Total Pressure

T_B Outlet Total Temperature

W_B Outlet Mass Flow Rate

As no mass flow rate loss is considered and the mass conservation law has to be followed, the mixer outlet mass flow rate is given from Eq. 3-51.

$$W_B = W_{A1} + W_{A2} \quad (3-51)$$

By assuming that the mixer is large enough to avoid the two flow streams mixing in this component not be pressurized, the outlet total pressure is equal to the inlet pressure. Compared with the main flow from the combustor exit, the cooling air stream is relatively small. Therefore, it is assumed that the mixer outlet total pressure is equal to the main flow total pressure from the combustor outlet.

$$P_B = P_{A1} \quad (3-52)$$

The outlet total temperature is based on the enthalpy conservation law (Eq. 3-53) and calculated from Eq. 3-49.

$$h(T_B) = h(T_{A1}) + h(T_{A2}) \quad (3-53)$$

Turbine:

The purpose of a turbine is to allow gas expansion to generate required turbine work. The high speed and high pressure and temperature exhaust gas from the combustion chamber flows through the gas path formed by a set of turbine stages. Meanwhile, it drives every turbine stage to rotate. When the gas passes through these stages, the thermal energy of hot gas is mainly converted to mechanical energy within the turbine. This mechanical energy is then utilised to drive the

compressor on the same shaft with the turbine, and to power other accessory components such as fuel pumps. In addition, the electrical power of the aircraft is mainly derived from turbine work. As with the compressor, turbine multi-stages are integrated as one component in the performance simulation. Gas expansion through this component is considered to be an isentropic process. The input and output parameters and main calculation equations of this component are listed below.

Input:

AW	Auxiliary Work Consumed by other Connecting Components
CW	Compressor Work
N_{DP}	Shaft Rotational Speed at Design Point
P_A	Inlet Total Pressure
P_B	Outlet Total Pressure
PCN_i	Previous Step Calculated Shaft Rotational Speed Relative to Design Point Value
T_A	Inlet Total Temperature
Δt	Calculation Time Step
η_i	Previous Step Turbine Isentropic Efficiency
η_m	Mechanical Efficiency

Output:

PCN_{i+1}	Shaft Rotational Speed Relative to the Design Point Value for Next Step Calculation
T_B	Outlet Total Temperature
W_A	Inlet Mass Flow Rate
W_B	Outlet Mass Flow Rate

As with the compressor calculation, turbine PR is first obtained (Eq. 3-27) by knowing the inlet and outlet total pressure. Gas expansion in the turbine is assumed to be an isentropic process. Thus, the turbine isentropic efficiency (η_{isTurb}) is introduced to calculate the turbine temperature ratio (Eqs. 3-54 and 3-55).

$$\eta_{is_{turb}} = \frac{h_A - h_B}{h_A - h'_B} = \frac{T_A - T_B}{T_A - T'_B} = \frac{1 - \frac{T_B}{T_A}}{1 - \left(\frac{P_B}{P_A}\right)^{\frac{\gamma-1}{\gamma}}} \quad (3-54)$$

$$\frac{T_B}{T_A} = 1 - \left[1 - \left(\frac{P_B}{P_A}\right)^{\frac{\gamma-1}{\gamma}} \right] \times \eta_{is_{turb}} \quad (3-55)$$

Here, the isentropic efficiency has to be interpolated from the turbine efficiency map using the work function DH (Eq. 3-45).

$$DH = \frac{\Delta h}{T_A} = \frac{h(T_B) - h(T_A)}{T_A} \quad (3-56)$$

As shown in formula 3-45, DH has to be calculated from the turbine inlet and outlet temperatures. In the engine design point simulation, shaft power balance between compressor and turbine work on the same shaft is maintained. Thus, the turbine outlet temperature can be obtained by knowing the compressor's consumed power. However, in the transient phase, this shaft power balance is broken. In that case, an isentropic efficiency from the previous step calculation is used to first calculate the outlet total temperature. With the value of outlet total temperature, DH is known to interpolate a new efficiency from the turbine map. Through a series of iterations, both the calculations of used efficiency and interpolated efficiency will finally converge into a quite close value which is taken in this step calculation. If the turbine temperature ratio is obtained, then the outlet total temperature can be calculated from Eq. 3-57.

$$T_B = T_A \times TR_{Turb} \quad (3-57)$$

To interpolate turbine characteristic maps, non-dimensional rotational speed CNT is also required. The value of this parameter for interpolation comes from PCN and CNTSF.

$$CNT = \frac{PCN_i \times CNTSF}{\sqrt{T_A}} \quad (3-58)$$

The turbine mass flow rate can be calculated from the non-dimensional mass flow rate (*NDMF*) interpolated from the mass flow characteristic map by using Eq. 3-59.

$$W_{turb} = \frac{NDMF \times P_A}{\sqrt{T_A}} \quad (3-59)$$

In the ICV method transient simulation, as the turbine produced work is not equal to the compressor consumed work, this work imbalance will lead to a speed variation at each time step. This is because the surplus power *SP* (Eq. 3-60) on one shaft produces an imbalance in torque as shown in Eq. 3-61.

$$SP = TW - CW - AW \quad (3-60)$$

$$SP = Q \times \omega = I\alpha \times 2\pi \times \frac{N}{60} = I \times \frac{d\omega}{dt} \times \frac{2\pi \times N}{60} = \frac{4\pi^2 \times I \times N \times dN}{3600 \times dt} \quad (3-61)$$

$$N_i = PCN_i \times N_{DP} \quad (3-62)$$

where *I* is shaft inertia, *N_i* is the previous step shaft real rotational speed.

Thus, the rotational speed increment is derived from Eq. 3-63.

$$\frac{dN}{dt} = \frac{SP \times 3600}{4\pi^2 \times I \times N_i} \quad (3-63)$$

Shaft rotational speed relative to the design point value (*PCN_{i+1}*) for next step calculation is given from Eq. 3-64.

$$PCN_{i+1} = \frac{N_i + \frac{dN}{dt} \times DT}{N_{DP}} \quad (3-64)$$

Nozzle:

Two types of nozzles are used in the aircraft engine system including the convergent nozzle and convergent-divergent nozzle. In this case, only the convergent nozzle is required. Simulation of this component treats it as a duct. Therefore, outlet gas mass flow rate, total pressure, and total temperature are equal to the inlet values.

Input:

A_{DP}	Nozzle Area
P_A	Inlet Total Pressure
T_A	Inlet Total Temperature
$V_{Sflight}$	Flight Speed
W_{ff}	Combustor Injected Fuel Flow Rate

Output:

NT	Net Thrust
p_B	Outlet Static Pressure
P_B	Outlet Total Pressure
SFC	Specific Fuel Consumption
t_B	Outlet Static Temperature
T_B	Outlet Total Temperature
V_{SB}	Outlet Exhaust Gas Velocity
W_A	Inlet Mass Flow Rate
W_B	Outlet Mass Flow Rate

As a constant area component, the flow capacity of this component has a maximum value to restrict the nozzle performance. Through the engine operation, two working conditions may exist which are the choked condition and the un-choked condition. If the nozzle operates under the former condition, pressure and

temperature ratios across the nozzle remain at their critical values. If, however, the nozzle is not choked, exhaust gas will fully expand and outlet static pressure will be equal to the ambient value. [97]

The critical values of the pressure and temperature ratios are calculated from formulae 3-65 and 3-66 by keeping the nozzle outlet Mach number (Ma_B) is 1.0.

$$\left(\frac{P_B}{p_B}\right)_{crit} = \left(1 + \frac{\gamma - 1}{2}\right)^{\frac{\gamma}{\gamma - 1}} \quad (3-65)$$

$$\left(\frac{T_B}{t_B}\right)_{crit} = 1 + \frac{\gamma - 1}{2} \quad (3-66)$$

If the nozzle is choked $\frac{P_B}{P_{amb}} > \left(\frac{P_B}{p_B}\right)_{crit}$, formulae 3-67 to 3-68 are taken to calculate the nozzle outlet static pressure and temperature.

$$p_B = P_B \times \frac{1}{\left(\frac{P_B}{p_B}\right)_{crit}} \quad (3-67)$$

$$\frac{T_B}{t_B} = \left(\frac{P_B}{p_B}\right)^{\frac{\gamma - 1}{\gamma}} \quad (3-68)$$

If the nozzle is unchoked $\frac{P_B}{P_{amb}} < \left(\frac{P_B}{p_B}\right)_{crit}$, formulae 3-68 and 3-69 are used.

$$p_B = P_{amb} \quad (3-69)$$

The nozzle outlet velocity calculation is also different under the choked and unchoked conditions.

To a choked nozzle, the local air speed equation is used because the flow quantity passing through the nozzle is constant.

$$V_{SB} = \sqrt{\gamma \times R \times t_B} \quad (3-70)$$

To an unchoked nozzle, the exhaust gas is assumed fully expanded to the ambient. Thus, the speed (Eq. 3-71) is calculated by considering the heat energy of exhaust gas being transformed into kinetic energy.

$$V_{S_B} = \sqrt{2 \times Cp \times (T_A - t_B)} \quad (3-71)$$

In this simulation, a fixed area nozzle is selected. To calculate the nozzle area, Eq. 3-72 is applied in the design point simulation. In the steady state and transient simulation, this area is kept constant to calculate the gas mass flow rate through the nozzle (Eq. 3-73).

$$A_{DP} = \frac{W_{B,DP} \times R \times t_{B,DP}}{p_{B,DP} \times V_{S_{B,DP}}} \quad (3-72)$$

$$W_B = \frac{A_{DP} \times p_B \times V_{S_B}}{R \times t_B} \quad (3-73)$$

The engine net thrust (NT) is then calculated after all the forementioned parameter values are known. Eq.3-74 is used for choked condition and Eq. 3-75 is used for the unchoked condition.

$$NT = W_A \times (V_{S_B} - V_{S_{flight}}) + A_B \times (p_B - P_{amb}) \quad (3-74)$$

$$NT = W_A \times (V_{S_B} - V_{S_{flight}}) \quad (3-75)$$

Specific fuel consumption is then calculated by knowing the combustor burned fuel flow rate and the generated engine net thrust.

$$SFC = \frac{W_{ff}}{NT} \quad (3-76)$$

Volume:

Volume is an assumed component introduced into the engine transient simulation using the traditional ICV method. During the transient operation, the equilibrium of mass inside the engine system is broken. The purpose of this component is to absorb this mass flow rate mismatch from its connecting components and produce a new volume pressure to finally eliminate the mismatch. The ideal gas equation will be taken for the volume pressure calculation will be taken from the volume air/gas mass storage or release.

Input:

P_i	Volume Pressure at Previous Step
T_A	Volume Inlet Total Temperature at Current Step
T_i	Volume Temperature at Previous Step
V	Volume of the Volume Chamber
W_A	Inlet Mass Flow Rate
W_B	Outlet Mass Flow Rate

Output:

P_A	Volume Inlet Total Pressure
P_B	Volume Outlet Total Pressure
T_B	Volume Outlet Total Temperature

Volume of stored gas has to be first calculated (Eq. 3-77) by following the mass conservation law inside the component. The previous step stored gas M_i is given from Eq. 3-78 by knowing the previous step volume pressure and temperature.

$$M_{i+1} = M_i + W_A - W_B \quad (3-77)$$

$$M_i = \frac{P_i \times V}{R \times T_i} \quad (3-78)$$

The current volume pressure P_{i+1} for next step calculation can be obtained from the ideal equation (Eq. 3-79). P_{i+1} is taken as the inlet and outlet total pressure provided for the connecting components calculation in the next step.

$$P_{i+1} = \frac{M_{i+1} \times R \times T_{i+1}}{V} \quad (3-79)$$

In the formula 3-79, volume current temperature T_{i+1} (Eq. 3-67) is the mean value of previous step temperature T_i and volume inlet total temperature T_A . This value is taken as the volume outlet temperature.

$$T_B = T_{i+1} = \frac{T_i + T_A}{2} \quad (3-80)$$

3.2 Engine Control System Simulation

The engine fuel control is a two-step process where three fuel schedules are designed: for steady state; acceleration; and deceleration. These fuel schedules schematically shown in Fig. 3.5 provide the required fuel flow rate W_{ff} signal to the fuel system based on the demand and measured engine shaft relative rotational speed PCN that is the handle of the engine.

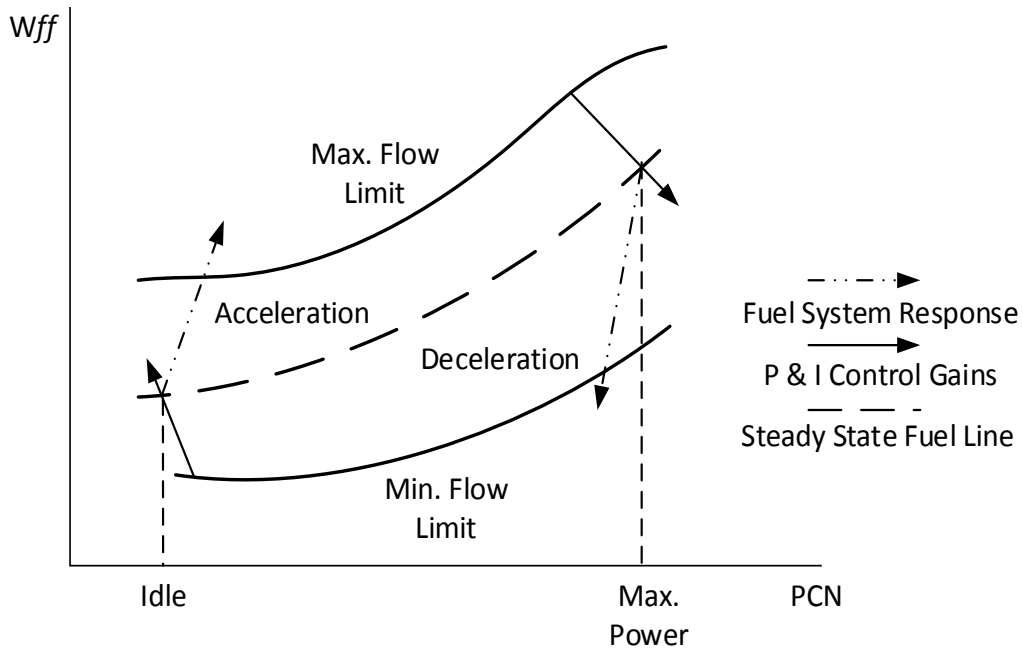


Figure 3.5 Fuel Schedule of Model Engine

As shown in Fig. 3.5, the steady state fuel line is represented by the dash line. In order to keep an engine transient process swift and safe, a minimum fuel selection logic called “Low Win Logic” and a maximum fuel selection logic called “High Win Logic” are embedded into the controller. For example, at an initial phase of the acceleration process, the controller may predict a required fuel flow rate based on cockpit shaft speed command and the measured shaft speed. This predicted fuel flow rate may be larger than the value limited by the fuel selection logic. Therefore, fuel flow rate will be regulated by the fuel selection logic. When the engine approaches the desired target point of the transient process, fuel flow rate signal provided by the fuel schedule will become smaller than that estimated

by the fuel selection logic. If that happens, the control process enters its second step and the controller will take over the fuel control until the engine reaches its desired steady state. The deceleration process is operated in a reverse process to the acceleration. The idea of the coupled two-step engine control and the fuel selection logic is represented in Fig. 3.6.

As shown in Fig. 3.6, the controller calculated control input for the current time step (Wff_{cal}) is first obtained, which is transferred from the speed error between engine current state and target steady state rotational speed difference, and the fuel flow rate given from the transient starting steady state point. Meanwhile, the engine current relative rotational speed, PCN, is used to interpolate both the acceleration and deceleration fuel schedule regulated fuel flow rates (Wff_{afs} for acceleration and Wff_{dfs} for deceleration). Afterwards, the introduced fuel selection logic is used to find a proper fuel flow given to the engine system to ensure its operational safety throughout the whole manoeuvre. The principle of fuel selection logic is to select the smaller value out of the controller calculated fuel flow rate and the fuel flow rate given from the fuel schedule for acceleration. For deceleration, a similar process is followed but a larger value will be obtained. The selected fuel flow rate will then be treated as the controller calculated required engine fuel flow rate. If the fuel delivery system exists in the simulated model, this fuel flow order will be transferred to the metering unit movement order for the fuel system to meter the engine required fuel flow. If not, this order will be regarded as the injected fuel flow rate into the engine combustor. With the given fuel flow rate from either the fuel system or the controller, the engine simulation will calculate a new rotational speed for next step simulation.

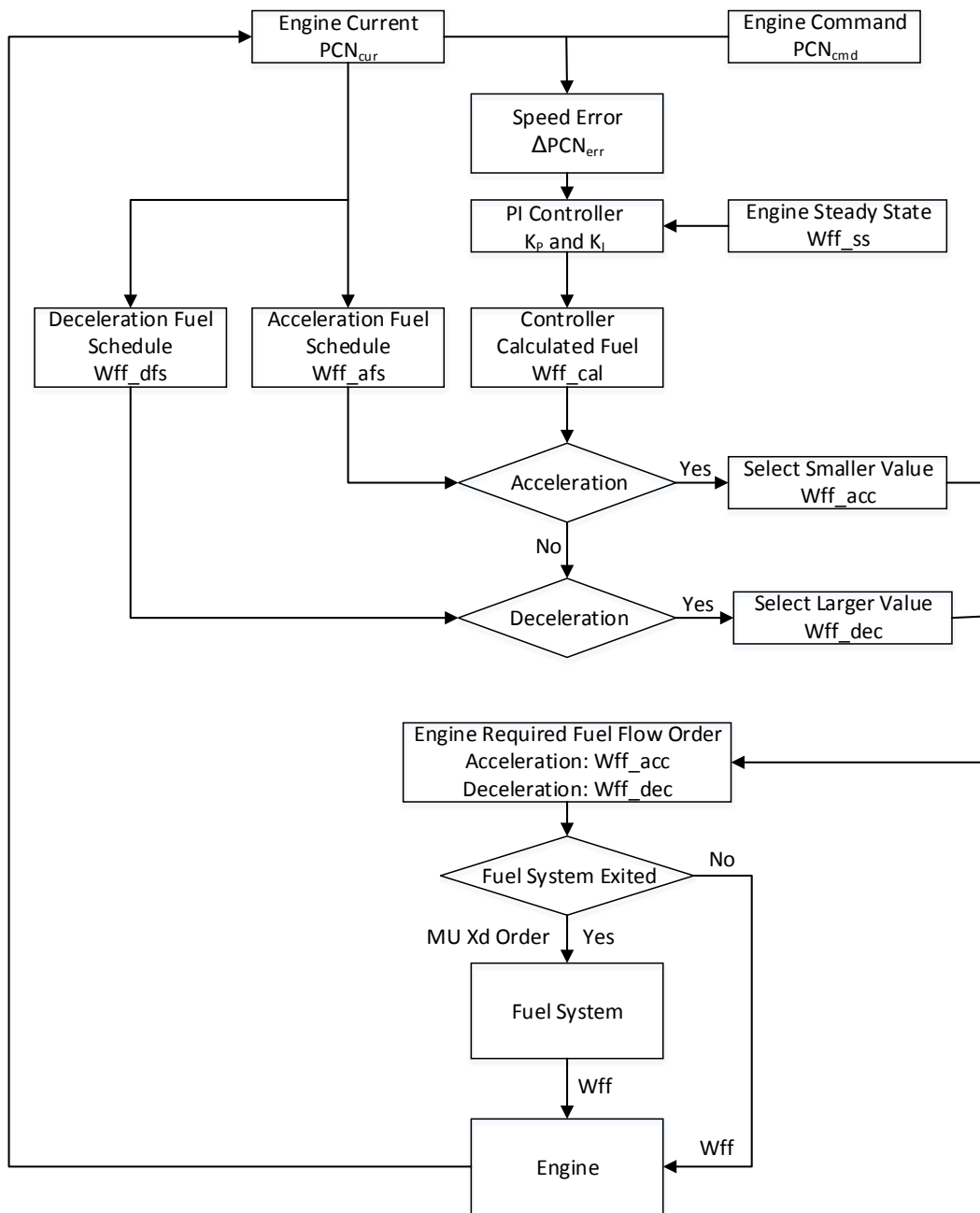


Figure 3.6 Diagram of Coupled Engine Controller and Fuel Selection Logic

A proportional-integral-derivative controller (*PID* controller), or its simplified form, may be used in the second step of the fuel control process. It is a closed loop feedback control widely used in industrial control systems. It historically has been considered to be the most useful controller [98]. *PID* Controller aims to minimise the error value as the difference between the desired and monitored system

variable by transferring the error into a controlled signal to govern the system operation. For a certain incoming error signal, the PID control algorithm involved three actions: P (proportional) action is proportional to the present error, I (integral) action depends on the accumulation of past errors and D (derivative) action is a prediction of future errors, based on current rate of change [99]. In this study, only PI controller is used and the derivative action has been omitted because the command variable shaft rotational speed has no obvious time lag to the control variable fuel flow rate.

Eq. 3-81 is the mathematical representation of the PI control algorithm [71].

$$u(t) = K_p e(t) + K_I \frac{1}{T_i} \int_0^t e(\tau) d\tau \quad (3-81)$$

where $u(t)$ is the control signal, $e(t)$ is the control error, K_p and K_I are the control gains of the proportional action and the integral action respectively, and T_i is a time constant of the integral action.

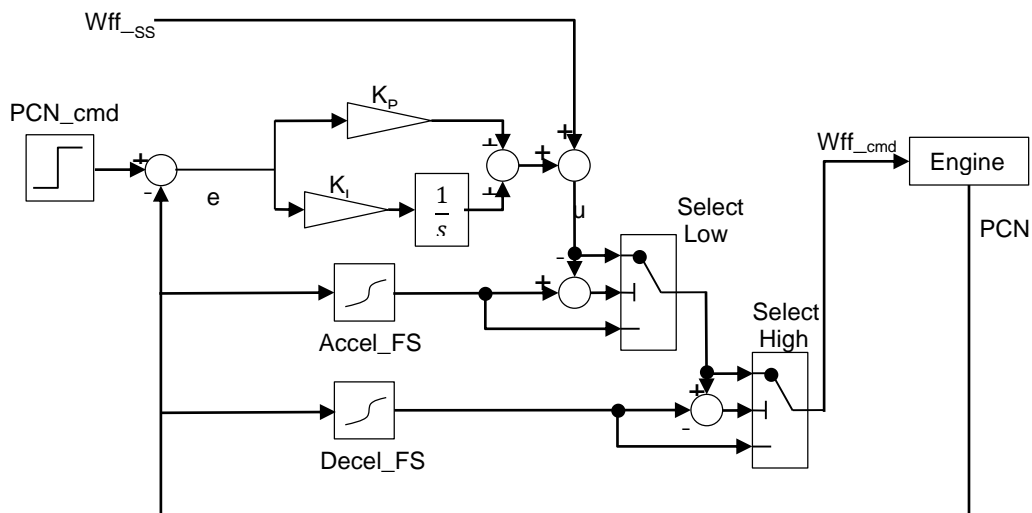


Figure 3.7 Diagram of Coupled Engine Controller and Fuel Selection Logic

The PI control algorithm can also be shown graphically in Fig. 3.7 where integral action is represented by a Laplace transfer function $\frac{1}{s}$. To implement a continuous-time control law in a simulation programme, the Laplace transformation of integral action may be approximated through Z-Transform discretization. Therefore, the PI algorithm in Fig. 3.7 may be more conveniently represented by Eq. 3-82.

$$u(j) = K_p \times e(j) + K_i \times \frac{T_i}{2} \times \frac{z + 1}{z - 1} \times e(j) \quad (3-82)$$

where T_i is equal to the calculation time step Δt , j is the j sampling point.

3.3 Engine Fuel System Simulation

3.3.1 Engine Fuel System Description

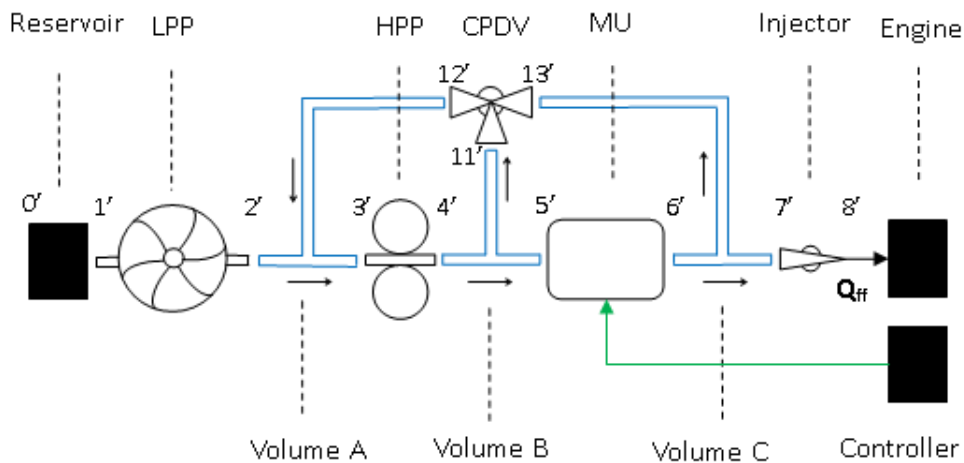


Figure 3.8 Schematic of Engine Fuel System

A fuel system is typically a hydraulic system and its function is to deliver the required fuel flow to the engine combustion chamber to maintain the propulsion system operation. A typical fuel system is shown in Fig. 3.8, which consists of a low pressure pump (*LPP*), a high pressure pump (*HPP*), a metering unit (*MU*), a constant pressure differential valve (*CPDV*), an injector, and tubes connecting these components.

In the fuel system shown in Fig. 3.8, three tubes connect different fuel system components. Fuel sucked from an oil reservoir is firstly pumped through the LPP

that delivers the fuel to the HPP with a proper fuel pressure to avoid fuel vaporization. The high pressure pump is used to pressurize the fuel further to ensure it has sufficient pressure to be injected into the engine combustion chamber. The fuel flow rate metered at an MU is the function of both the opening area and the pressure drop across the MU. If the pressure drop across the MU is maintained at a constant value, the fuel flow rate becomes proportional only to the MU orifice opening area that can be adjusted by the controller.

3.3.2 Engine Fuel System Performance Simulation Inter-Component Volume (ICV) Method

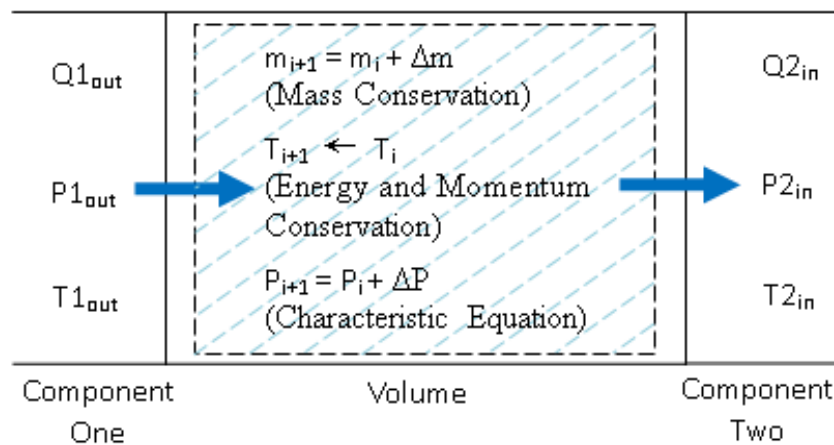


Figure 3.9 Schematic of Inter-Component Volume

Fuel system components are connected by tubes or ducts, named as inter-component volumes, filled with pressurized fuel fluid. During a transient process, the pressure inside the volume may vary due to the inconsistent fuel flow entering and leaving the volume. The ICV method [33] is based on such a phenomenon and has been effectively developed and used in gas turbine transient performance simulations where the working fluid is either air or gas being compressible and a perfect gas. In this study, it is the first time that the ICV method is introduced into the performance simulation of a hydraulic fuel system where the working fluid is fuel being highly incompressible. To assist the understanding of the ICV method, a typical inter-component volume may be schematically represented by Fig. 3.9.

It is assumed that the system running time is first divided into a series of calculation time steps. The varying system state is then calculated at each small time step during which the system is regarded as pseudo-steady and the transient process is calculated from one step to the other until the system reaches its aimed steady state.

Volume state variation is governed by the conservation of mass, energy and momentum. The conservation of mass is represented by Eq. 3-83.

$$m_{i+1} = m_i + \left(\sum W_{i_{in}} - \sum W_{i_{out}} \right) \times \Delta t \quad (3-83)$$

where m is the mass inside the volume, W is the fuel mass flow rate, Δt is the time step, subscript i represents current time moment, $i+1$ represents the next time moment, in is the volume inlet flow, and out is the volume outlet flow. In the fuel system, volumetric flow rate Q instead of mass flow rate W is normally used to represent the fuel flow rate because the metering unit only meters fuel volumetric flow. The fuel mass flow rate W can be calculated by Eq. 3-84.

$$W = \rho \times Q \quad (3-84)$$

where ρ is the fuel density. The conservation of energy is represented by Eq. 3-85.

$$T_{i+1} = \frac{\sum E_{i_{in}} + E_i - \sum E_{i_{out}} - \frac{1}{2} m_i V_{s_{i+1}}^2}{m_{i+1} C_{p_{i+1}}} \quad (3-85)$$

where T is the volume temperature, E the fuel flow energy and V_s the fuel flow velocity. The energy item E in Eq. 3-85 includes static and dynamic energy of the fuel flow that can be calculated by Eq. 3-86.

$$E = m \times C_p \times T + \frac{1}{2} m \times V_s^2 \quad (3-86)$$

In each volume, both inlet and outlet flow velocity can be calculated by Eq. 3-87.

$$V_s = Q/A \quad (3-87)$$

where A is the volume cross area. The conservation of momentum is represented by Eq. 3-88.

$$V_{S_{i+1}} = \frac{\sum(m_i V_{S_i})_{in} + (m_i V_{S_i}) - \sum(m_i V_{S_i})_{out}}{m_{i+1}} \quad (3-88)$$

To ensure these conservation laws are used correctly, the following three assumptions are made :

- The fuel entering the volume will be fully mixed immediately with the fuel already in the volume;
- The status of the fuel within a volume is kept unchanged within a time step;
- The fuel flow within a volume experiences an isentropic process.

The isothermal compressibility κ_T shown in Eq. 3-89 is introduced in Ref. 99 in this study.

$$\kappa_T = -\frac{1}{V} \left(\frac{\partial V}{\partial P} \right)_T \quad (3-89)$$

where κ_T is a pressure coefficient to measure fluid volume variation due to pressure change under constant temperature. Eq. 3-90 based on the equation of state for highly incompressible flow is used to represent the pressure variation within a volume affected by both temperature and volume change.

$$dP = \frac{\alpha}{\kappa_T} dT - \frac{1}{V\kappa_T} dV \quad (3-90)$$

where α is a temperature coefficient to measure how the fluid volume is affected by the temperature change under constant pressure. As both α and κ_T are derived from the same equation of state of fluid, it is not easy to specify these two coefficients' values accurately at the same time when the pressure variation needs to be calculated. To simplify the calculation, the temperature variation due to the fuel fluid compression or expansion in each calculation step is ignored since its effect on fuel volume change is very small compared to the flow

mismatch effect. Therefore the pressure variation within a volume is only affected by the fluid volume variation.

In addition, “bulk modulus” B is introduced to measure the resistance of a fluid to compression or expansion and it is defined as the ratio of pressure stress to volumetric strain. The “bulk modulus” is the function of fluid pressure at certain temperature in Ref. 101 shown in Eq. 3-91 [100].

$$B = \frac{1}{\kappa_T} = -V \left(\frac{\partial P}{\partial V} \right)_T \quad (3-91)$$

Therefore the volume pressure change dP produced by the fluid volume change dV can be estimated by Eq. 3-92 when the temperature variation is ignored.

$$dP = -\frac{B}{V} \times dV \quad (3-92)$$

where V is the volume chamber volume, and dV is given by Eq. 3-93.

$$dV = \sum Q_{in} - \sum Q_{out} \quad (3-93)$$

The new volume pressure produced at next time step P_{i+1} is then calculated by Eq. 3-94.

$$P_{i+1} = P_i + dP \quad (3-94)$$

3.3.3 Engine Fuel System Performance Simulation Newton Raphson (NR) Method

The previous section has illustrated the newly developed ICV method used in engine fuel system simulations. This method introduces the liquid fuel oil compression phenomenon inside the connecting ducts between conjunct components to implement the transient process operation. However, since liquid fuel oil is generally considered highly incompressible, this method used on fuel system simulation may be not as well accepted as that used for engine system simulation with compressible working fluid air/gas. In this section, a newly developed Newton-Raphson (NR) method applicable to engine fuel system transient simulation will be described. In this method, the ducts only transmit the

performance parameters from the previous outlet to the following component inlet but do not allow fuel compression inside it.

The Newton-Raphson method named after Isaac Newton and Joseph Raphson is a root-finding method to discover successively approximating roots (or zeros) of a real-valued function. [102] As shown in Fig. 3.10, the curve $y = f(x)$ meets the x-axis at point $(X_n, 0)$. The tangent line at $(X_0, f(X_0))$ is described by Eq. 3-95.

$$y = f(X_0) + (x - X_0)f'(X_0) \quad (3-95)$$

Geometrically, $(X_1, f(X_1))$ is the intersection point between the tangent line and x-axis. The value of X_1 is,

$$X_1 = X_0 - \frac{f(X_0)}{f'(X_0)} \quad (3-96)$$

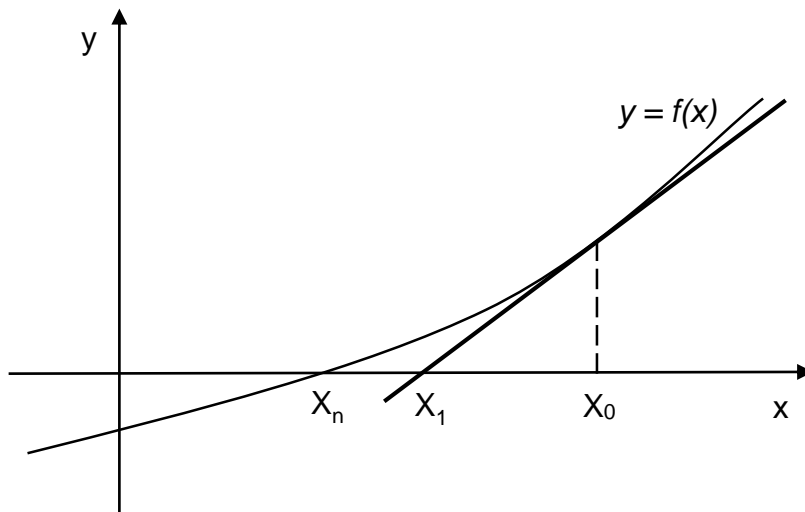


Figure 3.10 Newton Raphson Method on Finding X_n from Initial Value X_0

Compared to X_0 , X_1 is closer to the x-intercept X_n of the curve line. Thus, if repeated the process reported with Eq. 3-97, the value of X_n will finally be obtained.

$$X_{k+1} = X_k - \frac{f(X_k)}{f'(X_k)} \quad (3-97)$$

In the gas turbine engine system simulation, Macmillan [17] successfully employed this method on engine off-design steady state points' calculation. When the off-design (*OD*) is running, the system is not balanced because the equilibriums of work, mass flow rates, etc. are broken, given the disturbances between the target steady state point and the beginning steady state point. Errors produced by these imbalances are referred to as Base Errors (*BEs*). [17] These *BEs* are related to some engine variables such as turbomachinery outlet pressures and engine shaft speeds. NR method is applied to eliminate these errors by adjusting the variables' values through a series of iterations. If all the errors become zero, the system equilibriums are restored. Thus, the system reaches a new steady state operating point. In the fuel system transient phase, system equilibriums are also broken. In this case, the NR method is available on the fuel system transient simulation.

Just as in the ICV method, the system running time is divided into a series of calculation time steps. During each time step, the system is regarded as pseudo-steady to calculate the system state with NR method. By calculating the system state from one step to the other until the system reaches its aimed steady state, transient process simulation of fuel system will be implemented.

When the system equilibriums are broken under transient operation, the *BEs* produced by the fuel system imbalances form a system of equations named Residual Equation Set (*RES*) (Eq. 3-98).

$$\begin{cases} BE_1 = BE_1(x_1, x_2, \dots, x_n) = F_1 \\ BE_2 = BE_2(x_1, x_2, \dots, x_n) = F_2 \\ \dots \dots \dots \dots \\ BE_n = BE_n(x_1, x_2, \dots, x_n) = F_n \end{cases} \quad (3-98)$$

where x_1, x_2, \dots, x_n are the selected independent variables relating to the *BEs*. As shown in Eq. 3-98, the number of the selected variables is equal to the number of *BEs*. The vector form of Eq. 3-98 is represented by Eqs. 3-99 and 3-100.

$$BE = f(X) = 0 \quad (3-99)$$

$$\mathbf{X} \in \mathbf{R}^n \quad (3-100)$$

The calculation of the system pseudo-steady state in one time step is intended to solve all the variables \mathbf{X} at $\mathbf{BE} = 0$ condition. With these calculated variables' values, each system error becomes zero. In that case, system imbalances are eliminated and the system remains at a pseudo-steady state.

To illustrate the NR method applied on the system transient simulation, a system state at time step k is specified. To the system with n selected variables, the RES at initial variables' values \mathbf{X}_0 is,

$$\begin{cases} BE_1 = BE_1(x_1, x_2, \dots, x_n) = F_{k1} \\ BE_2 = BE_2(x_1, x_2, \dots, x_n) = F_{k2} \\ \dots \dots \dots \dots \\ BE_n = BE_n(x_1, x_2, \dots, x_n) = F_{kn} \end{cases} \quad (3-101)$$

If a slight increment of system variables $\Delta\mathbf{X}$ is provided, the variation of \mathbf{BE} is represented by Eq. 3-102.

$$\begin{cases} \Delta BE_1 = \frac{\partial BE_1}{\partial x_1} \Delta x_1 + \frac{\partial BE_1}{\partial x_2} \Delta x_2 + \dots + \frac{\partial BE_1}{\partial x_n} \Delta x_n \\ \Delta BE_2 = \frac{\partial BE_2}{\partial x_1} \Delta x_1 + \frac{\partial BE_2}{\partial x_2} \Delta x_2 + \dots + \frac{\partial BE_2}{\partial x_n} \Delta x_n \\ \dots \dots \dots \dots \\ \Delta BE_n = \frac{\partial BE_n}{\partial x_1} \Delta x_1 + \frac{\partial BE_n}{\partial x_2} \Delta x_2 + \dots + \frac{\partial BE_n}{\partial x_n} \Delta x_n \end{cases} \quad (3-102)$$

If it assumes that the system can reach its pseudo-steady state with this increment, Eq. 3-103 and Eq. 3-104 are obtained.

$$\mathbf{BE}(\mathbf{X}_1) = \mathbf{BE}(\mathbf{X}_0) + \Delta\mathbf{BE} = 0 \quad (3-103)$$

$$\Delta\mathbf{BE} = -\mathbf{BE}(\mathbf{X}_0) = -\mathbf{F}_k \quad (3-104)$$

The vector form of Eq. 3-104 can be represented by a matrix form shown in Eq. 3-105.

$$\begin{bmatrix} \frac{\partial BE_1}{\partial x_1} & \frac{\partial BE_1}{\partial x_2} & \dots & \frac{\partial BE_1}{\partial x_n} \\ \frac{\partial BE_2}{\partial x_1} & \frac{\partial BE_2}{\partial x_2} & \dots & \frac{\partial BE_2}{\partial x_n} \\ \dots & \dots & \dots & \dots \\ \frac{\partial BE_n}{\partial x_1} & \frac{\partial BE_n}{\partial x_2} & \dots & \frac{\partial BE_n}{\partial x_n} \end{bmatrix} \begin{bmatrix} \Delta x_1 \\ \Delta x_2 \\ \vdots \\ \Delta x_n \end{bmatrix} = \begin{bmatrix} -F_{k1} \\ -F_{k2} \\ \vdots \\ -F_{kn} \end{bmatrix} \quad (3-105)$$

Eq. 3-105 can be simplified as,

$$J(\mathbf{BE}, \mathbf{X})[\mathbf{X}_1 - \mathbf{X}_0] = -\mathbf{F}_k \quad (3-106)$$

where $J(\mathbf{BE}, \mathbf{X})$ is the Jacobian matrix which is the first-order partial differentials of Eq. 3-101.

$$J(\mathbf{BE}, \mathbf{X}) = \begin{bmatrix} \frac{\partial BE_1}{\partial x_1} & \frac{\partial BE_1}{\partial x_2} & \dots & \frac{\partial BE_1}{\partial x_n} \\ \frac{\partial BE_2}{\partial x_1} & \frac{\partial BE_2}{\partial x_2} & \dots & \frac{\partial BE_2}{\partial x_n} \\ \dots & \dots & \dots & \dots \\ \frac{\partial BE_n}{\partial x_1} & \frac{\partial BE_n}{\partial x_2} & \dots & \frac{\partial BE_n}{\partial x_n} \end{bmatrix} \quad (3-107)$$

According to Eq. 3-106, the equation used on each iteration in one time step is concluded as Eq. 3-108 to obtain the values of selected system independent variables.

$$\mathbf{X}_{j+1} = \mathbf{X}_j + J^{-1}(\mathbf{BE}, \mathbf{X}) \cdot \mathbf{BE}(\mathbf{X}_j) \quad (3-108)$$

The previous process introduces the principle of the NR method applied to non-linear system simulations. For the engine fuel system during transient, three flow equilibriums are selected to be the BE equations. The first is the equilibrium between LPP and HPP; the second is that between the HPP and MU; and the third is between MU and injector. According to the BE equations, three independent variables relating to these BEs are also selected. These three variables are the fuel pressure at each connecting tube between conjunct components. Calculation steps of the NR method applied to engine fuel system simulation in one time step are listed as follows:

1. Select the independent variables \mathbf{X} .

$$\mathbf{X} = [P_{V1}, P_{V2}, P_{V3}]^T \quad (3-109)$$

2. Establish the 3×3 Jacobian matrix $J(\mathbf{BE}, \mathbf{X})$ (Eq. 3-110) at \mathbf{X}_1 point. To the non-linear system consisting of many components, it is hard to find the system first-order partial derivatives at point \mathbf{X}_1 . An alternative method is to use the difference in quotients instead of differentials to find the Jacobian matrix at each calculation step. This is achieved by provide a slight increment of each system independent variable Δx_i , $i=1, 2, \dots, n$. To each given variable increment Δx_i , fuel system (Fig. 3.8) state will be varied to find the mass flow rates' variations relating to each flow equilibrium equation. (Eqs. 3-111 to 3-113)

$$J(\mathbf{BE}, \mathbf{X}) = \begin{bmatrix} \frac{\partial BE_1}{\partial P_{V1}} & \frac{\partial BE_1}{\partial P_{V2}} & \frac{\partial BE_1}{\partial P_{V3}} \\ \frac{\partial BE_2}{\partial P_{V1}} & \frac{\partial BE_2}{\partial P_{V2}} & \frac{\partial BE_2}{\partial P_{V3}} \\ \frac{\partial BE_3}{\partial P_{V1}} & \frac{\partial BE_3}{\partial P_{V2}} & \frac{\partial BE_3}{\partial P_{V3}} \end{bmatrix} \quad (3-110)$$

$$\begin{cases} \frac{\partial BE_1}{\partial P_{V1}} = \frac{\partial W_{LPP}}{\partial P_{V1}} + \frac{\partial W_{CPDV}}{\partial P_{V1}} - \frac{\partial W_{HPP}}{\partial P_{V1}} \\ \frac{\partial BE_1}{\partial P_{V2}} = \frac{\partial W_{LPP}}{\partial P_{V2}} + \frac{\partial W_{CPDV}}{\partial P_{V2}} - \frac{\partial W_{HPP}}{\partial P_{V2}} \\ \frac{\partial BE_1}{\partial P_{V3}} = \frac{\partial W_{LPP}}{\partial P_{V3}} + \frac{\partial W_{CPDV}}{\partial P_{V3}} - \frac{\partial W_{HPP}}{\partial P_{V3}} \end{cases} \quad (3-111)$$

$$\begin{cases} \frac{\partial BE_2}{\partial P_{V1}} = \frac{\partial W_{HPP}}{\partial P_{V1}} - \frac{\partial W_{MU}}{\partial P_{V1}} - \frac{\partial W_{CPDV}}{\partial P_{V1}} \\ \frac{\partial BE_2}{\partial P_{V2}} = \frac{\partial W_{HPP}}{\partial P_{V2}} - \frac{\partial W_{MU}}{\partial P_{V2}} - \frac{\partial W_{CPDV}}{\partial P_{V2}} \\ \frac{\partial BE_2}{\partial P_{V3}} = \frac{\partial W_{HPP}}{\partial P_{V3}} - \frac{\partial W_{MU}}{\partial P_{V3}} - \frac{\partial W_{CPDV}}{\partial P_{V3}} \end{cases} \quad (3-112)$$

$$\begin{cases} \frac{\partial BE_3}{\partial P_{V1}} = \frac{\partial W_{MU}}{\partial P_{V1}} - \frac{\partial W_{Injector}}{\partial P_{V1}} \\ \frac{\partial BE_3}{\partial P_{V2}} = \frac{\partial W_{MU}}{\partial P_{V2}} - \frac{\partial W_{Injector}}{\partial P_{V2}} \\ \frac{\partial BE_3}{\partial P_{V3}} = \frac{\partial W_{MU}}{\partial P_{V3}} - \frac{\partial W_{Injector}}{\partial P_{V3}} \end{cases} \quad (3-113)$$

3. Establish the system RES of BEs (Eq. 3-114) from the \mathbf{X}_1 values and system state values. Initially, the system is performed at a DP simulation. All the system state variables are kept at DP values at the beginning of transient simulation. In addition, as the fuel system state is decided by the engine system and its controller, pump rotational speed ratio and injector outlet fuel pressure are provided by the engine system current operating state. Engine required fuel flow rate at current state is also transferred to the metering unit opening area by the controller. By using these parameters' values, fuel system RES at \mathbf{X}_1 can be established to calculate each BE from the fuel volumetric flow imbalances.

$$\begin{cases} BE_1 = W_{LPP} + W_{CPDV} - W_{HPP} \\ BE_2 = W_{HPP} - W_{MU} - W_{CPDV} \\ BE_3 = W_{MU} - W_{Injector} \end{cases} \quad (3-114)$$

4. After the Jacobian matrix $J(\mathbf{BE}, \mathbf{X})$ has been found, the inverse matrix of Jacobian matrix $J^{-1}(\mathbf{BE}, \mathbf{X})$ (Eq. 3-115) can be calculated.

$$J^{-1}(\mathbf{BE}, \mathbf{X}) = [J(\mathbf{BE}, \mathbf{X})]^{-1} \quad (3-115)$$

5. Find point \mathbf{X}_2 with Eq. 3-108 by using NR method.
6. Repeat the steps 3 to 5 until the BEs' norm at point \mathbf{X}_{j+1} is less than the prescribed convergence value ξ . (Eq. 3-116) \mathbf{X}_{j+1} is the solution of RES. With this solution, a system pseudo-steady state at this time step will be obtained.

$$\|\mathbf{BE}_{j+1}\| = \sqrt[n]{BE_1^n + BE_2^n + \dots + BE_n^n} \leq \xi \quad (3-116)$$

where ξ is the convergence precision. The convergence value ξ instead of 0 is used because the base errors relating to the selected multi-

independent variables cannot be easily eliminated to zero from the NR iterations. In addition, when the calculated BEs' norm approaches to virtually zero, the calculated independent variables' change ΔX become very small to alter the variable values during each iteration. This will largely increase the consumption time of computer simulation.

7. Repeat the steps 2-6, a series of fuel system pseudo-steady states will be calculated until the system reaches its target steady state.

In practice, the system only converges to its pseudo-steady state when the selected beginning X_1 point is very close to the pseudo-steady state X_{j+1} point at each time step. However, in the transient simulation with hundreds of thousands of pseudo-steady state points to be calculated, it cannot be ensured that the system could be converged at each time step. If it is not, the system may not be converged and the transient simulation cannot be implemented. A technical solution to this problem is to introduce relaxation factors ω_k into the NR method. (Eq. 3-117)

$$X_{j+1} = X_j - \omega_k \cdot J^{-1}(BE, X) \cdot BE(X_j) \quad (3-117)$$

According to the Eq. 3-117, ω_k is able to control the amount of variation in the independent variable value X_j during each iteration. If the variation on one iteration is too large, the system cannot reach its pseudo-steady state. On the contrary, if the variation is too small, the convergence process may consume a large amount of time. Therefore, a good value of ω_k will lead to a fast and converged solution of NR method simulation. To the engine fuel system transient simulation with millions of pseudo-steady states to be calculated, it is hard to find a proper ω_k for the whole transient simulation. A tried and trusted method is to govern each independent variable (duct pressure) variation between 0.1 kPa to 10 kPa with ω_k in one iteration.

3.3.4 Engine Fuel System Components Calculation

Pumps:

Pumps are used to pressurize fuel flow in order that it can be transported and injected into the engine combustion system. Two types of pumps, i.e. centrifugal pumps as low pressure pumps and gear pumps as high pressure pumps are normally used in hydraulic fuel systems and the schematics are represented in Figs. 3.11 and 3.12 respectively.

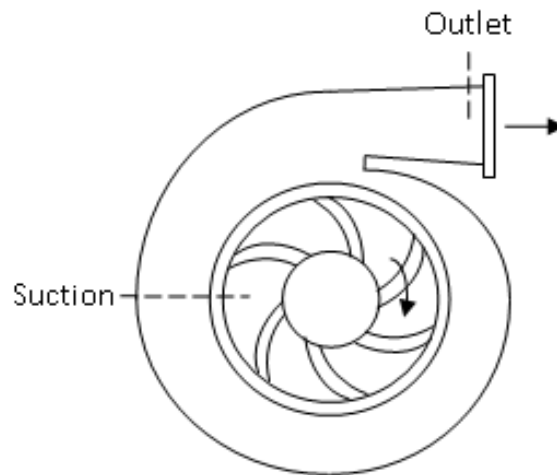


Figure 3.11 Schematic of Centrifugal Pump

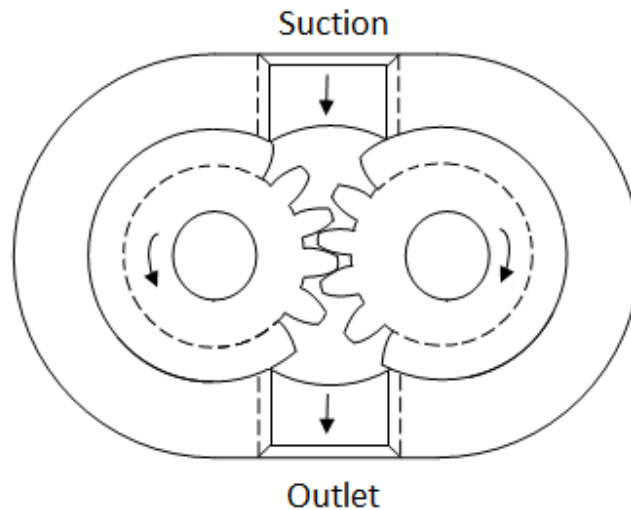


Figure 3.12 Schematic of Gear Pump

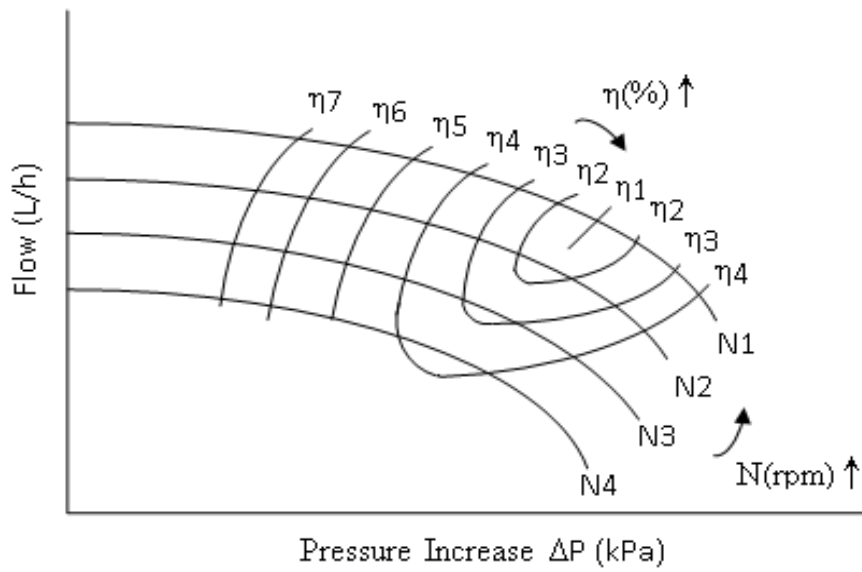


Figure 3.13 Typical Centrifugal Pump Characteristic Map

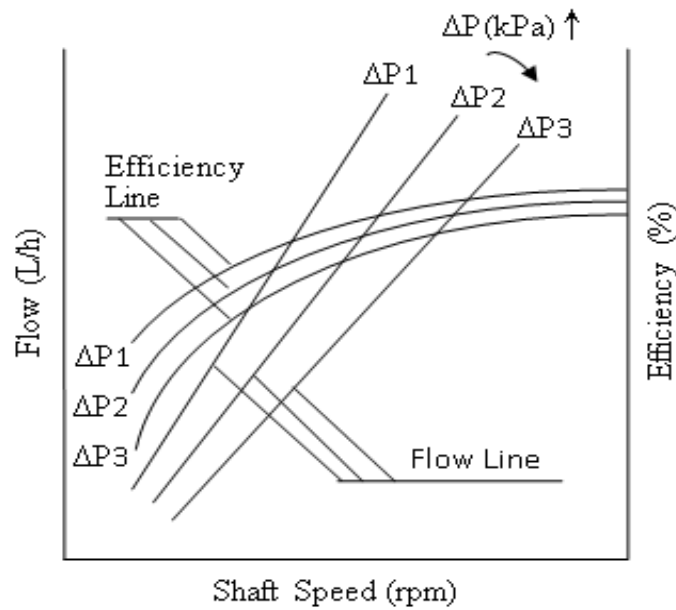


Figure 3.14 Typical Gear Pump Characteristic Map

In this study, empirical pump characteristic maps are used to describe the performance behaviour of the pumps. Four characteristic parameters including

shaft speed ratio PCN, volumetric flow rate Q, efficiency η , and pressure increase ΔP are used to describe the pump characteristics in the maps. Generally, the shaft speed ratio PCN and pressure increase ΔP are known, in order to obtain the required pump volumetric flow rate Q and efficiency η in the transient simulation. Figs. 3.13 and 3.14 show typical characteristic maps for centrifugal pumps and gear pumps, respectively.

As pumps are directly connected to engine shaft and are driven by an engine, pump shaft rotational speed is assumed to be equal to the engine shaft speed and there is no time delay between engine and pump shaft speeds during engine transient processes. The input and output parameters and main calculation equations of pumps are listed below.

Input:

- P_A Inlet Fuel Total Pressure
- P_B Outlet Fuel Total Pressure
- PCN Shaft Relative Rotational Speed (from Turbine)
- T_A Inlet Fuel Total Temperature

Output:

- PSP Pump Shaft Power
- Q_A Inlet Fuel Volumetric Flow Rate
- Q_B Outlet Fuel Volumetric Flow Rate
- T_B Outlet Fuel Total Temperature

Pump outlet total pressure P_B is calculated from its following volume (with ICV method) or duct (with NR method). Pressure increase ΔP is the difference between P_B and P_A .

$$\Delta P = P_B - P_A \quad (3-118)$$

Pump volumetric fuel flow rate Q and efficiency η are then interpolated from the scaled characteristic maps with ΔP and PCN. The scaled pump maps are obtained from pump design point calculation by specifying the pump pressure increase (ΔP_{DP}), volumetric flow rate (Q_{DP}), and efficiency (η_{DP}) of newly designed fuel systems at design point condition. The scaling factor of each parameter is then given from Eq. 3-119 to 3-121.

$$\Delta PSF = \frac{\Delta P_{DP}}{\Delta P_{DP,Map}} \quad (3-119)$$

$$QSF = \frac{Q_{DP}}{Q_{DP,Map}} \quad (3-120)$$

$$EtaSF = \frac{\eta_{DP}}{\eta_{DP,Map}} \quad (3-121)$$

The energy transformed to the fuel flow through a pump can be divided into two parts: one is used to pressurise the fuel flow and the other is to increase fuel temperature by assuming the pump is an adiabatic system. In other words, pump shaft power (PSP) can be obtained by Eq. 3-122 [89].

$$PSP = \frac{\Delta P \times Q}{\eta} \quad (3-122)$$

The thermal energy Φ absorbed by the fuel flow can be calculated by Eq. 3-123 [103].

$$\phi = PSP \times (1 - \eta) \quad (3-123)$$

Therefore, the temperature rise ΔT of the fuel flow can be then calculated by Eq. 3-124.

$$\Delta T = \frac{\phi}{W \times C_p} \quad (3-124)$$

where C_p is the specific heat of the fuel at constant pressure.

Valves:

Valves are the devices to regulate the quantity and pressure, and control the direction of fuel flow rate in the system. By controlling the opening and closing of a valve, the fuel flow rate can be controlled.

Constant Pressure Differential Valve:

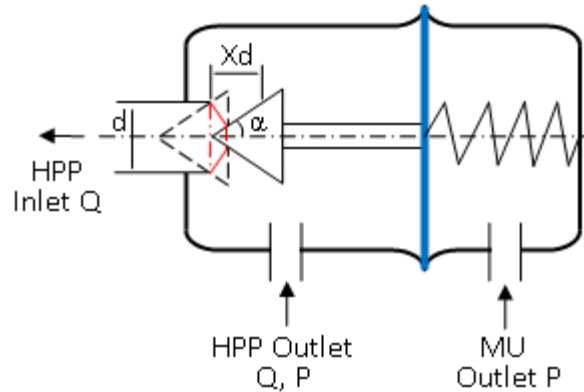


Figure 3.15 Schematic of Constant Pressure Differential Valve

A constant pressure differential valve (CPDV), a schematic of it shown in Fig. 3.15, is a device to maintain a constant pressure drop across a fuel metering unit (MU). It has two inlet ports, one connecting the HPP outlet and the MU inlet and the other connecting the MU outlet. It has an exit port where fuel will be bypassed from the inlet of the MU to the entry of HPP via a cone valve in order to keep a constant pressure drop. Inside the CPDV, a film connecting with a pressurized spring is installed to separate the CPDV into two independent chambers where pressure difference can be transferred but fuel cannot be. The pressure drop is balanced by the spring whose movement adjusts the opening area of valve orifice.

Input:

- P_{A1} Inlet Fuel Total Pressure from HPP Outlet
- P_{A2} Inlet Fuel Total Pressure from MU Outlet
- P_B Outlet Fuel Total Pressure from HPP Outlet
- T_A Inlet Fuel Total Temperature

T_m	Valve Mechanism Movement Delay Time Constant
X_d	Cone Valve Opening Displacement at Previous Calculation Step

Output:

Q	Return Fuel Volumetric Flow Rate from HPP Outlet to HPP Inlet
T_B	Outlet Fuel Total Temperature
$X_{d_{i+1}}$	Cone Valve Opening Displacement at Current Step

CPDV is designed to adjust the returned fuel flow rate from HPP outlet to the HPP inlet port to maintain the constant pressure drop across the MU. The fuel volumetric flow rate Q passing through a valve can be calculated from Eq. 3-125.

[89]

$$Q = Cd \times A \times \sqrt{\frac{2\Delta P}{\rho}} \quad (3-125)$$

where Cd is the valve orifice discharge flow coefficient, ρ is the fuel density and ΔP is the pressure difference across the valve orifice.

According to Eq. 3-125, the CPDV exit fuel flow rate is the function of the pressure drop ΔP_{CPDV} and the opening area A_c of the cone valve. ΔP_{CPDV} (Eq. 3-126) is the pressure difference between P_{A1} and P_B . A_c calculated from Eq. 3-127 is considered as the lateral area of a conical frustum formed by the cone gate and the valve orifice.

$$\Delta P_{CPDV} = P_{A1} - P_B \quad (3-126)$$

$$A_c = \pi \times d \times X_{d_{i+1}} \times \sin \alpha \quad (3-127)$$

where, d is the diameter of the valve orifice, $X_{d_{i+1}}$ is the moving distance of the cone gate at current step calculation, and α is the angle of the cone.

The moving distance X_d is governed by the CPDV film and its connecting spring. (Fig. 3.15) To maintain a pressure drop ΔP_{MU} (Eq. 3-128) between HPP and MU

outlet, the spring has to be pre-pressurized. The spring force (SF) produced by the pressurized spring is given by Eq. 3-129.

$$\Delta P_{MU} = P_{A1} - P_{A2} \quad (3-128)$$

$$SF = K \times (\tau - Xd_i) \quad (3-129)$$

where K is the spring stiffness, τ is the pre-pressurized distance of the spring.

The pressure drop ΔP_{MU} on the film also produces a pressure force (PF) estimated by Eq. 3-130.

$$PF = \Delta P_{MU} \times A_f \quad (3-130)$$

where A_f is the area of the film.

The valve moving distance variation ΔXd produced by imbalance between the pressure force and spring force can be obtained from Eq. 3-115. Thus,

$$\Delta Xd = (PF - TF)/K \quad (3-131)$$

A first order lag represented by a Laplace transfer function $\frac{1}{T_m s + 1}$ is added to represent the delay time ($4T_m$) of the mechanical movement corresponding to the moving distance variation ΔXd . The Laplace transform of the first order lag may be approximated through Z-Transform discretization. Therefore, the moving distance of the cone valve Xd_{i+1} in one time step can be calculated by Eq. 3-132.

$$Xd_{i+1} = Xd_i + \Delta Xd \times \frac{1 - e^{-\frac{\Delta t}{T_m}}}{z - e^{-\frac{\Delta t}{T_m}}} \quad (3-132)$$

where, T_s the time constant of first order lag, Δt the calculation time step.

The thermal energy Φ absorbed by the fuel flow passing through the orifice may be estimated by Eq. 3-133 [89].

$$\phi = \kappa \times \Delta P \times Q \quad (3-133)$$

where κ is the heat producing coefficient of the valve. By using Eq. 3-124, the fuel flow temperature rise across valve orifice can be calculated.

Metering Unit:

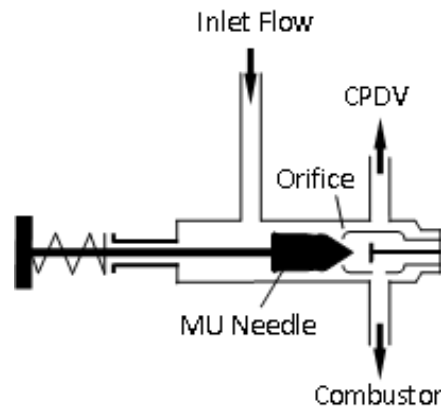


Figure 3.16 Schematic of Metering Unit Valve

A metering unit is the device to meter the engine required fuel flow rate based on the controller order. A typical metering unit consists of a stepper motor, a rack and pinion mechanism, and a metering valve. A schematic of a metering unit valve is represented in Fig. 3.16. A needle valve is selected as the metering valve which comprises a needle and an orifice. During the engine operation, the stepper motor drives the rack and pinion mechanism to open a discrete distance of the needle valve based on the controller order. The area formed by the needle and orifice is taken to measure the fuel pressurized by the HPP. The measured fuel flows through the injector and is burned in the engine combustor. The extra fuel from the HPP outlet will flow back to the HPP inlet through the CPDV to maintain the required pressure drop across the metering valve.

Input:

- P_A Inlet Fuel Total Pressure
- P_B Outlet Fuel Total Pressure
- T_A Inlet Fuel Total Temperature

T_m	Valve Mechanism Movement Delay Time Constant
Xd_i	Previous Step Metering Valve Opening Displacement
Xd_{order}	Metering Valve Opening Displacement Ordered by the Controller
ΔP_i	Previous Step Metering Valve Pressure Drop

Output:

Q	MU Metered Fuel Flow Rate
T_B	Outlet Fuel Total Temperature
Xd_{i+1}	Current Step Metering Valve Opening Displacement

The MU metered fuel volumetric flow rate is also calculated from Eq. 3-125 if the pressure drop ΔP_{MU} (Eq. 3-134) and opening area A_{MU} (Eq. 3-135) of the metering valve orifice are known.

$$\Delta P_{MU} = P_A - P_B \quad (3-134)$$

The opening area A_{MU} of the metering valve is assumed to be proportional to the moving distance of

$$A_{MU} = k \times Xd_{i+1} \quad (3-135)$$

where k is the opening coefficient of the metering valve.

The valve opening distance Xd_{order} is governed by the controller calculated required metering fuel volumetric flow rate order Q_{order} based on the engine speed error $e(PCN)$ and fuel density ρ .

$$Q_{order} = f[e(PCN), \rho] \quad (3-136)$$

$$Xd_{order} = \frac{Q_{order}}{Cd \times \sqrt{\frac{2\Delta P_i}{\rho}} \times k} \quad (3-137)$$

The valve moving distance variation ΔXd at the current step is calculated from Eq. 3-138 if the moving distance Xd_i at the previous step and the required opening distance Xd_{order} are known.

$$\Delta Xd = Xd_{order} - Xd_i \quad (3-138)$$

To represent the mechanical delay effect of the stepper motor and rack and pinion mechanism to vary the distance, a first order lag $\frac{1}{T_m s + 1}$ is also introduced. Thus, the current step metering valve opening distance can be obtained from Eq. 3-132.

Metering unit outlet total temperature is calculated from the thermal energy equation (Eq. 3-133) and temperature rise equation (Eq. 3-124).

Injector:

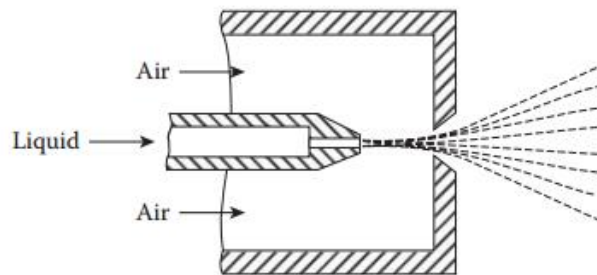


Figure 3.17 Schematic of Metering Unit Valve [104]

An injector is to deliver the metered fuel into the engine combustor. To ensure the fuel is burned efficiently, liquid fuel is mixed with air inside the injector and the fuel/air mixture is injected into the engine combustor. A schematic of an injector is shown in Fig. 3.17. This component is assumed to be a fixed area orifice in the simulation. The fuel and air mixing process and fuel mixture spray effect are considered as a first order lag added in the simulation.

Input:

- A Injector Fixed Area
- P_A Inlet Fuel Total Pressure

P_B	Outlet Fuel Total Pressure (Combustor Back Pressure)
T_A	Inlet Fuel Total Temperature
T_f	Fuel Spray Delay Time Constant

Output:

T_B	Outlet Fuel Total Temperature
W_{ff}	Injected Fuel Flow Rate into Engine Combustor

As a fixed area orifice in the simulation, the injector orifice area is known from its DP calculation (Eq. 3-139) by knowing the fuel pressure drop and designed fuel volumetric flow rate through this component.

$$A = \frac{Q_{DP}}{Cd \times \sqrt{\frac{2\Delta P_{DP}}{\rho}}} \quad (3-139)$$

The injector pressure drop ΔP_{DP} is the pressure difference between MU outlet total pressure and combustor back pressure (inlet total pressure) at design point operating condition.

In the transient process, the fuel volumetric flow rate Q_{i+1} through the injector at the current time step is also calculated from Eq. 3-125 by knowing its pressure drop and area. The fuel spray delay effect in the injector is also considered as a first order lag represented by a Laplace transfer function $\frac{1}{T_f s + 1}$. The injected fuel flow rate into the engine combustor is then calculated by Eq. 3-140. Outlet total temperature is calculated from the thermal energy equation (Eq. 3-133) and temperature rise equation (Eq. 3-124).

$$W_{ff,i+1} = Q_{i+1} \times \frac{1 - e^{-\frac{\Delta t}{T_f}}}{z - e^{-\frac{\Delta t}{T_f}}} \times \rho \quad (3-140)$$

3.4 Integrated Engine, Control and Fuel System

With the models of all the system components becoming available, the engine and its fuel and control system can be separately built by using the previous introduced methods. The flow charts of each individual system are listed in Appendix A. The integrated engine, fuel and control system has been established and shown in Fig. 3.18.

Engine shaft speed is measured by a speed sensor and the measured signal is transmitted to the engine controller with a first order lag $\frac{1}{T_s s + 1}$. In this research, two different engine types: a turbojet engine and a turboshaft engine are examined to test the applicability of newly developed fuel system simulation methods. For the turbojet engine with a single shaft, there is only one shaft where its speed is measured. However, in the case of the turboshaft engine with a free turbine, the free turbine shaft speed is measured to regulate the required fuel flow rate.

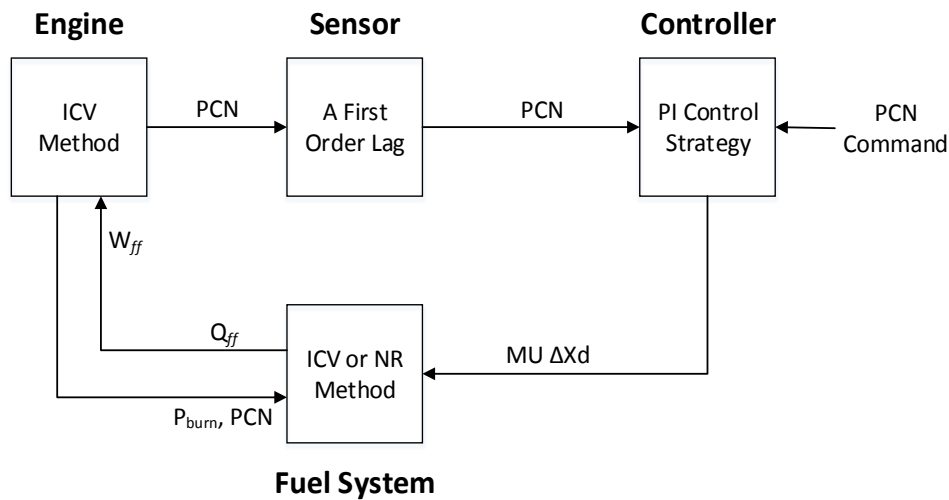


Figure 3.18 Schematic of Integrated Engine, Control and Fuel System

The controller receives the measured speed signal and speed demand indicated by a cockpit power level angle (*PLA*) to calculate the required fuel flow rate Q_{ff} using the PI control schedule. Q_{ff} is then turns into the movement ΔX_d of the mechanism in the fuel system to adjust the orifice opening area of the metering

unit. The metered fuel flow rate W_{ff} from the fuel system will then be injected into the engine combustion chamber to maintain the engine transient operation.

4 Application, Results, and Analysis

4.1 Application of Engine and its Control and Fuel Systems

4.1.1 Model Engine System

The developed integrated engine, control and fuel system transient performance simulation method has first been applied to a model turbojet gas turbine engine shown in Fig. 3.1. Two inter-component volumes are included in the transient engine performance model, one located between the compressor and the turbine and the other between the turbine and the nozzle. Spool percentage corrected rotational speed PCN is chosen as the handle and is controlled by the controller to determine the operating condition of the engine. Table 4-1 lists the turbojet engine performance specification at ISA sea level static condition and the key performance parameters used in the performance modelling.

Table 4-1 Turbojet Model Engine Performance Specification at Design Point and Key Parameters

Parameters	Value
Air Flow Rate (kg/s)	77.2
Compressor Pressure Ratio	8.8
Compressor Isentropic Efficiency	0.84
Splitter Remained Flow Coefficient	0.9
Combustion Efficiency	0.99
Burner Exit Temperature (K)	1141
Volume A (m ³)	0.4
Turbine Isentropic Efficiency	0.87
Volume B (m ³)	0.2
Thrust (kN)	47.29
SFC (g/kN·s)	22.36

To validate the flexibility of the newly developed method on engine fuel system transient simulation, the turboshaft engine shown in Fig. 3.2 has also been selected as a model. Compared with the turbojet engine, this turboshaft engine introduces an additional free turbine between the core generator turbine and engine nozzle. An external loading (EL) is driven by this free turbine through a connecting shaft. In this simulation, the external loading (Eq. 4-1) is assumed to be proportional to the cube of the free turbine shaft speed.

$$EL = \sigma \times PCN_{FT}^3 \quad (4-1)$$

Table 4-2 Turboshaft Model Engine Performance Specification at Design Point and Key Parameters

Parameters	Value
Air Flow Rate (kg/s)	65
Compressor Pressure Ratio	18.4
Compressor Isentropic Efficiency	0.92
Splitter Remained Flow Coefficient	0.9
Combustion Efficiency	0.99
Burner Exit Temperature (K)	1443
Volume A (m ³)	0.4
Core Turbine Isentropic Efficiency	0.9
Volume B (m ³)	0.2
External Loading (MW)	21.8
Free Turbine Isentropic Efficiency	0.89
Fuel Flow Rate (kg/s)	1.269

Two inter-component volumes also exist in the turboshaft transient model, where one volume is introduced between compressor and turbine and the other between

the core gas generator turbine and free turbine. In this engine model, the handled speed is not the core shaft speed, but the free turbine speed. The performance specification at ISA SLS condition and the key performance parameters of this turboshaft engine are listed in Table 4-2.

4.1.2 Model Fuel System

4.1.2.1 Model Fuel System Simulated with ICV Method

The model fuel system used in this study for both the turbojet and turboshaft engine is shown in Fig. 3.8. The developed ICV method illustrated in section 3.3.2 has been applied for the fuel system simulation. Table 4-3 lists key parameters of the turbojet model fuel system. Table 4-4 lists key parameters of the turboshaft model fuel system.

Table 4-3 Fuel System Parameters at Design Point for Turbojet Model

Component		Value
Low Pressure Pump	Fuel Flow Rate (L/h)	4759.7
	Pressure Rise (kPa)	600
	Efficiency	0.6
Volume A	Volume (m ³)	0.0001
High Pressure Pump	Fuel Flow Rate (L/h)	7615.4
	Pressure Rise (kPa)	3500
	Efficiency	0.8
Volume B	Volume (m ³)	0.00003
Metering Unit	Fuel Flow Rate (L/h)	4759.7
	Pressure Drop (kPa)	1000
	Opening Coefficient	0.009
Volume C	Volume (m ³)	0.00003
Injector	Fuel Flow Rate (L/h)	4759.7

	Area (mm ²)	28.5
Constant Pressure Differential Valve	Spring Stiffness (N/m)	9000
	Valve Orifice Diameter (m)	0.0087
	Cone Angle (°)	22.5
	Film Area (m ²)	0.0005
	Pre-pressurized Spring Distance (m)	0.055

Table 4-4 Fuel System Parameters at Design Point for Turboshaft Model

Component		Value
Low Pressure Pump	Fuel Flow Rate (L/h)	5706
	Pressure Rise (kPa)	600
	Efficiency	0.6
Volume A	Volume (m ³)	0.0001
High Pressure Pump	Fuel Flow Rate (L/h)	9130
	Pressure Rise (kPa)	3500
	Efficiency	0.8
Volume B	Volume (m ³)	0.00003
Metering Unit	Fuel Flow Rate (L/h)	5706
	Pressure Drop (kPa)	1000
	Opening Coefficient	0.009
Volume C	Volume (m ³)	0.00003
Injector	Fuel Flow Rate (L/h)	5706
	Area (mm ²)	43.7
	Spring Stiffness (N/m)	9000

Constant Pressure Differential Valve	Valve Orifice Diameter (m)	0.0087
	Cone Angle (°)	22.5
	Film Area (m ²)	0.0005
	Pre-pressurized Spring Distance (m)	0.055

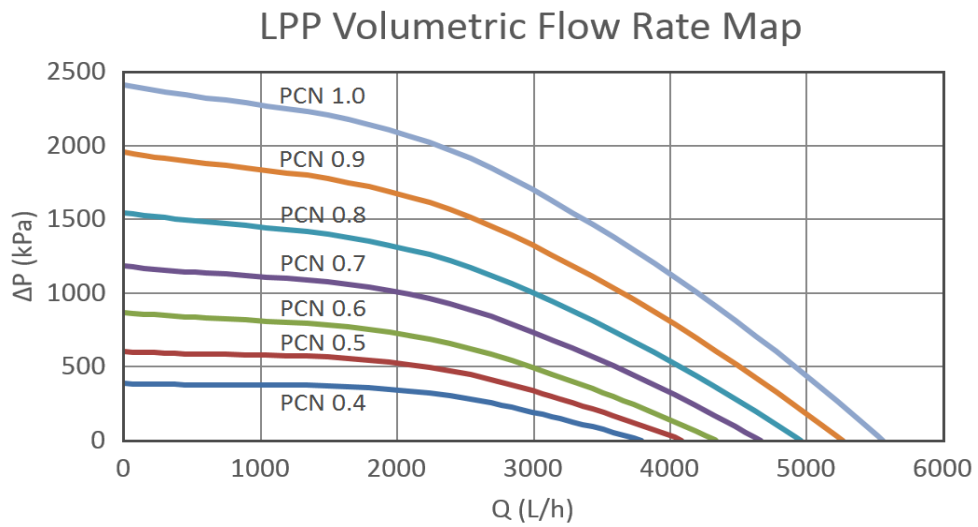


Figure 4.1 Low Pressure Pump Volumetric Flow Rate Map

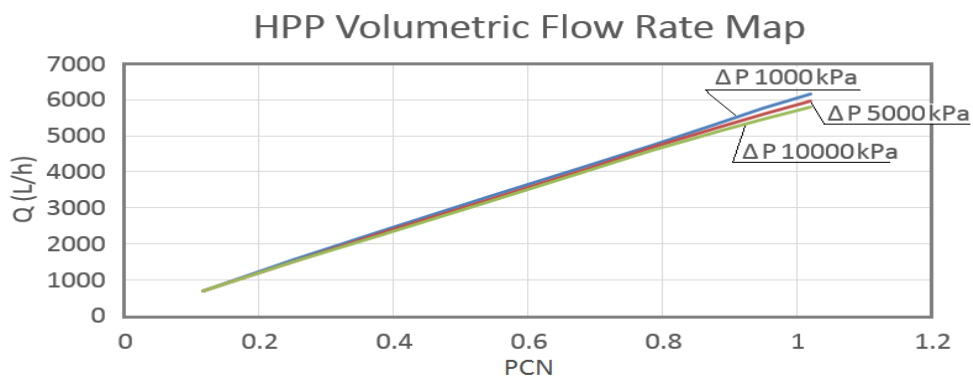


Figure 4.2 High Pressure Pump Volumetric Flow Rate Map

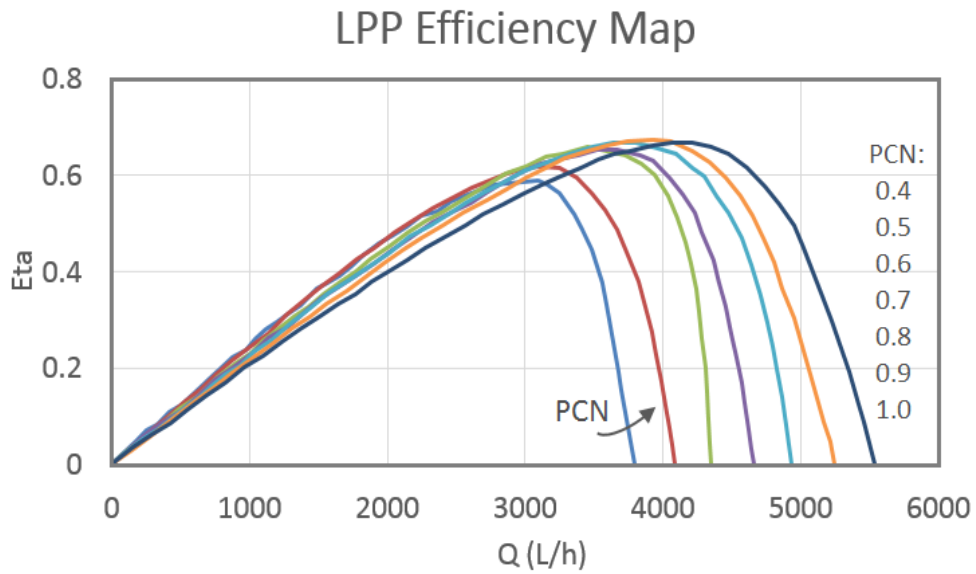


Figure 4.3 Low Pressure Pump Efficiency Map

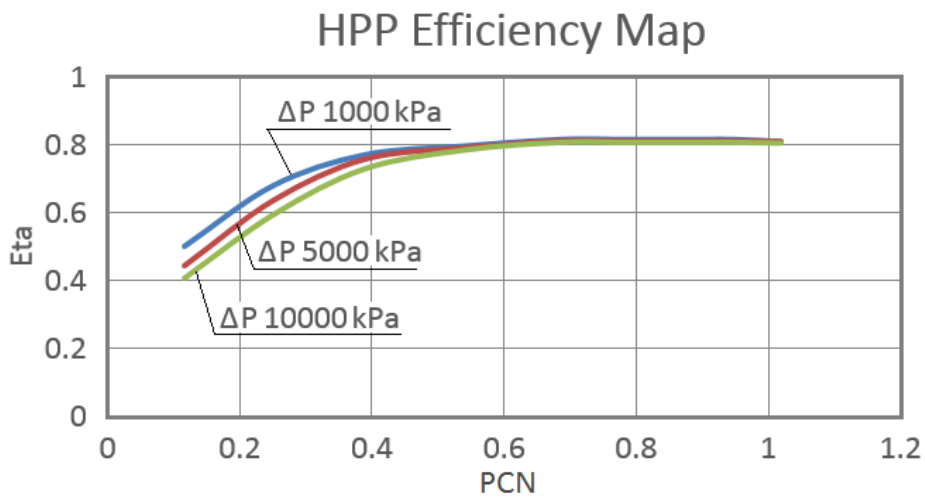


Figure 4.4 High Pressure Pump Efficiency Map

The typical volumetric flow characteristic map shown in Fig. 4.1 is for the centrifugal pump and the map shown in Fig. 4.2 is for the gear pump. The efficiency maps of these two pumps are shown in Fig. 4.3 and Fig. 4.4. These pumps' characteristic maps can be scaled for different model simulations. The developed ICV method and NR method described in an earlier part of the thesis

were applied to the fuel system for its transient performance simulation. In practice, the determination of the fuel schedule should consider keeping a large enough safety margin for compressor surge, turbine over-heating, shaft over-speeding, combustor blow out, and other similar eventualities, which are not rigorously considered in this study.

4.1.2.2 Model Fuel System Simulated with NR Methods

Previous section has illustrated the key fuel system input data and pump characteristic maps used for ICV method simulation. The input data and characteristic maps given for the model fuel system simulated with NR method are the same as the fuel system using ICV method, except the introduced inter-component volumes between system conjunct components. Those assumed volumes are used to calculate the connecting ducts' (volumes shown in Fig. 3.8) pressures to consider the flow mismatch through the system transient operation. In contrast, the NR method used for fuel system transient simulation also considers the flow mismatch, but eliminates this mismatch through a series of iterations instead of the volume dynamics calculation.

A general principle for fuel system simulation using the NR method has been described in the section 3.3.3. To the model fuel system used for research shown in Fig. 3.8, the three connecting ducts' pressures are the selected independent parameters (\mathbf{X}) whose values are calculated through the NR method iterations during each time step. The system flow mismatch at each connecting duct is calculated and the value of this flow mismatch is referred to as the mentioned Base Error (BE). The NR method aims to eliminate the values of these BE s to virtually zero which means the system reaches its pseudo steady state at current time step and can move to the calculation for the next step. After the selected variables \mathbf{X} (ducts' pressures) and the function value (BE s calculated from Eq. 3-114) have been obtained, an inverse of the system BE s Jacobian matrix which can be regarded as the $f'(X_k)$ shown in Eq. 3-97, is needed. This inverse matrix can be calculated from the Eqs. 3-110 to 3-113 and 3-115. By plugging these three arrays into the Eq. 3-108, the new variables' values which are the ducts' pressures are known for the next iteration. These ducts' pressures are given to

the fuel system to simulate the new system BEs. By comparing the norm of the BEs with the prescribed small value epsilon which is given by 0.0007 kg per time step in this research, the system pseudo steady state at this time step may be achieved or not achieved. If the system reaches its pseudo steady state at current time step, it moves to the next step calculation to obtain new ducts' pressures and system BEs until the system reaches its target steady state.

4.1.3 Model Control System

The PI control strategy has been applied to establish the model control system. The block diagram of a PI controller in co-operation with an acceleration and deceleration fuel selection logic has been represented in Fig. 3.7. The control gains of the PI controller for two model engines are given in Table 4-5 and Table 4-6. Two different integral gains are provided to the acceleration and deceleration processes to eliminate the oscillation phenomenon around the target speed. The control gains of two engine models are all obtained from manual adjustment. The engine transient fuel schedules against steady state fuel lines of model turbojet and turboshaft engines are represented in Fig. 4.5 and 4.6.

Table 4-5 PI Controller Gains for Turbojet Engine Model

	Acceleration	Deceleration
Proportional Gain K_P	8	8
Integral Gain K_I	2.8	1.03

Table 4-6 PI Controller Gains for Turboshaft Engine Model

	Acceleration	Deceleration
Proportional Gain K_P	6	6
Integral Gain K_I	2.65	1.3

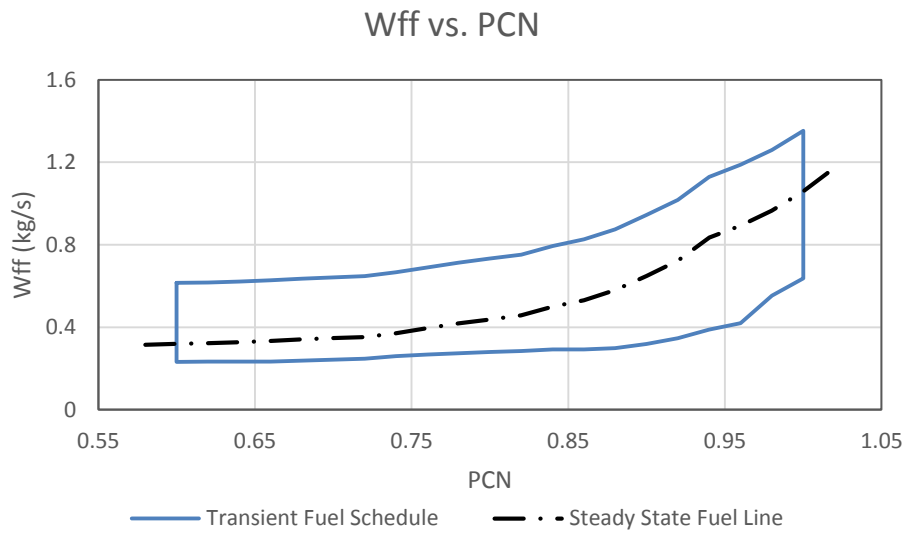


Figure 4.5 Turbojet Engine Fuel Schedule and Steady State Fuel Lines

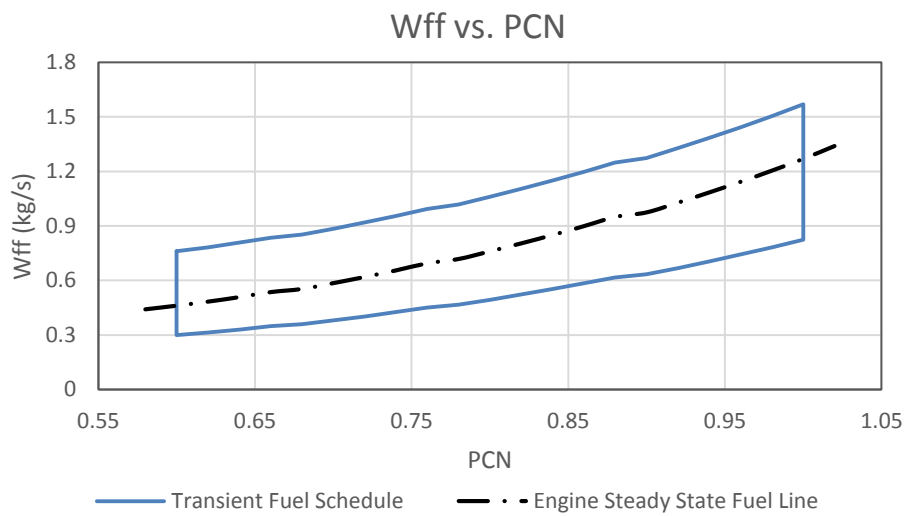


Figure 4.6 Turboshaft Engine Fuel Schedule and Steady State Fuel Lines

4.2 Engine Model Validation

4.2.1 Off-Design Steady State Validation

The newly developed engine fuel system method has first been applied to the simulation of a model single-spool turbojet aircraft engine co-operating with its fuel and control system. To ensure the accuracy of this simulation, the simulated model engine requires to be validated. Due to the lack of real experimental data from rig tests, the simulated results from newly developed model engine are compared with the same system established on both the sophisticated Cranfield gas turbine performance software TurboMatch [17] and MTU commercial software GasTurb [50].

As both the TurboMatch and GasTurb simulation platforms do not allow the fuel and control systems simulation, only a single spool turbojet engine model has been established on these two platforms, to prove the accuracy of the developed numerical engine model used in this research. The new platform, for the engine coupling its fuel and control systems simulation, is developed as a lumped component level gas turbine engine performance software, the same as TurboMatch. A similar format of the system input data file and the same compressor and turbine characteristic maps, as with TurboMatch, are used in the new platform to simulate the engine transient behaviours.

GasTurb is also a component level simulation platform but the engine structure is fixed. In mark contrast to establish the engine model based on the provided engine component bricks inside the input file of new system and TurboMatch. Engine design point input data for the validation GasTurb model are the same with the input data used for engine simulation on the newly developed platform and TurboMatch. The compressor and turbine characteristic maps can be plotted using the user required parameters' values and manually input into the software.

The compressor map is consisted of the four functions of compressor non-dimensional mass flow rate, shaft relative rotational speed, pressure ratio, and isentropic efficiency. The compressor map used for GasTurb simulation is the same with the map used for new software and TurboMatch. The turbine map for

GasTurb shows the four functions of turbine corrected relative speed, non-dimensional mass flow rate, pressure ratio (minimum and maximum) and isentropic efficiency. The turbine map used for GasTurb uses the same non-dimensional mass flow rate and isentropic efficiency with newly developed system and TurboMatch. However, the corrected rotational speed and pressure ratio use the GasTurb original map values. This is because the map for TurboMatch uses the enthalpy drop instead of pressure ratio. For the turbine corrected rotational speed, as GasTurb and TurboMatch use different scaling method, the values of this parameter on different rotational speeds are also not changed.

Engine compressor exit pressure (P_3), turbine entry temperature (TET), net thrust (NT) and specific fuel consumption (SFC) are selected to represent this validation. All these parameters are calculated at five different steady state points inside the transient simulation at sea level, ISA condition. The errors of engine key performance parameters of newly simulated engine models against with TurboMatch and GasTurb are represented at Fig. 4.7, 4.8 and Table 4-7, 4-8.

Engine design point is first calculated on each software simulation. The results on Fig. 4.7 show less than 1% errors of the key performance parameters between the new platform simulated results and TurboMatch results at the point PCN equals to 1.0. In the comparison with GasTurb results, less than 2% errors of the key parameters are also shown in Fig. 4.8.

When the shaft relative rotational speed decreases, the errors shown in Fig. 4.7 become larger. The reason produced such errors is mainly affected by a prescribed constant relative pressure drop across the combustor in the newly developed platform. This consideration reduces the turbine work at the given fuel flow rate. It results in the increase of the air stream at lower rotational speed which produces lower turbine entry temperature and engine net thrust but higher engine SFC.

Off-Design Simulation Results Comparison between TurboMatch and Newly Simulated Engine Models

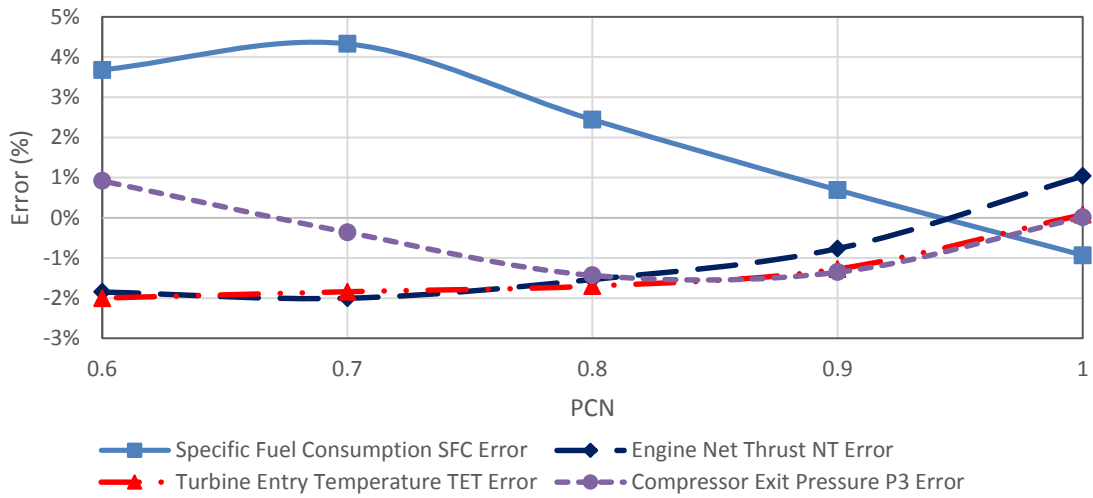


Figure 4.7 Off-Design Steady State Results Comparison at Sea Level, ISA Condition between TurboMatch and Newly Simulated Engine Models

Off-Design Simulation Results Comparison between GasTurb and Newly Simulated Engine Models

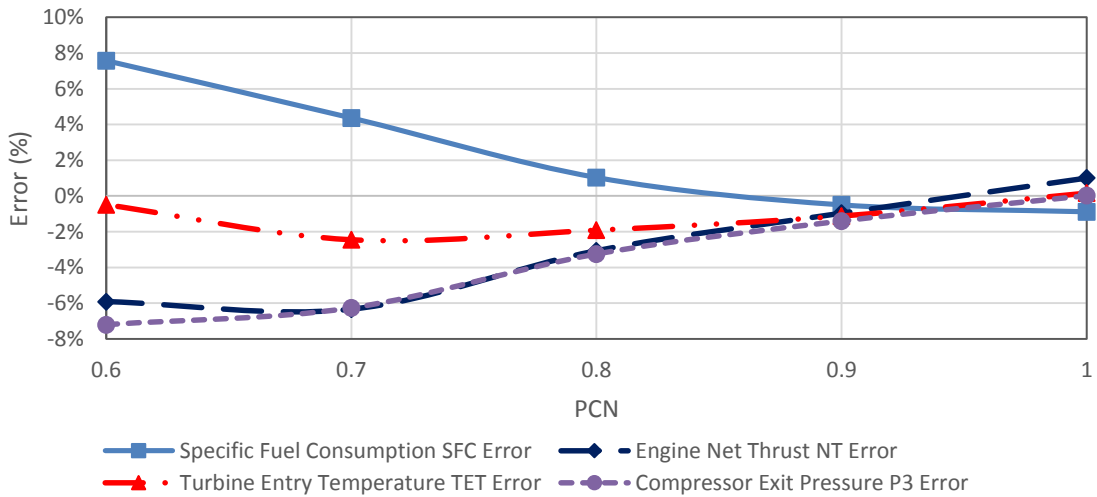


Figure 4.8 Off-Design Steady State Results Comparison at Sea Level, ISA Condition between GasTurb and Newly Simulated Engine Models

The errors shown in Fig. 4.8 on low engine shaft speeds also become larger. In addition to the combustor constant pressure drop mentioned in the comparison with TurboMatch model, the different turbine maps used in the new system and GasTurb model are also the reasons producing larger errors between the two models at lower shaft relative rotational speeds.

A detailed illustration of the differences are represented in Tables 4-7 and 4-8 below, in percentages. Table 4-7 shows that the parameters' differences with TurboMatch results are less than 5%. The comparison with GasTurb model in Table 4-8 shows the differences are less than 8%. Therefore, according to the comparison of key performance parameters between the new model and validation model of TurboMatch and GasTurb, the new engine model used for engine integrated with its fuel and control system simulation is acceptable.

Table 4-7 Off-Design Key Performance Parameters Comparison between Newly Simulated Engine Model and TurboMatch Simulated Engine Model (%)

Parameters PCN	Compressor Outlet Pressure (P_3)	Turbine Entry Temperature (TET)	Net Thrust (NT)	Specific Fuel Consumption (SFC)
1.0	0.02%	0.08%	1.04%	-0.93%
0.9	-1.35%	-1.28%	-0.76%	0.69%
0.8	-1.43%	-1.70%	-1.53%	2.44%
0.7	-0.36%	-1.84%	-2.00%	4.10%
0.6	0.92%	-2.00%	-1.85%	3.68%

Table 4-8 Key Performance Parameters Comparison between Newly Simulated Engine Model and GasTurb Simulated Engine Model (%)

Parameters PCN	Compressor Outlet Pressure (P_3)	Turbine Entry Temperature (TET)	Net Thrust (NT)	Specific Fuel Consumption (SFC)
1.0	0.02%	0.16%	1.00%	-0.89%
0.9	-1.41%	-1.12%	-0.96%	0.50%
0.8	-3.25%	-1.91%	-3.07%	1.03%
0.7	-6.27%	-2.45%	-6.34%	4.37%
0.6	-7.21%	-0.49%	-5.92%	7.57%

4.2.2 Transient Validation

Fig. 4.9 is the transient trajectories of engine key performance parameters: spool PCN, W_{ff} , TET, engine net thrust NT and compressor exit pressure responding to the rotational speed command between GasTurb and newly simulated engine models. It can be seen that through most of the transient process, the errors of all the listed parameters are less than 10% against the GasTurb engine model. However, there are several points where the errors do exceed 10%. The reason produces such errors is the fuel trajectories used to regulate the engine transient processes on the newly developed platform and GasTurb are different. In the new software, the engine fuel schedule is given as the prescribed fuel flow rate against the shaft relative rotational speed (shown in Fig. 4.5). The engine controller, working in co-operation with the fuel selection logic, decides the proper engine required fuel flow rate based on the engine current rotational speed and its command speed. In contrast, the fuel schedule used for GasTurb platform simulation is the engine required fuel flow rate against time. The differences between two fuel schedules result in the errors, green dot line shown in Fig. 4.9,

between the two engine actual fuel flow rate lines for both platforms simulated models. The errors for other listed parameters which exceed 10% are all happened at the points where the fuel flow rate errors are large.

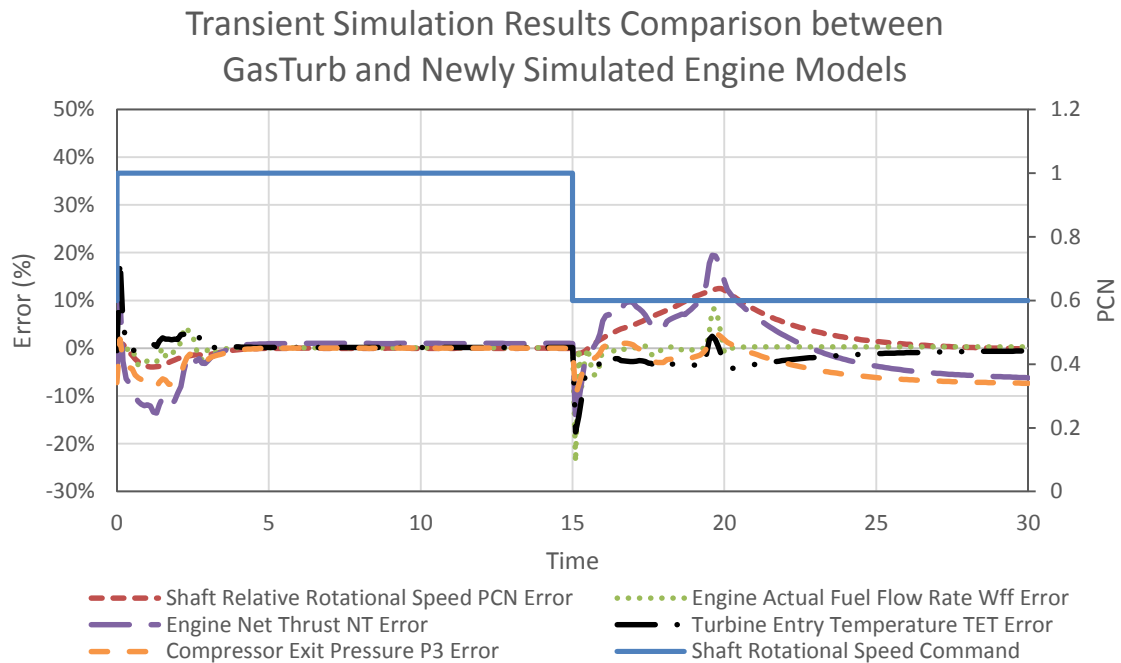


Figure 4.9 Transient Trajectories Comparison at Sea Level, ISA Condition between GasTurb and Newly Simulated Engine Models

4.3 Engine Transient Performance Simulation Co-operating with its Control and Fuel System

4.3.1 Turbojet Engine with Fuel System Developed Using ICV Method

The transient performance of the model turbojet engine has been simulated using the integrated engine, control and fuel system shown in Fig. 3.18. It is assumed that the model engine is operating at sea level, ISA condition. It is also assumed that the engine starts acceleration from its steady state condition at PCN of 0.6, accelerates to its maximum power at PCN of 1.0, stays at the maximum condition for about 16 seconds and then decelerates back to the PCN of 0.6.

Fig. 4.10 shows the PCN command signal against the actual PCN variation during the whole transient process of 60 seconds. Compared with the command signal in this figure, the delay of the actual PCN response is due to the transient response to the engine and its control and fuel systems. According to the transient requirement of military engines at sea level condition in Ref. 18, typical acceleration time from idle to 0.98 PCN should be less than 4s and deceleration time from take off thrust to the 75% thrust change between take off and minimum idle is about 4s. For civil engines, the transient time should be regulated a little bit longer than the military engines. Typical acceleration time at sea level condition is about 5s and deceleration time should be less than 4.5s.

In this turbojet engine model co-operating with its fuel and control system, in which the fuel system is simulated with ICV method, it is assumed that the idle speed at sea level condition is PCN 0.6. The acceleration time from PCN 0.6 to PCN 0.98 (Thrust 95%) is registered at about 3.2s and deceleration time from PCN 1.0 to PCN 0.65 (Thrust 75% change) at about 4.0s. By selecting different fuel schedules and PI control gains, the transient time will be adjusted to fulfil the requirements of different applications.

Fig. 4.11 shows a comparison between the fuel command signal provided by the fuel selection logic and the actual fuel flow rate delivered by the control and fuel system over time. It can be seen that during the acceleration process the delivered fuel flow rate follows the fuel schedule initially and then deviates from the fuel schedule at about 3.6s. This is because the fuel controller takes over the fuel control task and controls the fuel flow rate based on the difference between the desired and actual engine shaft speed PCN. A similar phenomenon can be observed during the deceleration process where the fuel flow rate follows the fuel schedule until at around 34.8s and then the controller takes over the fuel control until the engine reaches its desired steady state end condition. It can be seen that during the acceleration and deceleration processes, the actual injected fuel flow rate into the combustor is delayed, compared to the fuel command, when the fuel schedule governs the fuel flow rate. This phenomenon is a result of the

response of engine fuel system introduced into the system transient performance simulation.

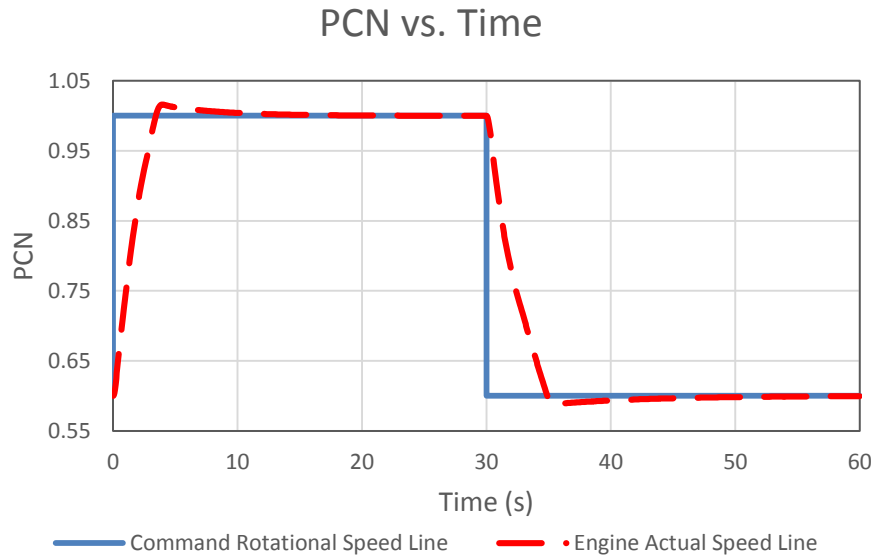


Figure 4.10 Model Turbojet Engine PCN vs. Time at Sea Level, ISA Condition

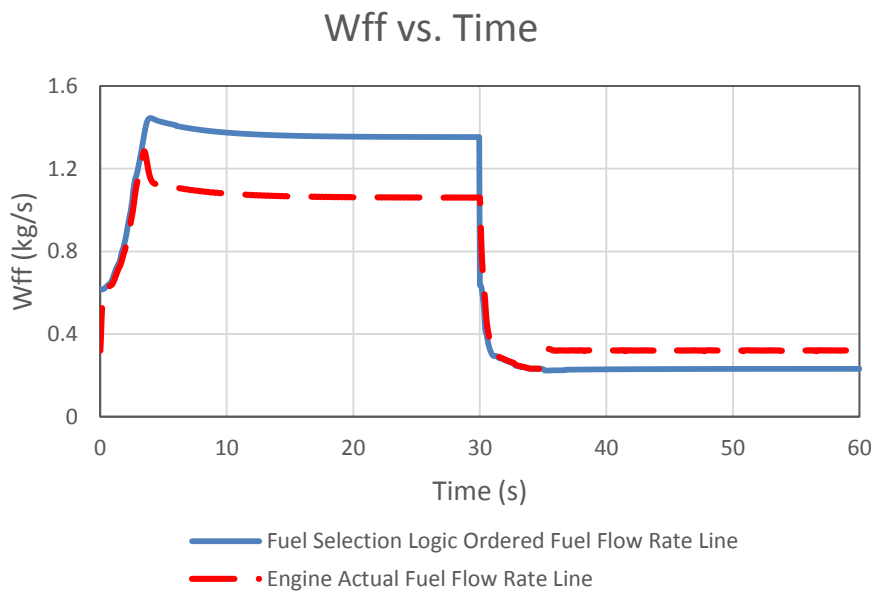


Figure 4.11 Model Turbojet Engine Wff vs. Time at Sea Level, ISA Condition

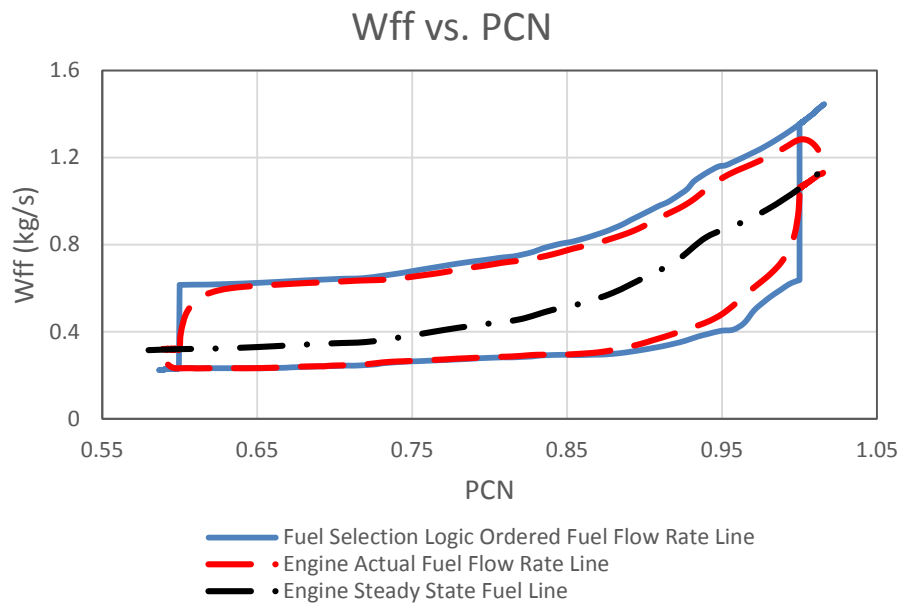


Figure 4.12 Model Turbojet Engine Wff vs. PCN at Sea Level, ISA Condition

Fig. 4.12 above shows a comparison of the trajectory of actual fuel flow variation against those from the fuel schedules for the acceleration and the deceleration processes. It is also compared with the engine fuel flow rate at steady state conditions. There appears to be a gap between fuel schedule regulated fuel line and engine actual fuel line. This is produced by the delay response of the fuel system to the controller fuel command. From Fig. 4.10 to 4.12, the applicability of developed ICV method on engine fuel system transient simulation has been proved.

4.3.2 Turbojet Engine with Fuel System Developed Using NR Method

The last section has represented the simulated transient process of a turbojet model engine with its fuel and control system. In that model, the fuel system transient performance is simulated using the recently developed ICV method. However, as the liquid fuel oil is mostly considered highly incompressible, the fuel system simulation using ICV method may not be convincing. In that case, a freshly developed Newton Raphson method has been introduced to simulate the fuel system of the same model engine with its control and fuel system. In this new

model, it is also assumed that the model engine is running at sea level, ISA condition. The same transient processes, including acceleration from PCN 0.6 to 1.0 and deceleration from PCN 1.0 to 0.6, are also applied in order to validate the results.

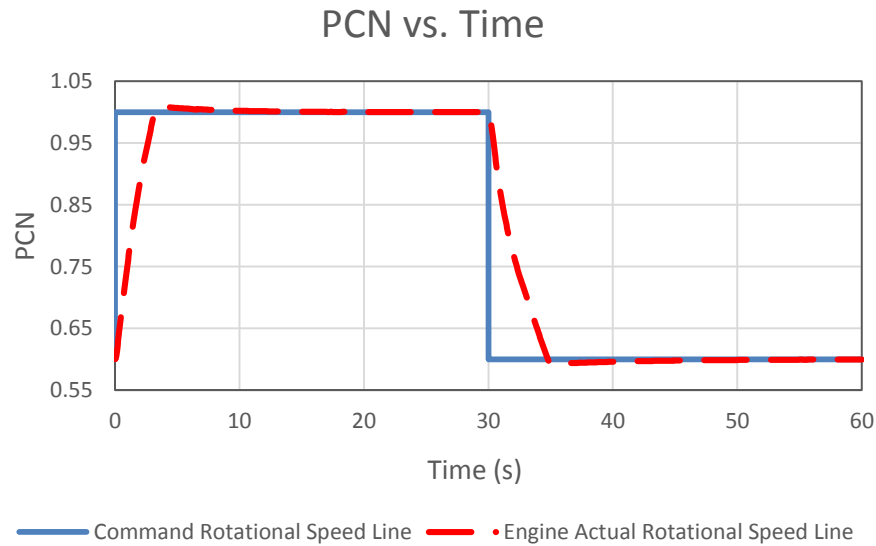


Figure 4.13 Model Turbojet Engine PCN vs. Time at Sea Level, ISA Condition

Fig. 4.13 above shows the variation of PCN command signal against the actual PCN during the whole transient process of 60 seconds. A similar process shown in Fig. 4.10 shows that the actual engine PCN lags behind the PCN command because of the transient response of engine and its control and fuel systems. The acceleration time from PCN 0.6 to PCN 0.98 (Thrust 95%) is registered at about 3.0s and deceleration time from PCN 1.0 to PCN 0.65 at about 3.9s. Compared with the model fuel system simulation with ICV method, the transient time of this model is faster. In addition, when the engine's actual rotational speed approaches its target speed commands in both acceleration and deceleration processes, less overshoots appear.

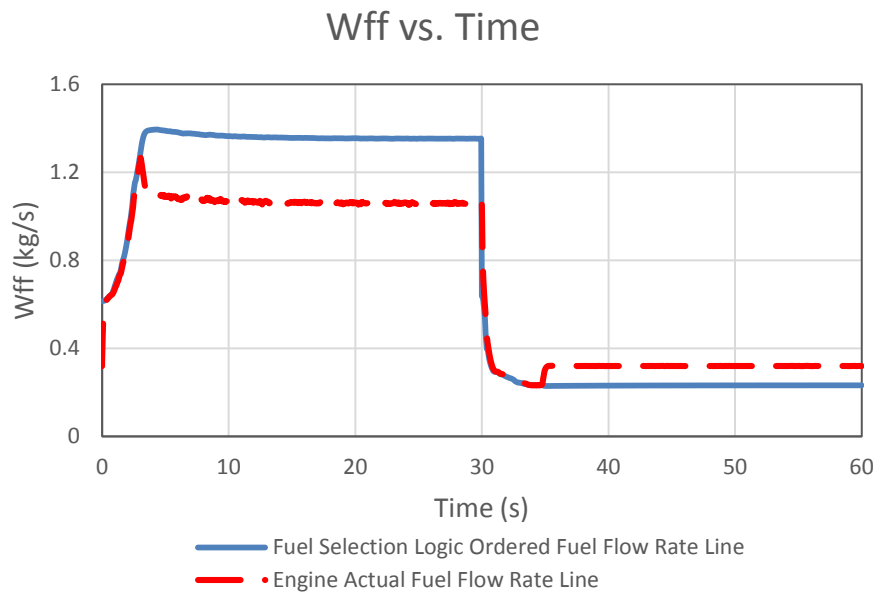


Figure 4.14 Model Turbojet Engine Wff vs. Time at Sea Level, ISA Condition

Fig. 4.14 above shows the comparison between fuel selection logic regulated fuel command signal and the actual engine fuel of the model engine. As with the previous model, the delivered fuel flow rate follows the fuel schedule initially and then deviates from the fuel schedule at about 3.1 seconds. During deceleration, the time when the controller takes over the fuel flow regulation task, based on the speed error, is at about 34.8s. In the acceleration process after the engine speed approaches its target, small oscillations of engine actual fuel flow keep appearing to regulate the engine rotational speed. However, from the engine speed line point of the view in Fig. 4.13, the engine speed line is very smooth approaching its target command and stays at the target speed until the deceleration process begins. Therefore, these small oscillations around target fuel command are acceptable.

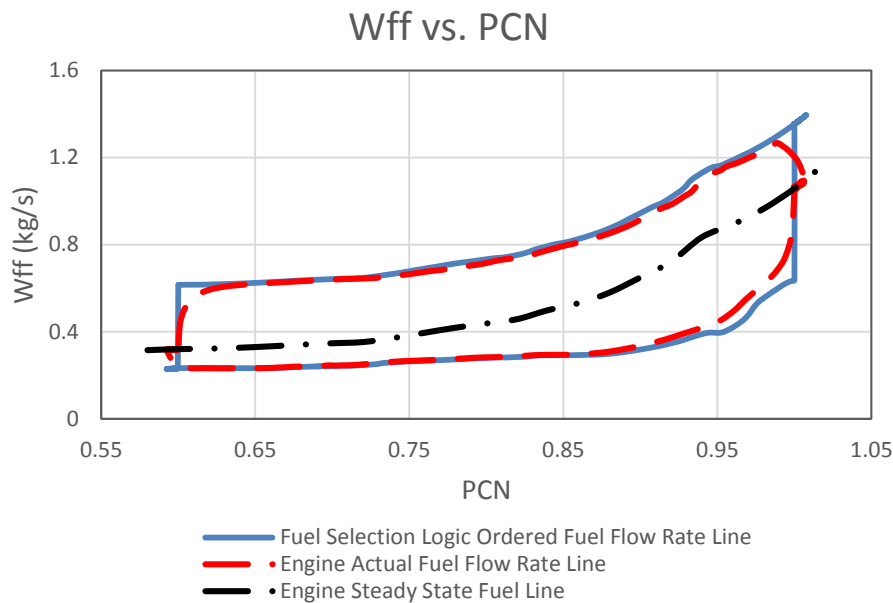


Figure 4.15 Model Turbojet Engine Wff vs. PCN at Sea Level, ISA Condition

Fig. 4.15 above shows the comparison between actual fuel flow trajectories and fuel schedules for the acceleration and deceleration processes of a turbojet engine model for which the fuel system is simulated with NR method. The engine steady state fuel line is also compared with the transient trajectories. From Figs. 4.13 to 4.15, the availability of a freshly developed NR method on engine fuel system transient simulation has been proved. A more detailed illustration of the comparison between the fuel system using both a newly developed ICV method and NR method for the same model engine, coupled with its fuel and control system, will be presented in section 4.3.4.

4.3.3 Turbojet Engine with and without Fuel System Transient Simulation Results Comparison

To demonstrate the impact of the inclusion of the fuel system model in the engine transient performance simulation, a comparison of the simulated transient processes with and without the fuel system model is made in the following figures. The represented fuel system involved in the transient process has been simulated based on the developed ICV method. By applying the same transient processes of acceleration and deceleration just described in Section 4.3.1, the fuel flow rate

variations of the model engine are shown in Fig. 4.16 where the delayed transient responses (by about 0.5 seconds during acceleration, and 0.3 seconds during deceleration), clearly enable the engine to reach its target rotational speed due to the inclusion of the fuel system model is obvious.

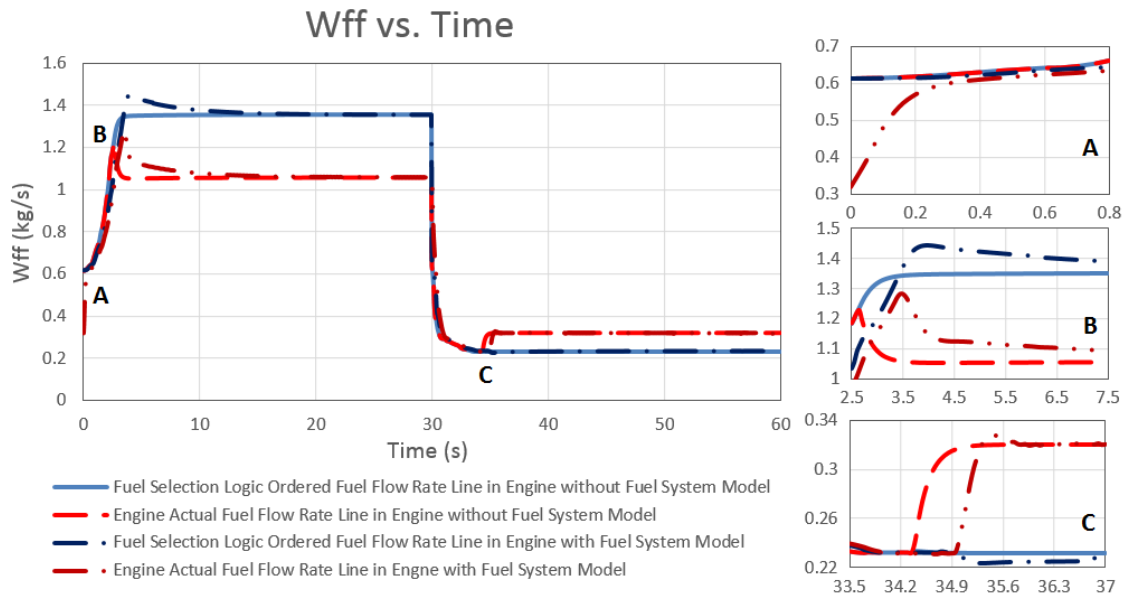


Figure 4.16 Model Turbojet Engine Wff vs. Time Comparison at Sea Level, ISA Condition between Engine with and without Fuel System Transient Simulation

The most significant delays happen at the points where the fuel flow control is switched between the fuel schedule and the fuel controller. Through the acceleration process, the delay time around the switching region shown in Fig. 4.16 point B is about 0.8s. The deceleration delay time around point C is about 0.5s. However, as the fuel system introduced into the model engine transient simulation produces overshoots of the fuel selection logic ordered fuel line, the model engine, in reaching its target acceleration speed PCN 0.98, has a 0.5s delay. A similar phenomenon occurs during deceleration, so in reaching PCN 0.65, there is a 0.3s delay compared with the model engine without fuel system. This phenomenon can be observed from the rotational speed comparison in Fig. 4.18.

Another obvious difference between the model engine with and without fuel system simulation is at the starting point of the transient simulation at Fig. 4.16 point A. In the engine without fuel system model, the actual fuel flow rate into the engine combustor directly jumps to the fuel selection logic ordered fuel flow rate and overlaps with the ordered fuel line until the controller takes over the regulation task. However, in the engine with a fuel system model, the actual fuel flow rate starts from the steady state point fuel flow rate. It is then smoothly varied approaching the fuel selection logic ordered fuel line. This process takes about 0.3s shown in Fig. 4.16 point A.

In addition to the illustrated differences observed from Fig. 4.16, the inclusion of the fuel system in the engine transient performance also extends the calculation time of the whole transient process. For the engine *without* the fuel system simulation, the actual computer calculation time is 19.3 seconds, whereas for the engine *with* fuel system developed with ICV method, the simulation time takes 25.9 seconds.

Fig. 4.17 below is the actual engine fuel trajectories and fuel schedules comparison between model turbojet engine with and without fuel system. As shown in Fig. 4.17, the fuel schedules of two engine models are overlapped. It demonstrates that both these models utilize the same transient fuel schedules (Wff versus PCN). A slight extension of both the acceleration and deceleration fuel selection logic ordered fuel line of the engine with fuel system model (Blue Long Dash Line with one Dot) can be observed due to the overshoot phenomenon of the engine actual fuel (Red Long Dash Line with two Dots). The red long dash line which represents the model engine without fuel system actual fuel line overlaps with the fuel schedule (Blue Solid Line). It can be also observed that a gap between the engine actual fuel line (Red Long Dash Line with two Dots) and fuel selection logic ordered fuel line (Blue Long Dash Line with one Dot) exists. This is due to the delay caused by the action of the fuel system components and the effect of the inter-component volumes introduced into the fuel system simulation.

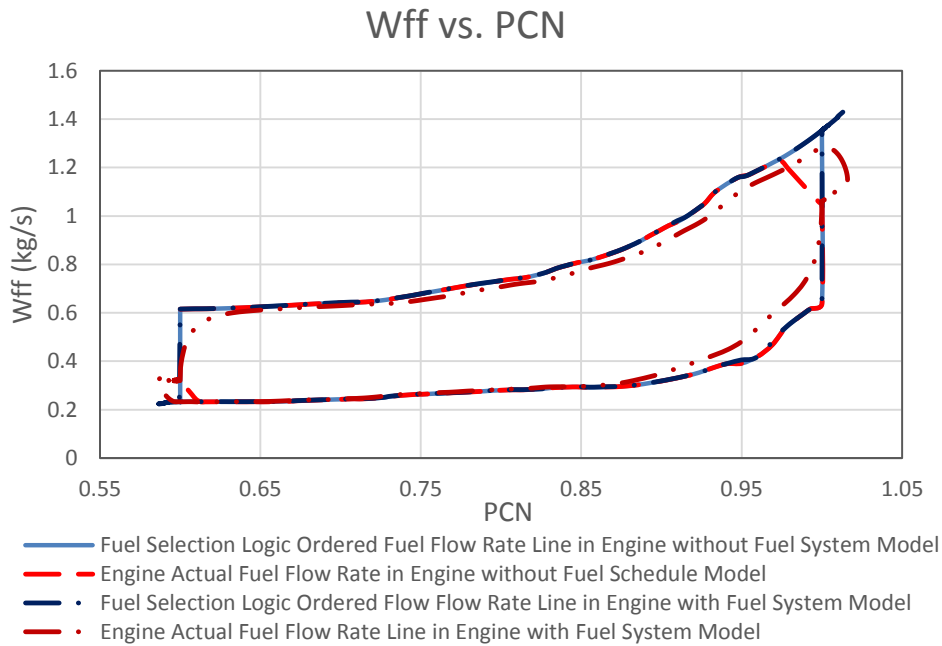


Figure 4.17 Model Turbojet Engine Wff vs. PCN Comparison at Sea Level, ISA Condition between Engine with and without Fuel System Transient Simulation

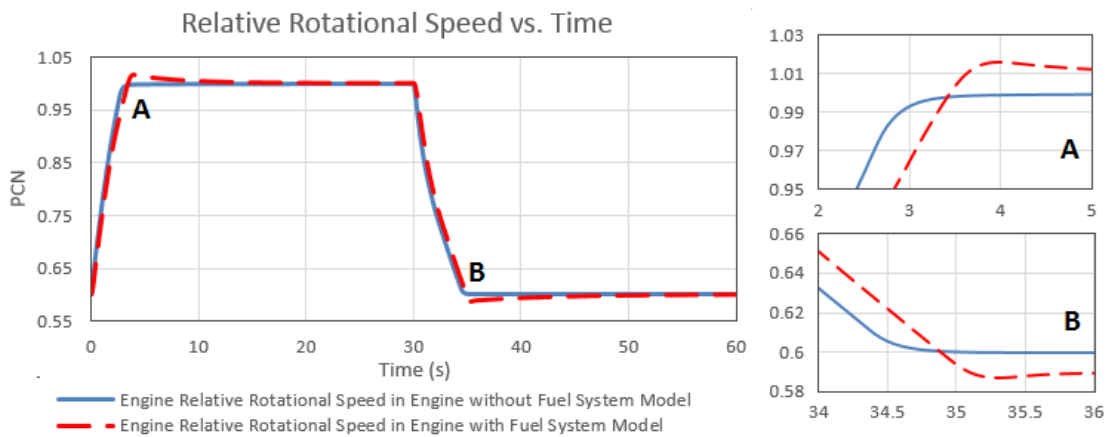


Figure 4.18 Model Turbojet Engine PCN vs. Time Comparison at Sea Level, ISA Condition between Engine with and without Fuel System Transient Simulation

More engine parameters, such as PCN, TET and compressor exit pressure P_3 varying over time for the same transient process are also shown in Figs. 4.18 to 4.20. It can be seen from the figures that the predicted variations of these

parameters with and without the inclusion of the fuel system model follow the same pattern as that shown in Fig. 4.16 and that the differences are small.

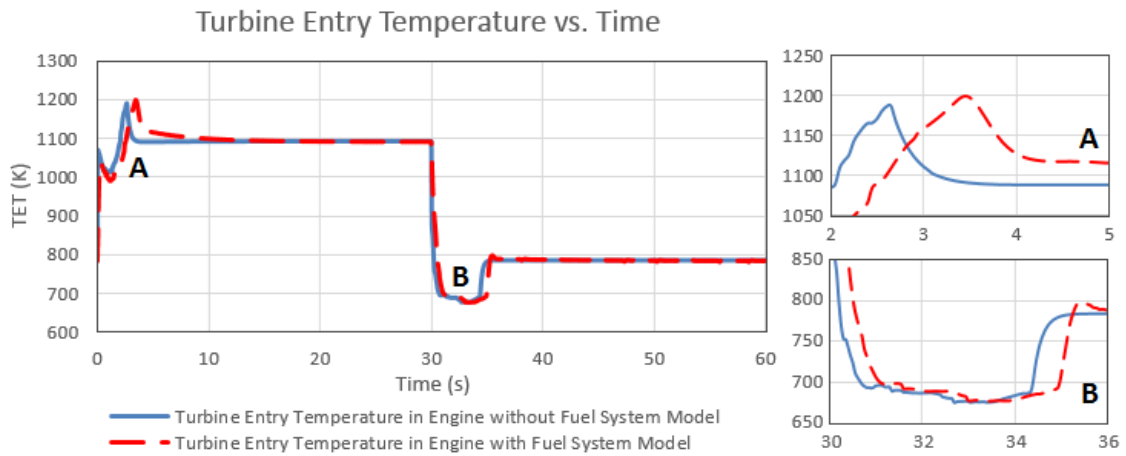


Figure 4.19 Model Turbojet Engine TET vs. Time Comparison at Sea Level, ISA Condition between Engine with and without Fuel System Transient Simulation

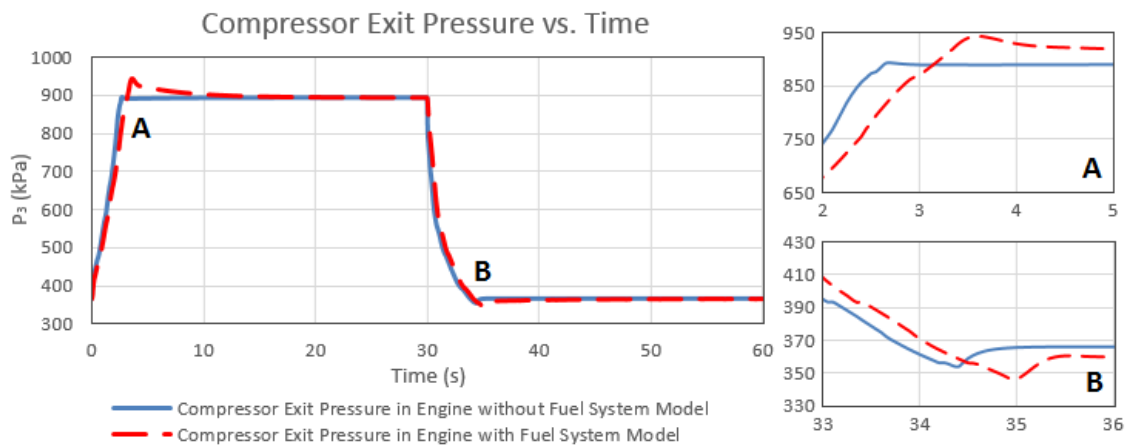


Figure 4.20 Model Turbojet Engine P_3 vs. Time Comparison at Sea Level, ISA Condition between Engine with and without Fuel System Transient Simulation

4.3.4 Turbojet Engine with Fuel System Transient Simulation Results Comparison between the Developed ICV and NR Method Applied for Fuel System Simulation

To demonstrate the impact of the developed two methods of fuel system simulation, a comparison of the simulated transient processes with the fuel system model developed, based on ICV and NR methods, is made in the following. For the same transient process of acceleration and deceleration just described above, the fuel flow rate variations of the model engine are shown in Fig. 4.21.

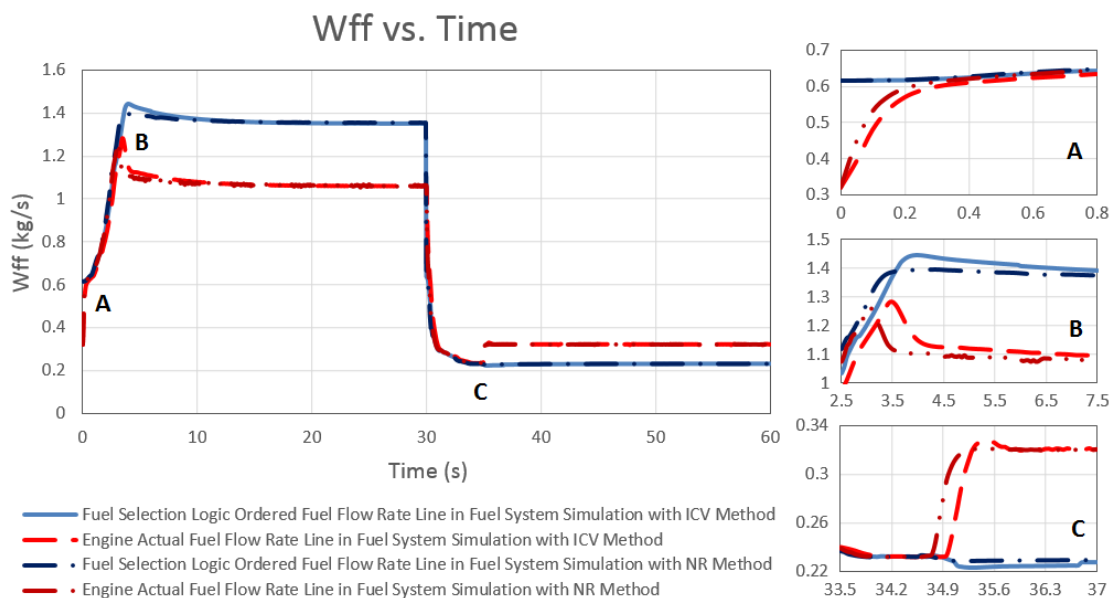


Figure 4.21 Model Turbojet Engine Wff vs. Time Comparison at Sea Level, ISA Condition between the Developed ICV and NR Methods Applied on the Fuel System Transient Simulation

In the last section, the comparison between the model engine without fuel system and the model engine with fuel system developed with ICV method has represented a 0.5s delay effect to the target speed due to the fuel system included in the engine system. This phenomenon is produced by the action of the fuel system components and the effect of the inter-component volumes. In the fuel system model developed with NR method, the inter-component volumes

have been omitted to ignore the fuel compression effect between the conjunct fuel system components. Therefore, it can be observed that both the fuel selection logic ordered fuel line (Blue Long Dash Line with two Dots) and fuel actual fuel line (Red Long Dash Line with one Dot) of NR method simulated model (Case Two) are in advance of the fuel lines of ICV method simulated fuel system model (Case One). The most significant advance phenomenon also happens at the points where the fuel flow control is switched between the fuel schedule and the fuel controller. Through the acceleration process, the advance time around the switching region shown in Fig. 4.21 point B is about 0.5s. The deceleration advance time around point C is about 0.3s. This is due to the omission of inter-component volumes introduced in the ICV method.

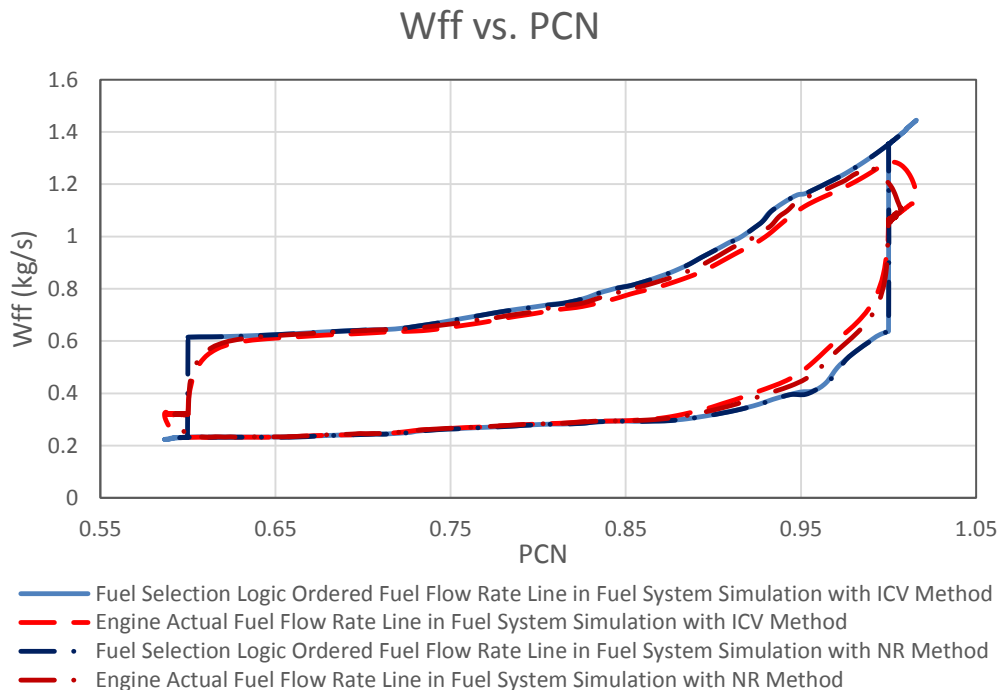


Figure 4.22 Model Turbojet Engine Wff vs. PCN Comparison at Sea Level, ISA Condition between the Developed ICV and NR Methods Applied on the Fuel System Transient Simulation

Fig. 4.22 above is the comparison between the engine actual fuel and fuel selection logic ordered fuel trajectories of two model cases. The overlap of the

fuel trajectories proves that the same transient fuel schedule has been applied. Compared with case one, the case two model (NR method) represents fewer overshoots around both the acceleration and deceleration setpoint speed. The actual fuel line of case two is also closer to the fuel selection logic ordered fuel line. The phenomenon also follows the same rationale introduced in Fig. 4.21.

More engine parameters, such as PCN, TET, and compressor exit pressure P_3 varying over time for the same transient process are also shown in Figs. 4.23 to 4.25. It can be seen from the figures that the predicted variations of these parameters of the fuel system model simulated with the developed ICV method and NR method follow the same pattern as that shown in Fig. 4.21 and that the differences are small.

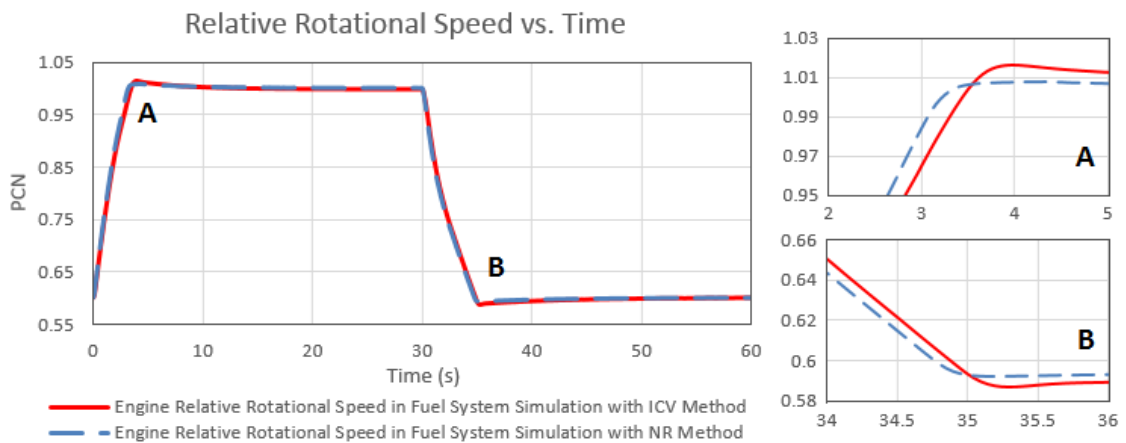


Figure 4.23 Model Turbojet Engine PCN vs. Time Comparison at Sea Level, ISA Condition between the Developed ICV and NR Methods Applied on the Fuel System Transient Simulation

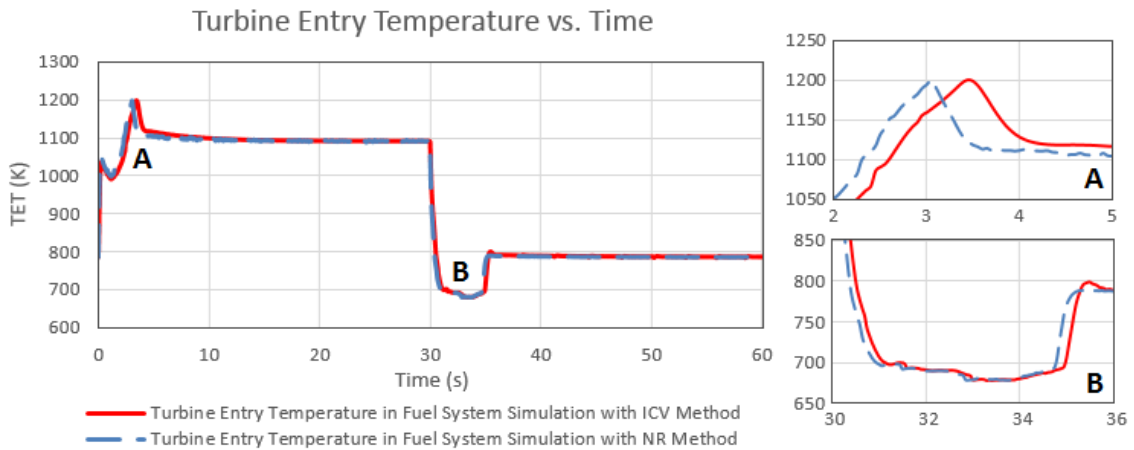


Figure 4.24 Model Turbojet Engine TET vs. Time Comparison at Sea Level, ISA Condition between the Developed ICV and NR Methods Applied on the Fuel System Transient Simulation

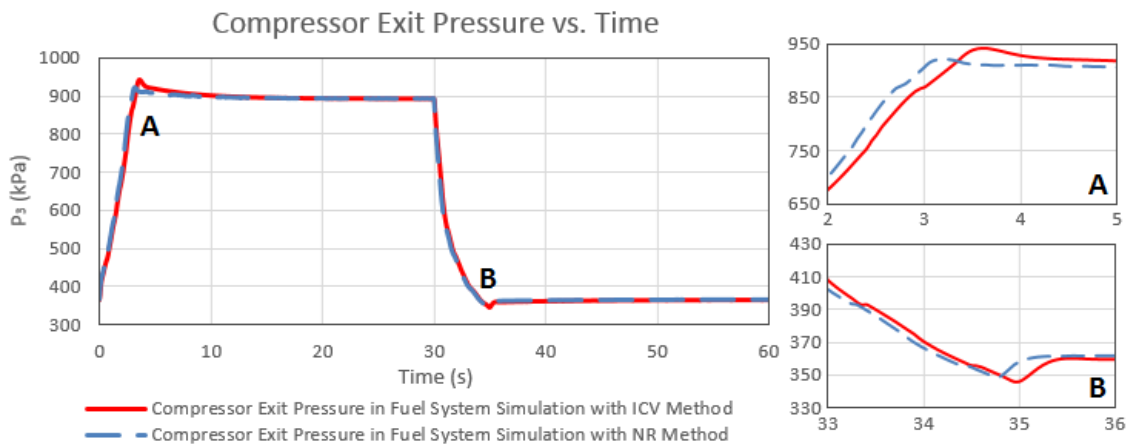


Figure 4.25 Model Turbojet Engine P_3 vs. Time Comparison at Sea Level, ISA Condition between the Developed ICV and NR Methods Applied on the Fuel System Transient Simulation

4.3.5 Turboshaft Engine with Fuel System Developed Using ICV Method

The previous two models in Sections 4.3.1 and 4.3.2 have represented the application of the developed ICV method and NR method on engine fuel system simulation by simulating the same model turbojet engine coupled with its fuel and control system. To investigate the flexibility of these two methods on the fuel system simulation of other types of engines, a turboshaft engine is selected to be modelled. The transient performance of the model turboshaft engine has also been simulated using the integrated engine, control and fuel system shown in Fig. 3.18. However, in contrast to the turbojet engine to handle the gas generator shaft speed, the rotational speed ratio of the free turbine shaft is measured to regulate the transient required fuel flow rate. It is assumed that the model engine is running at sea level, ISA condition. It is also assumed that the engine starts acceleration from its free turbine speed at PCN of 0.6, accelerates to its maximum output power at PCN of 1.0, stays at the maximum condition for about 20 seconds and then decelerates back to the PCN of 0.6.

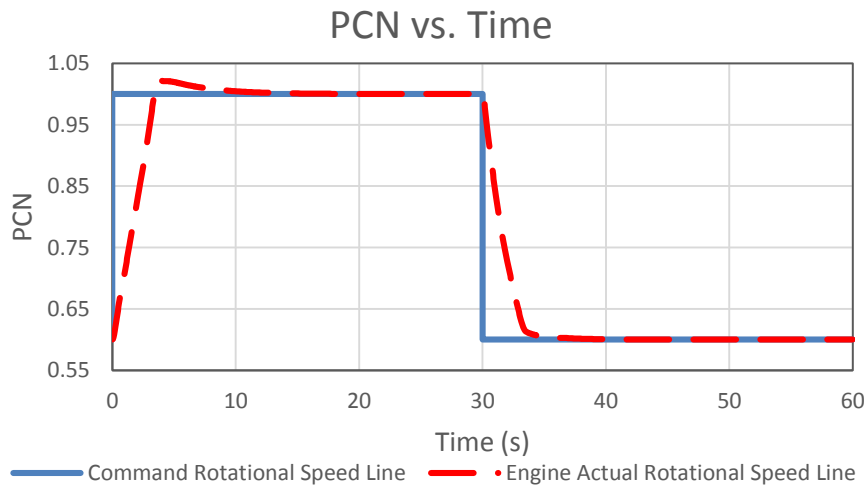


Figure 4.26 Model Turboshaft Engine PCN vs. Time at Sea Level, ISA Condition

Fig. 4.26 shows the turboshaft engine free turbine PCN command signal against the actual PCN variation during the whole transient process of 60 seconds. The acceleration time from PCN 0.6 to PCN 0.98 is registered at about 3.26s and

deceleration time from PCN 1.0 to PCN 0.65 is at about 2.88s. For the same reason, the delay of engine PCN to command is due to the transient response of the engine and its control and fuel systems.

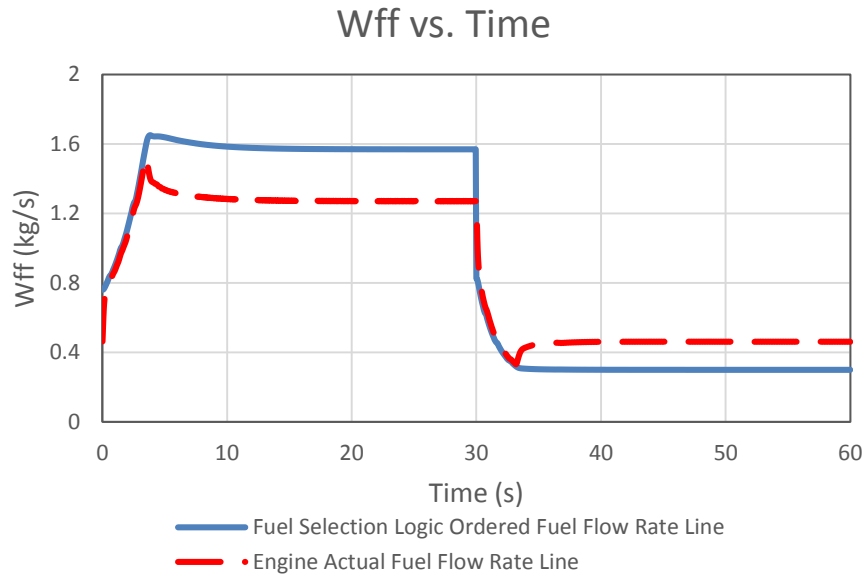


Figure 4.27 Model Turboshaft Engine Wff vs. Time at Sea Level, ISA Condition

Fig. 4.27 above shows the comparison between the fuel selection logic regulated fuel order and the actual consumed fuel flow rate of a turboshaft engine. The separation time when the controller handle adjusts the fuel regulation from the speed error during acceleration is at about 3.55s. A similar phenomenon during deceleration process is at about 33.2s.

Fig. 4.28 is the comparison between actual fuel flow trajectories and fuel schedules for the acceleration and deceleration processes of a model turboshaft engine coupled with its fuel and control system simulation. The engine steady state fuel line is also represented in this figure in order to compare with the transient trajectories. From the transient simulation results shown in Fig. 4.26 to 4.28, the flexibility of the ICV method used for a turboshaft engine fuel system simulation has been proved.

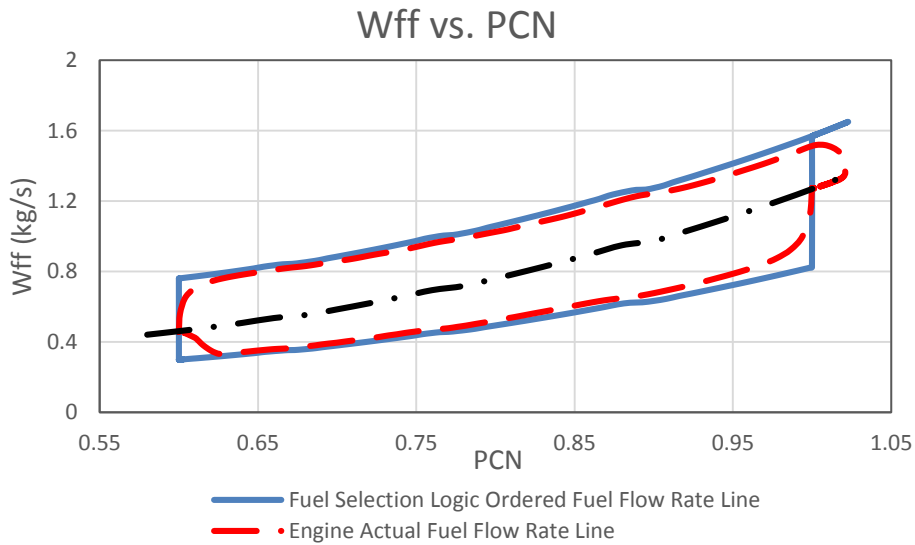


Figure 4.28 Model Turboshhaft Engine Wff vs. PCN at Sea Level, ISA Condition

4.3.6 Turboshhaft Engine with Fuel System Developed Using NR Method

By using the same turboshhaft engine model in conjunction with its fuel and control systems represented in Section 4.3.5, the transient processes of model turboshhaft engine with the fuel system simulated using NR method will also be represented in this section.

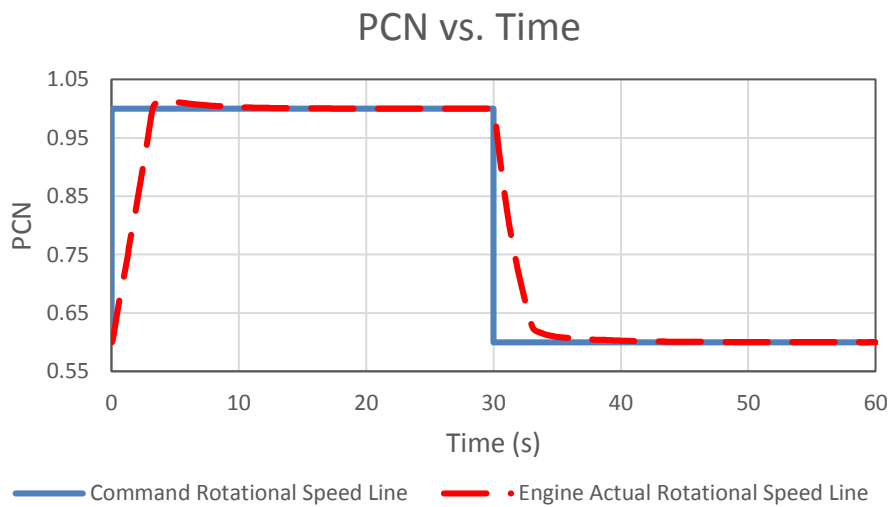


Figure 4.29 Model Turboshhaft Engine PCN vs. Time at Sea Level, ISA Condition

Fig. 4.29 above shows the turboshaft engine free turbine PCN command signal against the actual PCN variation during the whole transient process of 60 seconds. The acceleration time reaching PCN 0.98 is at about 3.08s and deceleration time to PCN 0.65 is at about 2.72s. Compared with the turboshaft engine with the fuel system modelled with ICV method in Fig. 4.26, the transient time of NR method simulated model is faster. During the acceleration, a smaller overshoot can be observed when the shaft rotational speed approaches its target command.

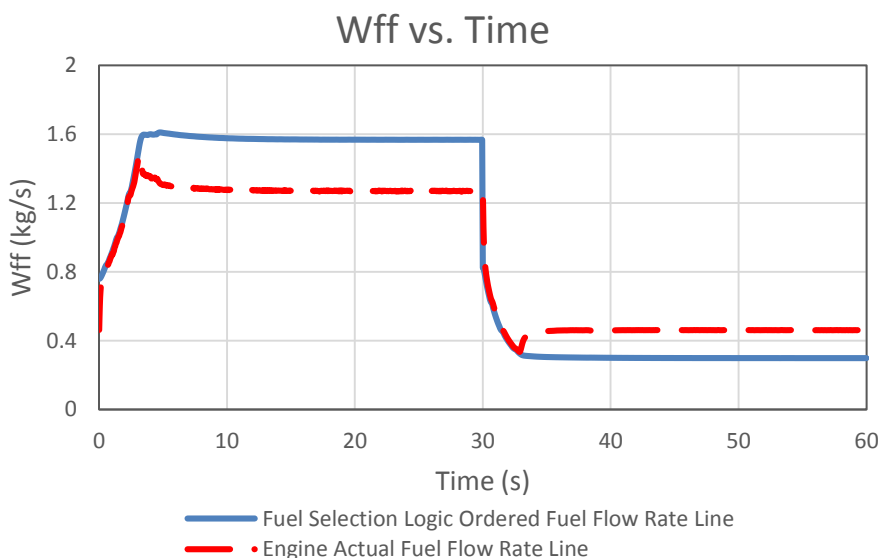


Figure 4.30 Model Turboshaft Engine Wff vs. Time at Sea Level, ISA Condition

Fig. 4.30 above is the comparison between the fuel selection logic ordered fuel flow rate signal and the engine actual fuel flow rate. The separation time of acceleration process from the fuel schedule regulated fuel to the controller governed fuel from rotational speed error is at about 3.2s. During the deceleration process, this separation time is at about 32.9s. Compared with the fuel system modelled with the ICV method in Fig. 4.27, the fuel system modelled with NR method does not represent any obvious delay phenomenon to the controller command in Fig. 4.30.

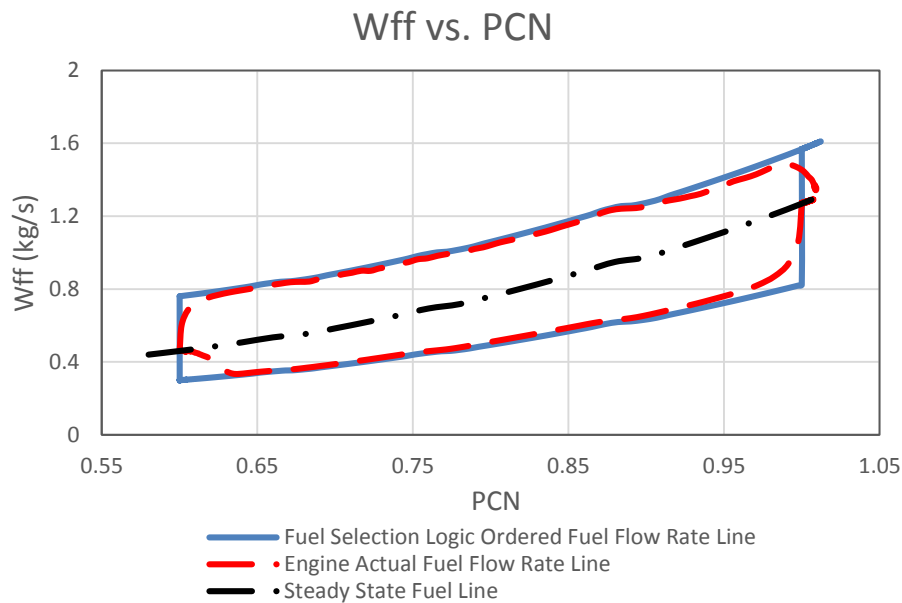


Figure 4.31 Model Turboshhaft Engine Wff vs. PCN at Sea Level, ISA Condition

Fig. 4.31 above is the turboshhaft actual fuel trajectories compared with the transient fuel schedules and the engine steady state fuel line. Compared with Fig. 4.28 in which the turboshhaft engine fuel system model is simulated with ICV method, the engine actual fuel flow rate line in this model almost overlaps with the transient fuel schedule line; the controller taking over the fuel regulation work is faster; and a smaller overshoot at the acceleration target speed is also demonstrated. From the transient simulation results shown in Figs. 4.29 to 4.31, the flexibility of the NR method when applied to turboshhaft engine fuel system simulation has been proved.

4.4 Sensitivity Analysis of Key Fuel System Parameters on Engine Transient Behaviour

In this research, physically based fuel system models have been established with the newly developed methods and added into the engine transient models to investigate the coupling effect of engine integrated with its fuel and control systems. For the developed fuel system model, some selected key parameters may have large effects on the engine transient behaviours. In this section,

investigations of the sensitivities of those selected parameters, which are, the volumes of the assumed volume chambers in ICV method; fuel system components' delay time constants; and some physical parameters of the fuel system components have been achieved and discussed.

4.4.1 The Sensitivity of Selected Volume of Fuel System Volume Chambers

In the fuel system model investigated in this project shown in Fig.3.8, three assumed volumes are added by using the developed ICV method to simulate the system transient behaviours. These volumes store or release the extra fuel produced by the flow mismatch between system conjunct components. This phenomenon causes a time delay effect on the fuel delivered to the engine system, thereby, affects the engine transient performance. The amounts of the volumes of those assumed volume chambers are main factors to produce such delay effects. Therefore, the first investigation on fuel system parameters' sensitivity focuses on the volume effect. For each assumed volume, a 100% increase of the volume amount has been given. The engine actual fuel trajectory of each simulated cases has been compared with the reference system model, which has no increase on the selected parameters, to analysis the sensitivity of the selected volumes.

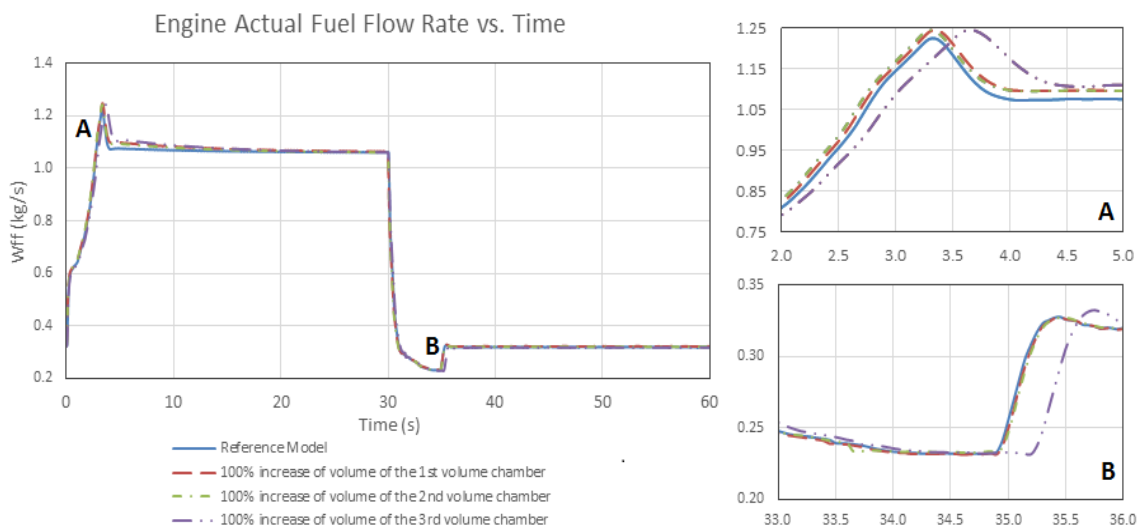


Figure 4.32 Engine Actual Fuel Trajectories Comparison for Fuel System Volume Sensitivity Analysis

Fig. 4.32 shows the engine actual fuel trajectories comparison between the reference model and three increased volume models. The four trajectories follow the same trend through the whole transient manoeuvre. Relatively small but obvious delay effects have been found at point A and B when the controller handles the fuel regulation task from the fuel selection logic. For the scaling point A, the gaps between the fuel trajectories for the first and second increased volume models and the reference model are about 0.05s and 0.1s. For the third increased volume case, the maximum fuel trajectory delay during acceleration is about 0.5s. For deceleration process at the scaling point B, the first and second increased volume models' fuel lines are almost overlapped with the reference model. The maximum delay time for the third increased volume model during this period is about 0.35s. Therefore, it can be concluded that the first and second volumes have less effect on the engine actual fuel line which will finally affect the engine system transient performance. In contrast, the volume of the third assumed volume chamber between the MU and injector has an obvious delay effect on engine injected fuel. A 100% increase of the amount of volume produces a 0.5s delay during acceleration and a 0.35s delay during deceleration.

The reason producing such phenomena is that the first and second volumes, HPP and CPDV form a closed fuel delivery loop to return the excess fuel from HPP outlet to its inlet. This fuel stream is not involved in the system fuel metering task but only used to maintain the system operation safety. Therefore, the amounts of the first and second volumes have less effect on the metered fuel injected into the engine combustor. On the contrary, the MU metered fuel has to flow through the third volume and the injector before it entering into the engine system. The variation of the volume amount of the third volume chamber largely affects the engine actual fuel trajectory.

4.4.2 The Sensitivity of Fuel System Components' Delay Time Constant

Except the assumed volumes introduces delay effects to the engine fuel trajectories, the valve movement delay and fuel spray effects simulated as first order lags for fuel system transient simulation also introduce delay effects into

the engine consumed fuel. In the reference fuel system model, the metering valve movement delay time constant is defined as 10ms meaning the movement delay is 40ms, which is four times to the time constant. The CPDV valve movement delay time constant is 5ms. The fuel spray delay time constant is 75ms. To investigate the sensitivity of each time delay issue, a 5ms is added to each delay time constant and the engine actual fuel trajectories comparison between the new models with new time constants and the reference model has been shown in Fig. 4.33.

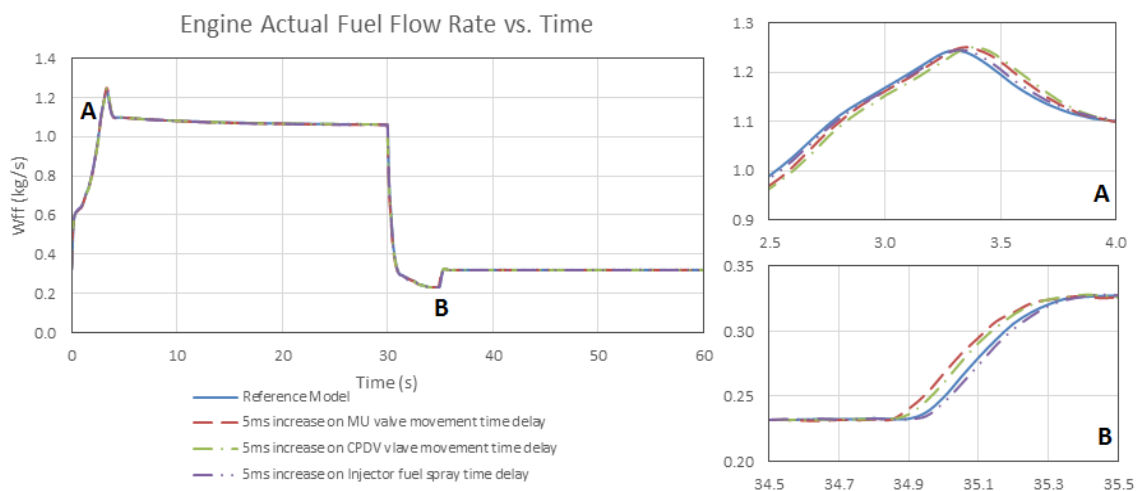


Figure 4.33 Engine Actual Fuel Trajectories Comparison for Fuel System Components' Delay Time Constant Sensitivity Analysis

The simulation results comparison shown in Fig. 4.33 represent that the fuel trajectory of each investigated case follows the same trend with the reference model. The differences appear at the scaling points A and B, although relatively small. For the point A, the increased time constants for MU and CPDV valve movement, and injector fuel spray effect cause the delay of engine actual consumed fuel trajectories. Among these three delay issues during acceleration process, a time constant increase on the injector fuel spray delay has a less effect on the engine fuel trajectory. The increase of the time constant on the CPDV valve movement delay has the largest effect. The maximum delay time for 5ms increase on MU delay time constant through acceleration is about 0.07s; for

CPDV valve movement delay time constant increase is about 0.09s; and for injector is about 0.03s. For the scaling point B during deceleration process, the increases of MU and CPDV valve movement delay time constants do not delay the fuel trajectories but lead to them ahead of the reference model's fuel trajectory. Only the increase on fuel spray delay time constant still produces a further time delay effect comparing with the reference model. The maximum ahead time for MU movement delay time constant increase is about 0.06s and for CPDV valve is about 0.04s. The delay time for injector delay time constant increase is about 0.02s.

4.4.3 The Sensitivity of Fuel System Components' Performance and Structural Key Parameters

Section 4.4.1 and 4.4.2 have investigated the sensitivity of the selected volumes and components' delay time constants which produce delay effect to the engine actual fuel trajectories. In addition to these two considerations, the sensitivity of the selected fuel system components' key performance and structural parameters are also required to be investigated. The selected parameters used to represent the fuel system performance are the components' volumetric flow rate, pressure, and temperature. The input data for design point simulation shown in Table 4-3 and 4-4 are each component's fuel volumetric flow rate and pressure increase or drop through the component. The temperature variation through each component will then be calculated from the simulation.

The components' volumetric flow rates are designed based on the engine system fuel requirements. Therefore, the selected performance parameters used for the sensitivity investigations are the components' pressure increase or drop, that is to say, the LPP pressure increase, HPP pressure increase and the MU pressure drop. For the structural parameters, the MU valve opening coefficient and CPDV spring elastic stiffness sensitivity on engine actual fuel trajectories have been investigated. A 10% increase on each selected parameter has been given to simulate the engine transient performance variation. The simulated results which are the engine actual fuel trajectories are also compared with the reference model result.

Fig. 4.34 shows the engine actual fuel lines comparison between a 10% increase on each selected fuel system performance and structural parameters and the reference model fuel line. The results have shown that all the investigated fuel trajectories are overlapped. For the scaling points A and B, only the increase of HPP pressure increase results in a slight delay which is about 0.05s during acceleration and 0.02s during deceleration. Therefore, it can be concluded that the selected fuel system performance and structural parameters have no obvious effect on engine transient behaviours.

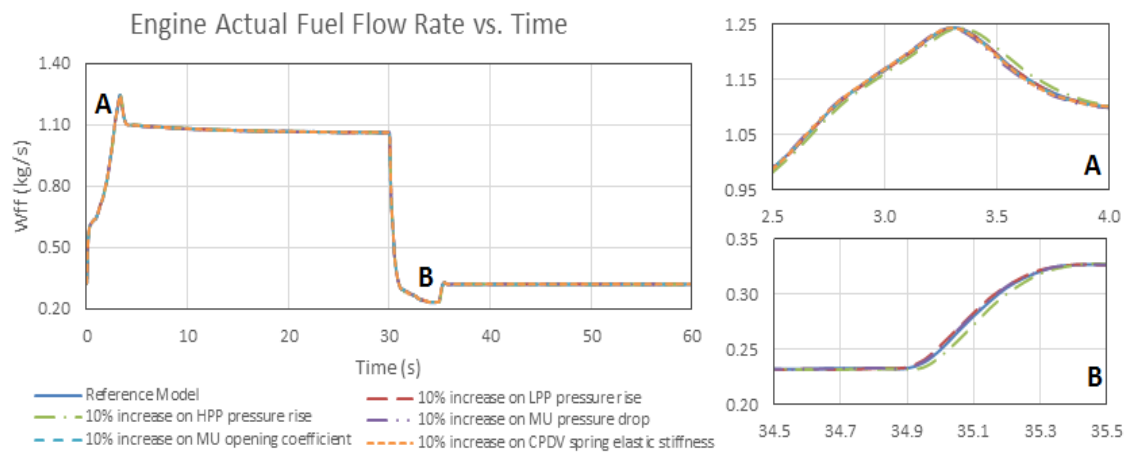


Figure 4.34 Engine Actual Fuel Trajectories Comparison for Fuel System Components' Performance and Structural Key Parameters' Sensitivity Analysis

5 Conclusion

The research of gas turbine transient simulation integrated with its fuel and control systems analysis has been concluded here. Two novel transient performance simulation methods for engine hydraulic fuel systems have been presented.

- Inter-Component Volume (*ICV*) Method
- Newton Raphson (*NR*) Method

The *ICV* method introduces assumed volumes into the system conjunct components to consider the volume fluid storage or release due to the flow mismatch between physical components during the transient process. This causes the fluid compression or expansion inside the volume which will result in the volume pressure variation. This phenomenon will change the volume connected components' operation until the system reaches its steady state condition when the flow mismatch has disappeared. The *ICV* method was first developed and applied to estimate gas turbine transient performance. In this research, the *ICV* method has also been introduced into the engine fuel delivery system transient simulation.

Now the *NR* method is an alternative method introduced into the fuel system simulation. With the introduced volumes, the *ICV* considers the fluid compressibility to implement the calculation. However, for the liquid oil in a fuel delivery system - which is generally considered highly incompressible - the *ICV* method based on fluid compressibility may not be stringent enough. In these cases, the iterative *NR* method for engine hydraulic fuel system simulation has been developed as an alternative simulation method. This method uses iterative processes to modify the connecting ducts pressure to eliminate the flow mismatch between conjunct components during transient operations.

Both the two developed methods allow physically-based simulation models to be built up for gas turbine engines with the inclusion of control and fuel systems, which are potentially more accurate than the methods using transfer functions. The coupling effect between model gas turbine engines and their control and fuel

system during engine transient processes have also been investigated. The developed ICV-based and NR-based fuel system simulation methods have been successfully applied to the performance simulations of the transient processes of a model turbojet and a model turboshaft gas turbine engine where acceleration and deceleration processes of the model engines are simulated and demonstrated.

The validation results comparisons between a single spool turbojet engine model simulated on newly developed simulation platform and validation platforms (TurboMatch and GasTurb) show that the off-design results for engine key performance parameters are less than 5% against TurboMatch model and less than 8% against GasTurb model. The transient parameters' trajectories against GasTurb model also show small differences.

The simulated results comparison between a model turbojet engine with and without its fuel system, which is developed based on the newly developed ICV method shows that the fuel flow delay during the transient process due to the inclusion of fuel system components and the effect of inter-component volumes is around 0.5 seconds during acceleration (PCN 0.6 to 1.0) and 0.3 seconds during deceleration (PCN 1.0 to 0.6). The maximum delay time during acceleration is about 0.8s and is about 0.5s during deceleration, The comparison between the two developed ICV and NR methods on fuel system simulation shows that both the simulated fuel systems have a delay effect to the engine transient simulation but the NR method is around 0.25 seconds during acceleration and 0.1 seconds during deceleration, ahead of the ICV method applied to an engine coupled with its fuel and control system transient processes. The maximum ahead time is about 0.5s during acceleration and is about 0.3s during deceleration. Both of the comparisons have shown that the noticeable effects occur during the process when the fuel control is switched between the fuel selection logic and the fuel controller, although such differences are relatively small.

The sensitivity analysis on fuel system key parameters have been investigated on three sets of parameters, that is to say, the amount of volume for each

assumed volume used for fuel system ICV method simulation; time constants of valve movement delay and injector fuel spray delay; and the fuel system key performance and structural parameters. 100% increase on each volume case comparison shows the volume between LPP and HPP and the volume between HPP and MU have smaller effects on engine actual fuel trajectory which affects the engine transient performance. The increase on the volume between MU and injector introduces an obvious delay effect which is about 0.5s during deceleration and 0.35s during deceleration.

On the sensitivity analysis of the defined time constants for the introduced first order lags to simulate valve movements and injector fuel spray effects, a 5ms time constant increase on MU movement delay provides a maximum 0.07s delay during acceleration but 0.06s ahead on engine actual fuel trajectory during deceleration. The CPDV valve delay time constant increased with 5ms also introduces a 0.09s delay during acceleration but 0.04s ahead of the engine fuel lines during deceleration. Only the time constant increase on injector fuel spray introduces a 0.03s and 0.02s delay on both acceleration and deceleration processes for the engine injected fuel trajectory.

For the fuel system performance and structural parameters' sensitivities analysis, 10% increase on the LPP and HPP pressure increase, MU pressure drop, MU valve opening coefficient and spring elastic stiffness have been analysed. The results of engine actual fuel trajectory have shown no obvious delay effects observed due to the increase of these listed parameters, except only the increase of the HPP pressure rise produces a 0.05s delay during acceleration and 0.02s delay during deceleration.

6 Future Work

In this research, two developed engine fuel system simulation methods have been introduced into the model engine coupled with its fuel and control systems to predict the systems' transient behaviour. The results have represented the availability and flexibility of developed methods and the effects of fuel systems on different methods of simulation. To improve the practicability and reliability of the developed engine with its fuel and control systems models on real industry applications, the following listed issues should be further addressed and implemented.

6.1 Model Accuracy Verification

Model accuracy is an important issue which should be considered for the numerical simulation of physical systems. In this research, the physical engine and fuel system components have been modelled with experiential equations and components' characteristic maps. Those characteristic maps are scaled from empirical, existing component maps. The accuracy of the developed engine model has only been validated by comparing the steady state operating parameters' values against the numerical simulated models at TurboMatch and GasTurb. To further validate the numerical simulation results, real system parameters and component characteristic maps from rig tests should be introduced into the simulations.

6.2 Engine Transient Model Improvement

There are a variety of engine transient phenomena which should be considered in the numerical simulations. However, in this research, only shaft imbalances, volume dynamics, fuel schedules, and fuel delivery components' delay effects have been simulated. Some other phenomena such as the effects of heat soakage, turbomachinery tip clearance changes, and heat transfer between compressor and turbine multi-stages should be considered in future engine model development. [18]

6.3 Fuel Control Algorithms

Fuel schedules are very important issues when regulating engine transient operations. In this research, it is assumed that the engine shaft speed is the only command variable to schedule the engine actual fuel flow rates. Some other specifications like turbine entry temperature, engine thrust, and specific fuel consumption also can be introduced to fulfil different applications' requirements.

6.4 Engine Limit Protection Control Logic

During engine transient operation, a series of limitations should be considered such as compressor surge, turbine over-heating, shaft over-speeding and combustor blow out. Limit protection control is to protect the engine from experiencing such dangerous malfunctions during extreme conditions. A simple fuel selection logic has been introduced in the model engine simulation to regulate transient actual fuel flow in this study. By using researcher defined protection fuel schedules, the model engine could be operated safely. However, if the model engine has already fallen into a dangerous operating status, such selection logic cannot provide solutions to get the engine out of the dangerous situations. A limit protection control logic will monitor the engine operation margin between current status and its limitations. If the margin is too small which is considered unsafe, the new control logic will regulate the engine fuel flow to reach an acceptable margin as soon as possible.

6.5 Dynamic Flight Parameters Introduced into Engine Transient Performance Simulation

For the aero-engines which have to experience the whole flight envelope, the ambient conditions and flight parameters may alter rapidly. Engine transient simulation in this research only permits the alteration of flight dependent parameters at the beginning from a user defined input parameter file. It would be very useful for an aero-propulsion system application to allow flight dependent parameters variation during the transient behaviour to consider an integral aircraft/engine performance simulation.

REFERENCES

- [1] R. Friend, "Turbine Engine Research in the United States Air Force", Air Force Res. Lab., Wright Patterson Air Force Base, OH, USA, 2001;
- [2] L.C. Jaw, J.D. Mattingly, "Aircraft Engine Controls: Design, System Analysis, and Health Monitoring", AIAA 1801 Alexander Bell Drive, Suite 500 Reston, VA 20191-4344, USA, 2009;
- [3] US Department of Transportation, "Airframe & Powerplant Mechanics: Powerplant Handbook", 1976;
- [4] A.R. Howell, "Fluid Dynamics of Axial Compressors", Proc. I. Mech. Eng., 1945;
- [5] A.R. Howell, R. Bonham, "Overall and Stage Characteristics of an Axial Flow Compressor" Proc. I. Mech. Eng., Vol. 164, no. 1, pp. 235-248, 1950;
- [6] D.H. Mallinson, W.G.E. Lewis, "The Part Load Performance of Various Gas Turbine Engine Schemes", Proc. I. Mech. Eng., Vol. 159, No. 1, pp. 198-219, 1948;
- [7] A.W. Goldstein, S. Alpert, W. Beede, K. Kovach, "Analysis of Performance of Jet Engine from Characteristics of Components II-Interaction of Components as Determined from Engine Operation", NACA Rept. 928, 1948;
- [8] R.J. May, B.J. Brownstein, S.J. Przybylko, R.L. McTasney, A.T. Molisse, "A Review of Current and Projected Aspects of Turbine Engine Performance Evaluation", Tech. Rpt. AFAPL-TR-71-34, 1972;
- [9] M.S. Chappell, E.P. Cockshutt, C.R. Sharp, "Gas Turbine Cycle Calculations: Design Point Performance of Turbojet and Turbofan Engine", National Research Council of Canada, Aero. Rept., LR-407, 1964;
- [10] E.P. Cockshutt, C.R. Sharp, "Gas Turbine Cycle Calculations: Design Point Performance of Turbopropellor and Turboshaft Engines", National Research Council of Canada, Aero. Rept., LR-448, 1965;

- [11] J.R. Palmer, "The 'Turbocode' Scheme for the Programming of Thermodynamic Cycle Calculations on an Electronic Digital Computer", College of Aeronautics Rept., Aero 198, 1967;
- [12] J.R. Palmer, K.P. Annand, "Description of the Algol Version of the 'Turbocode' Scheme for the Programming of Thermodynamic Cycle Calculations on an Electronic Digital Computer", College of Aeronautics Report, Aero 203, 1968;
- [13] J.S. McKinney, "Simulation of Turbofan Engine, Part 1, Description of Method and Balancing Technique", United States Air Force, Aero Propulsion Lab, AFAPL-TR-67-125-Part I, 1967;
- [14] J.S. McKinney, "Simulation of Turbofan Engine, Part 2, Users' Manual and Computer Listing", United States Air Force, Aero Propulsion Lab, AFAPL-TR-67-125-Part 2, 1967;
- [15] R.W. Koenig, L.W. Fishbach, "GENENG – A Program for Calculating Design and Off Design Performance for Turbojet and Turbofan Engines", NASA TND-6552, 1972;
- [16] L.W. Fishback, R.W. Koenig, "GENENG II – A Program for Calculating Design and Off Design Performance of Two and Three-Spool Turbofans with as Many Nozzles", NASA TN D-6553, 1972;
- [17] W.L. Macmillan, "Development of a Modular Type Computer Programme for the Calculation of Gas Turbine Off-Design Performance", Ph.D. Thesis, Cranfield Institute of Technology, 1974;
- [18] P.P. Walsh, P. Fletcher, "Gas Turbine Performance", 2nd edition, 2004;
- [19] V. A. Pachidis, "Gas Turbine Performance Simulation", Cranfield Thermal Power MSc Course Notes, 2011.
- [20] L.C. Jaw, S. Garg, "Propulsion Control Technology Development in the United States", NASA TM - 2005-213978;

- [21] E.W. Otto, B.L. Taylor, III, "Dynamics of a Turbojet Engine Considered as a Quasi-static System", NACA Rept. 1011, 1950;
- [22] M.F. Heidmann, "Analysis of the Effect of Variations in Primary Variables on Time Constant, and Turbine Inlet Temperature Overshoot of Turbojet Engines", NACA TN 2182, 1950;
- [23] D. Novik, "Some Linear Dynamics of Two-Spool Turbojet Engines", NACA TN 3274;
- [24] P. Pilidis, "Digital Simulation of Gas Turbine Performance", Ph.D. Thesis, University of Glasgow, 1983;
- [25] V.L. Larrowe, M.M. Spencer, S.R. Lampert, "A Dynamic Performance Computer for Gas Turbine Engines", Transactions ASME October., 1957;
- [26] C. Denison, "General Nonlinear Digital Simulation Methods Applied to Gas Turbine Dynamic Behavior", Ph.D. Thesis, University of London, 1968;
- [27] G.S. Mueller, "Gas Turbine Simulation Using One-Dimensional Flow Relationships", Ph.D. Thesis, University of Manchester, 1969;
- [28] H.P. Durand, "Simulation of Jet Engine Transient Performance", ASME Paper 65, WA/WD-16, 1965;
- [29] A.L. Bates, "Dynamic Analysis Techniques for Turbine Engine Controls", Air Force Aero Propulsion Laboratory, Tech. Rept. AFAPL-TR-67-117, 1967;
- [30] K. Bauerfeind, "A New Method for the Determination of Transient Jet Engine Performance Based on the Non-Stationary Characteristics of the Components", AGARD Conference Proc. No. 34, Part 2, Paper 32, 1968;
- [31] H.I.H Saravanamuttoo, A.J. Fawke, "Simulation of Gas Turbine Dynamic Responses", ASME Paper 70, GT-23, 1970;
- [32] A.J. Fawke, H.I.H. Saravanamuttoo, "Experimental Investigation of Methods for Improving the Dynamic Response of a Twin Spool Turbojet Engines", Transactions of ASME, *J. Engineering for Power*, Vol. 93, pp. 418-424, 1971;

- [33] A.J. Fawke, H.I.H. Saravanamuttoo, "Digital Computer Methods for Prediction of Gas Turbine Dynamic Response", Society of Automotive Engineers Ret. 710550, 1971;
- [34] N.U. Rahman, J.F. Whidborne, "Real-Time Transient Three Spool Turbofan Engine Simulation: A Hybrid Approach", Dynamics, Simulation and Controls Group, Cranfield University, 2009;
- [35] W.J. Tong, "A High Bypass Ratio Geared Turbofan Engine Transient Performance Modeling and Simulating Research", MSc. Thesis, Cranfield University, 2009;
- [36] Y.G. Li, N.R.L. MacCallum, P. Pilidis, "Pressure Waves in Volume Effect in Gas Turbine Transient Performance Models", *J. Propulsion and Power*, Vol. 17, No.3, pp. 706-710, 2001;
- [37] K. Seldner, J.R. Mihalow, "Generalized Simulation Technique for Turbojet Engine System Analysis", NASA TN D-6610, 1972;
- [38] P.H. Naylor, "Gas Turbine Transient Performance: Heat Soakage Modeling", Ph.D. Thesis, Cranfield University, 2004;
- [39] C.J. Daniele, "A Generalized Computer Code for Developing Dynamic Gas Turbine Engine Models (DIGTEM)", NASA TM-83508, 1984;
- [40] J.R. Szuch, W.M. Bruton, "Real Time Simulation of the TF30-P-3 Turbofan Engine Using a Hybrid Computer", NASA TM X-3106;
- [41] J.R. Szuch, K.Seldner, D.S. Cwunar, "Development and Verification of Real-Time Hybrid Computer Simulation of F100-PW-100(3) Turbofan Engine", NASA TP-1034, 1977;
- [42] R.A. Blech, D.J. Arpasi, "An Approach to Real-Time Using Parallel Processing", NASA TM-81371, 1981;
- [43] C.J. Daniele, S.M. Krosel, J.R. Szuch, E.J. Westerkamp, "Digital Computer Program for Generating Dynamic Turbofan Engine Models(DIGTEM)", NASA TM-83446, 1983;

- [44] J.K. Lytle, "The Numerical Propulsion System Simulation: A Multidisciplinary Design System for Aerospace Vehicles", NASA TM-209194;
- [45] J.K. Lytle, "The Numerical Propulsion System Simulation: An Overview", NASA M-209195;
- [46] C.G. Naiman, G.J. Follen, "Numerical Propulsion System Simulation – A Common Tool for Aerospace Propulsion Being Developed", NASA TM-210605;
- [47] R.D. May, J. Csank, T.M. Lavelle, J.S. Litt, T.H. Guo, "A High-Fidelity Simulation of a Generic Commercial Aircraft Engine and Controller", AIAA-2010-6629, 46th AIAA/ASME/SAE/ASEE Joint Propulsion Conference and Exhibit, Nashville, TN, 2010;
- [48] D.K. Frederick, J.A. DeCastro, J.S. Litt, "User's Guide for the Commercial Modular Aero-Propulsion System Simulation (C-MAPSS)", NASA TM-215026;
- [49] J. Kurzke, "Advanced User-Friendly Gas Turbine Performance Calculations on a Personal Computer", ASME Conference in Houston, TX, USA, ASME 95-GT-147;
- [50] GasTurb website URL: "<http://www.gasturb.de>", 2013;
- [51] W.P.J. Visser, M.J. Broomhead, "GSP, A Generic Object-Oriented Gas Turbine Simulation Environment", NLR-TP-2000-267, National Aerospace Laboratory, NLR, 2000;
- [52] W.P.J. Visser, M.J. Broomhead, J. van der Vorst, "TERTS, A Generic Real Time Gas Turbine Simulation Environment", NLR-TP-2002-069;
- [53] H.I.H. Saravanamuttoo, "Overview on Basis and Use of Performance Prediction Method", AD-P007 890, 1992;
- [54] J.G. Sun, "Advanced Multivariable Control Systems of Aeroengines", Press. Of BUAA, ISBN-7810775901, 2005;
- [55] J. Lutambo, J.Q. Wang, H. Yue, G. Minirovsky, "Aircraft Turbine Engine Control Systems Development: Historical Perspective",

- [56] C.B. Maher-Homji, "The Development of the Whittle Turbojet", *J. Eng. Gas Turbines Power*, 120(2), pp. 249-256, 1998;
- [57] E.A. Watson, "Fuel Control and Burning in Aero Gas Turbine Engine", James Clayton Lecture, IMechE, London, pp. 25-56, 1955;
- [58] O.N. Lawrence, "Fuel Systems for Gas Turbine Engines", *J.R. Aeronaut. Soc.*, November, pp. 727-737, 1955;
- [59] Wikipedia URL: https://en.wikipedia.org/wiki/Fuel_control_unit, 2015;
- [60] L.K. Bernard, "Gas Turbine Technology Evolution: A Designer's Perspective", *J. Propulsion and Power*, Vol.20, No.4, pp. 577-595, 2003;
- [61] T.A. Flanders, "The Architecture of a Turbine Engine Control", Joint Royal Aeronautical Society and Institute of Electrical Engineering Symposium, The Application of Electrical Control to Aircraft Propulsion System, London, UK, 1974;
- [62] D.M. Griffiths, R.D. Powell, "The Use of Digital Control for Complex Power Plant Management", AGARD Conference Proceedings N.151, Power Plants Controls for Aircraft Gas Turbine Engines, Ustaoset, Norway, 1974;
- [63] F.W. Burcham Jr., L.P. Myers, K.R. Walsh, "Flight Evaluation of a Digital Electronic Engine Control in an F-15 Airplane", *J. Aircraft*, Vol.22, No.12, pp.1072-1078, 1985;
- [64] NASA Technology Facts, "Digital Electronic Engine Control", TF-2004-03 DFRC, 2004;
- [65] M. Joby, "FADEC Widens its Application Base", *World Aerospace Technology*, pp. 103-106, 1991;
- [66] S. Garg, "Aircraft Turbine Engine Control Research at NASA Glenn Research Center", NASA TM-217821, 2013;
- [67] W.C. Merrill, C.F. Lorenzo, "A Reusable Rocket Engine Intelligent Control", NASA TM-100963, AIAA-88-3114, 1988;

- [68] Industry Representatives Distributed Engine Control Working Group, "Distributed Engine Control –Proposed 5 Year Plan: System Benefits and Implementation Challenges", NASA Propulsion Controls and Diagnostics Workshop, 2009;
- [69] A. Vick, K. Cohen, "Genetic Fuzzy Controller for a Gas Turbine Fuel System", Chapter 8 of *Advances in Intelligent and Autonomous Aerospace Systems*, pp. 229-272, 2012;
- [70] W.I. Rowen, "Design Considerations for Gas Turbine Fuel Systems", *Turbomachinery International*, 1990;
- [71] K. Astrom, T. Haggund, "PID Controllers: Theory, Design and Tuning", 2nd Edition, ISBN 1-55617-516-7, 1995;
- [72] S. Skogestad, "Probably the Best Simple PID Tuning Rules in the World", *J. Process Control*, July, 2001;
- [73] J.G. Ziegler, N.B. Nichols, "Optimum Settings for Automatic Controllers", *Trans. ASME*, Vol. 64, pp. 759-768, 1942;
- [74] D.E. Rivera, M. Morari, S. Skogestad, "Internal Model Control. 4. PID Controller Design", *Ind. Eng. Chem. Process Des. Dev.*, Vol. 25, pp. 252-265, 1986;
- [75] G.J. Michael, F.A. Farrar, "Development of Optimal Control Modes for Advanced Technology Propulsion Systems" United Aircraft Research Laboratories, East Hartford, Connecticut 06108, 1974;
- [76] A.E. Bryson, Jr., Y.-C. Ho, "Applied Optimal Control – Optimization, Estimation, and Control", Tayler & Francis Group, New York, 1975;
- [77] J.R. Szuch, J.F. Soeder, "F100 Multivariable Control Synthesis Program – Evaluation of a Multivariable Control Using a Real-Time Engine Simulation", NASA TP-1056, 1977;
- [78] H.H. Rosenbrock, "Design of Multivariable Control Systems Using the Inverse Nyquist Array", *Proc. IEE*, Vol. 116, pp. 1929-1936, 1969;

- [79] P.D. McMorrان, "Design of Gas-Turbine Controller Using Inverse Nyquist Method", *Proc. IEE*, Vol.117, pp. 2050-2056, 1970;
- [80] M. Nagahara, Y. Yamamoto, S. Miyazaki, T. Kudoh, N. Hayashi, " H^∞ Control of Microgrids Involving Gas Turbine Engines and Batteries", IEEE, 2012;
- [81] H. Richter, "Advanced Control of Turbofan Engines", ISBN 978-1-4614-1170-3, Springer, 2011;
- [82] I.V. Kolmanovsky, L.C. Jaw, W. Merrill, H. Tran Van, "Robust Control and Limit Protection in Aircraft Gas Turbine Engines", *IEEE. International Conf. Control Applications*, Dubrovnik, Croatia, 2012;
- [83] L.A. Zadeh, "Fuzzy Sets", *Information and Control*, Vol. 8, Issue. 3, pp. 338-353, 1965;
- [84] L.A. Zadeh, "Outline of a New Approach to the Analysis of Complex Systems and Decision Processes", *IEEE Transactions on Systems, Man, and Cybernetics*, Vol. SMC-3, No. 1, 1973;
- [85] S.R. Balakrishnan, S.K. Mishra, V. Sundararajan, K.A. Damodaran, "Fuzzy Computing for Control of Aero Gas Turbine Engines", *J. Defence Science*, Vol. 44, No. 4, pp. 295-304, 1994;
- [86] S.R. Balakrishnan, S. Santhakumar, "A Fuzzy Logic Approach in the Control of a Twin-Spool Aircraft Gas Turbine Engine under Development", *Proc. Instn. Mech. Engrs.*, Vol. 210, 1996;
- [87] B. Wang, H.C. Zhao, L. Yu, Z.F. Ye, "Study of Temperature Effect on Servovalve-Controlled Fuel Metering Unit", *J. Eng. Gas Turbine Power*, Vol. 137, No. 6, 061503, 2015;
- [88] H.A. Spang III, H. Brown, "Control of Jet Engines", *Control Engineering Practice*, Vol. 7, Issue. 9, Sep. 1999, pp. 1043-1059;
- [89] S.Q. Fan, D. Li, D. Fan, "Aero-Engine Control on the Book I", ISBN 9787561221617, Xi'an, CHINA, 2008;

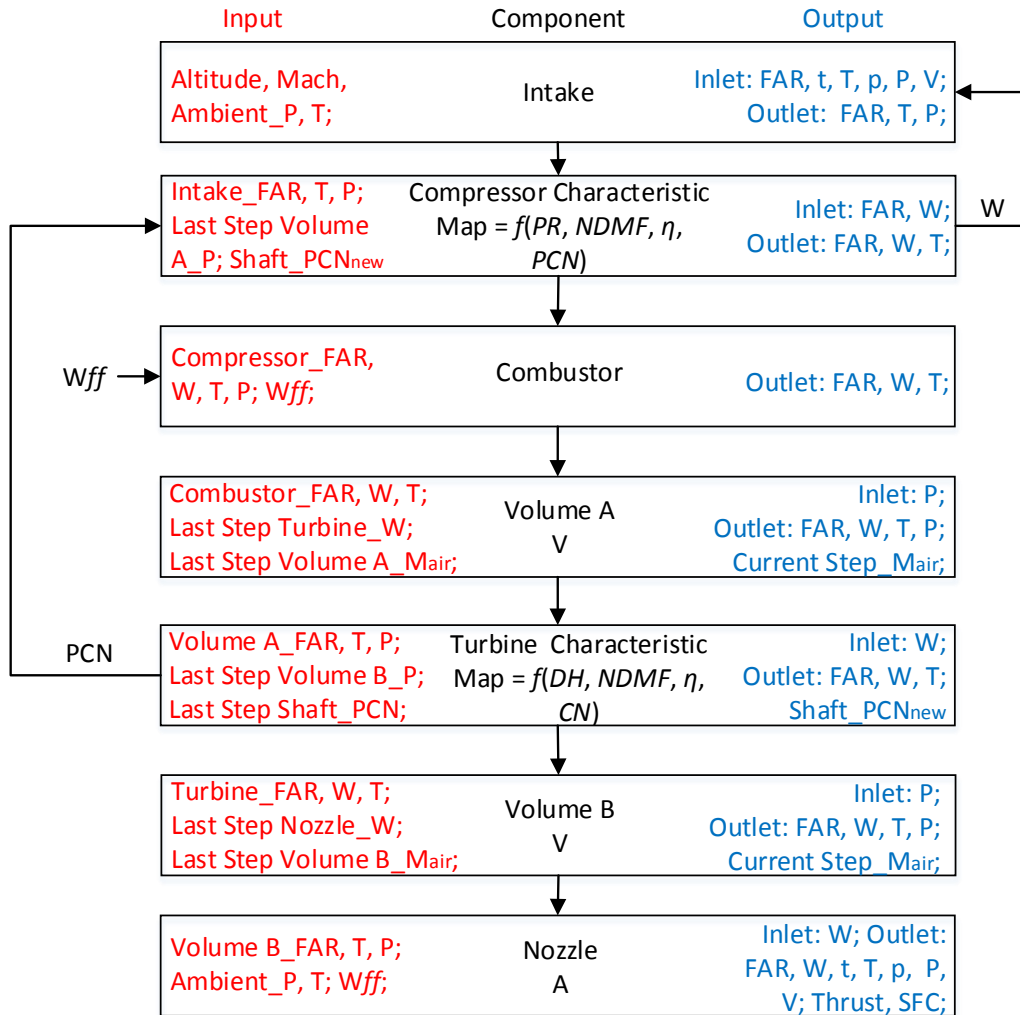
- [90] “Stepper Motor Basics”, Industrial Circuits Application Note, URL: <http://www.solarbotics.net/library/pdflib/pdf/motorbas.pdf>, 2013;
- [91] “Stepper Motor Reference Design”, Silicon Labs AN155;
- [92] H. Cohen, G.F.C. Rogers, H.I.H. Saravanamuttoo, “Gas Turbine Theory”, 4th Edition, ISBN 0-582-23632-0, 1996;
- [93] J.F. Sellers, and C.J. Daniele, “DYNGEM. A Program for Calculating Steady State and Transient Performance of Turbojet and Turbofan Engines”, NASA TN D-7901, 1975;
- [94] N.U. Rahman, J.F. Whidborne, “A Numerical Investigation into the Effect of Engine Bleed on Performance of a Single-Spool Turbojet Engine”, *Journal of Aerospace Engineering*, Vol. 222, No. 7, pp. 939-949, 2008;
- [95] A. Sobester, “Tradeoffs in Jet Inlet Design: A Historical Perspective”, *Journal of Aircraft*, Vol. 44, No. 3, May-Jun. 2007;
- [96] S. Yarlagadda, “Performance Analysis of J85 Turbojet Engine Matching Thrust with Reduced Inlet Pressure to the Compressor”, The University of Toledo Thesis, 2010;
- [97] P. Pilidis, J.R. Palmer, “Gas Turbine Theory and Performance”, Cranfield MSc Course Notes, 2011;
- [98] S. Benner, “A History of Control Engineering”, IET, 1993;
- [99] Wikipedia URL: http://en.wikipedia.org/wiki/PID_controller, 2015;
- [100] Matsuoka H, “Isobaric Thermal Expansion and Isothermal Compression”, Illinois State University, Thermal Physics, URL: [http://www2.phy.ilstu.edu/~hmb/phy325/TPCh.5.6.1\(11\).pdf](http://www2.phy.ilstu.edu/~hmb/phy325/TPCh.5.6.1(11).pdf), 2014;
- [101] Coordinating Research Council, “Handbook of Aviation Fuel Properties”, Society of Automotive Engineers, Inc. Warrendale, Pennsylvania, pp. 84-87, 1983;
- [102] Wikipedia, URL: http://en.wikipedia.org/wiki/Newton%27s_method, 2015;

[103] Z.L. Pu, "Aircraft Pump Design [M]", Academic Press, 12: 7-132, 1983;

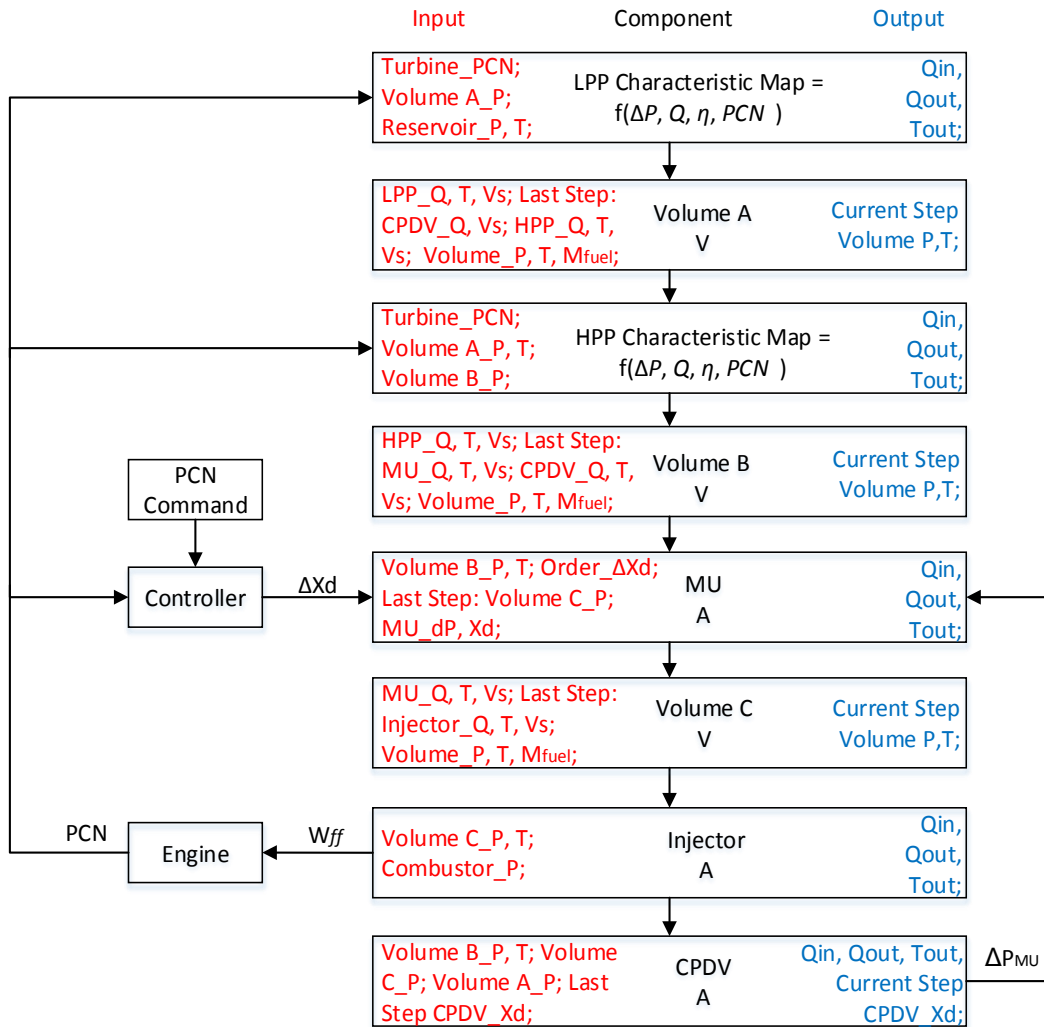
[104] H.L. Arthur, and R.B. Dilip, "Gas Turbine Combustion: Alternative Fuels and Emissions", 3rd ed, CRC Press, Boca Raton, London, New York, 2010, Chap.6;

APPENDICES

A.1 Engine System Simulation Flow Chart Using Inter-Component Volume (ICV) Method



A.2 Flow Chart of Inter-Component Volume (ICV) Method on Fuel System Simulation



A.2 Flow Chart of Newton Raphson (NR) Method on Fuel System Simulation

